Geological Society, London, Special Publications Online First

Crustal evolution, intra-cratonic architecture and the metallogeny of an Archaean craton

D. R. Mole, M. L. Fiorentini, K. F. Cassidy, C. L. Kirkland, N. Thebaud, T. C. McCuaig, M. P. Doublier, P. Duuring, S. S. Romano, R. Maas, E. A. Belousova, S. J. Barnes and J. Miller

Geological Society, London, Special Publications, first published December 3, 2013; doi 10.1144/SP393.8

Crustal evolution, intra-cratonic architecture and the metallogeny of an Archaean craton

D. R. MOLE[1,6]*, M. L. FIORENTINI[1], K. F. CASSIDY[1], C. L. KIRKLAND[2], N. THEBAUD[1], T. C. MCCUAIG[1], M. P. DOUBLIER[2], P. DUURING[1], S. S. ROMANO[2], R. MAAS[3], E. A. BELOUSOVA[4], S. J. BARNES[5] & J. MILLER[1]

[1]*Centre for Exploration Targeting, ARC Centre of Excellence for Core to Crust Fluid Systems, School of Earth and Environment, University of Western Australia, Stirling Hwy, Crawley 6009, Perth, Australia*

[2]*Geological Survey of Western Australia, 100 Plain Street, East Perth 6004, Australia*

[3]*School of Earth Sciences, University of Melbourne, Parkville, Victoria 3010, Australia*

[4]*ARC Key Centre for the Geochemical Evolution and Metallogeny of Continents (GEMOC), ARC Centre of Excellence for Core to Crust Fluid Systems, Macquarie University, North Ryde, NSW 2109, Australia*

[5]*CSIRO Earth Science & Resource Engineering, 26 Dick Perry Ave, Kensington 6151, Australia*

[6]*Current address: Department of Applied Geology, Curtin University, GPO Box 1987, Perth WA 6845, Australia*

**Corresponding author (e-mail: david.mole@curtin.edu.au)*

Abstract: The generation of the Earth's continental crust modified the composition of the mantle and provided a stable, buoyant reservoir capable of capturing mantle material and ultimately preserving ore deposits. Within the continental crust, lithospheric architecture and associated cratonic margins are a first-order control on camp-scale mineralization. Here we show that the evolving crustal architecture of the Archaean Yilgarn Craton, Western Australia, played a key role in controlling the localization of camp-scale gold, iron and nickel mineralized systems. The age and source characteristics of Archaean lithosphere are heterogeneous in both space and time and are recorded by the varying Nd isotopic signature of crustal rocks. Spatial and temporal variations in isotopic character document the evolution of an intra-cratonic architecture through time, and in doing so map transient lithospheric discontinuities where gold, nickel and iron mineral systems were concentrated. Komatiite-hosted nickel deposits cluster into camps localized within young, juvenile crust at the isotopic margin with older lithosphere; orogenic gold systems are typically localized along major structures within juvenile crust; and banded iron formation (BIF)-hosted iron deposits are localized at the edge of, and within, older lithospheric blocks. Furthermore, this work shows that crustal evolution plays an important role in the development and localization of favourable sources of nickel, gold and iron by controlling the occurrence of thick BIFs, ultramafic lavas and fertile (juvenile) crust, respectively. Fundamentally, this study demonstrates that the lithospheric architecture of a craton can be effectively imaged by isotopic techniques and used to identify regions prospective for camp-scale mineralization.

The continental crust is a physical and geochemical record of Earth history and is unique within our solar system (Taylor & McLennan 1985; Blichert-Toft & Albarède 1997; Bizzarro *et al.* 2003; Hawkesworth *et al.* 2010). Its formation began *c.* 200 myr after the formation of the planet at around 4.4 Ga (Wilde *et al.* 2001; Harrison *et al.* 2005; Blichert-Toft & Albarède 2008), but large continental blocks did not stabilize until after *c.* 3.2–3.0 Ga (Smithies *et al.* 2003; Shirey & Richardson 2011; Naeraa *et al.* 2012; Dhuime *et al.* 2012). The formation and stabilization of continental masses changed the composition of the mantle, creating two new geochemical reservoirs: the depleted upper mantle and the complementary enriched crust (Jacobsen & Wasserburg 1979; O'Nions *et al.* 1980; DePaolo 1981; Allègre *et al.* 1983; Hawkesworth & Kemp 2006; Hawkesworth *et al.* 2010). The creation of these reservoirs changed the geochemical budget of the Earth, whereby elements that

From: JENKIN, G. R. T., LUSTY, P. A. J., MCDONALD, I., SMITH, M. P., BOYCE, A. J. & WILKINSON, J. J. (eds) *Ore Deposits in an Evolving Earth*. Geological Society, London, Special Publications, **393**, http://dx.doi.org/10.1144/SP393.8

preferentially partition into silicate melts (incompatible elements) were concentrated in the new crust (Rudnick 1995; Hawkesworth & Kemp 2006).

This new crustal reservoir was dominated by lower-density minerals that made it more buoyant and gravitationally stable than oceanic crust, which being relatively dense is recycled back into the asthenosphere at subduction zones (Carlson & Raskin 1984; Cloos 1993; Hawkesworth *et al.* 2010; Cawood *et al.* 2013). As a result, the preservation potential of the new continental crust relative to oceanic material was much greater (Hawkesworth & Kemp 2006; Hawkesworth *et al.* 2009; Hawkesworth *et al.* 2010). In addition, the new continental crust had a rheology conducive to capturing and storing mantle-derived magmas that allowed both the generation and the preservation of metallic ore deposits.

The continental crust is not only essential for the capture and storage of ore deposits, but also has a first-order control on their localization and formation at a variety of scales (Cassidy *et al.* 2002; Champion & Cassidy 2007; Begg *et al.* 2009, 2010). The spatial evolution of the crust and the distribution of Precambrian cratons, Proterozoic fold belts and Phanerozoic crust create a diverse lithospheric architecture (Cawood *et al.* 2013) that effectively controls the preferential pathways of magmas and fluids as well as sites of structural complexity (Begg *et al.* 2009). Subsequently, Precambrian cratons and their boundaries are a major control on the location of mineral deposits worldwide (Groves & Batt 1984; Begg *et al.* 2009, 2010; Blewett *et al.* 2010*b*). However, there is clearly potential for major mineralization events/processes *within* cratonic blocks, as demonstrated by large nickel (Barrie *et al.* 1993; Houlé *et al.* 2008; Fiorentini *et al.* 2012; Houlé *et al.* 2012), platinum-group element (PGE; Zientek *et al.* 2002; Maier 2005), gold (Groves & Batt 1984; Robert *et al.* 2005; Ispolatov *et al.* 2008; Bateman *et al.* 2008), base metal (Ashley *et al.* 1988; Hannington *et al.* 1999*a*, *b*; Cantwell *et al.* 2009) and iron deposits (Khan & Naqvi 1996; Angerer & Hagemann 2010; Duuring *et al.* 2012; Angerer *et al.* 2012*a*) found within many Archaean cratons (e.g. Yilgarn, Superior, Kaapvaal). Consequently, understanding the internal temporal and spatial evolution of Archaean cratons is important in understanding the localization of Archaean mineral deposits (Ketchum *et al.* 2008; Blewett *et al.* 2010*b*).

To achieve this, Sm–Nd isotope data for Archaean crustal granites and felsic volcanic rocks of the Yilgarn Craton, Western Australia, were used to map spatial variations in the age and source of the crust. Previous Sm–Nd and Lu–Hf isotopic work by Cassidy *et al.* (2002), Griffin *et al.* (2004), Champion & Cassidy (2007) and Blewett *et al.* (2010*b*) showed that the Yilgarn Craton has an internal crustal architecture consisting of a number of discrete lithospheric blocks of varying age and origin. Several studies have linked this isotopic architecture to the localization of mineral systems (Barley *et al.* 2003; Begg *et al.* 2010); however a coherent, multicommodity study has been lacking. The primary aims of this work were to consolidate and extend the Sm–Nd isotope coverage of the Yilgarn Craton, develop a comprehensive understanding of the crustal evolution of the craton in space and time and relate this to the spatial and temporal occurrence of komatiite-hosted nickel, orogenic gold and banded iron formation (BIF)-hosted iron systems.

The Yilgarn Craton is one of the largest preserved pieces of Archaean crust on Earth (Cassidy *et al.* 2006; Champion & Cassidy 2007) and records a history of continental crust from *c.* 4400 Ma (Jack Hills, Illara and Maynard Hills metasediments; Wilde *et al.* 2001; Wyche *et al.* 2004) to 2600 Ma (late, post-tectonic 'cratonizing' granites; Cassidy *et al.* 2002; Champion & Cassidy 2007), and a supracrustal record dating from 3010 to 2650 Ma (Wilde & Pidgeon 1986; Pidgeon *et al.* 1990; Wang *et al.* 1996; Nelson 1997; Wang *et al.* 1998; Witt 1999; Chen *et al.* 2003; Robert *et al.* 2005; Kositcin *et al.* 2008; Ivanic *et al.* 2010). The Yilgarn Craton is also one of the most intensely mineralized crustal terranes on Earth, with multiple gold, iron and nickel camps (Groves 1993; Groves *et al.* 1995; Barley *et al.* 1998, 2003; Barnes 2006*a*, *b*; Angerer & Hagemann 2010; Angerer *et al.* 2012*a*, *b*; Fiorentini *et al.* 2012; Duuring & Hagemann 2013*a*, *b*). As a result, it represents an excellent case study area to investigate the effects of crustal evolution and intra-cratonic architecture on the localization of multiple mineral systems.

Geological setting and previous work

The Archaean Yilgarn Craton is located in the SW of Western Australia and consists of approximately 70% granite–gneiss and 30% greenstone belts (meta-igneous and meta-sedimentary sequences; Myers 1995; Cassidy *et al.* 2006). The craton has been divided into a number of terranes and domains by Cassidy *et al.* (2006) based on detailed stratigraphic, structural, geochemical and geochronological data (see Fig. 1). The Eastern Goldfields Superterrane comprises the eastern half of the Yilgarn Craton and consists of the Yamarna, Burtville, Kurnalpi and Kalgoorlie Terranes (Cassidy *et al.* 2006; Pawley *et al.* 2012). The South West, Narryer and Younami Terranes occur to the west of the Ida Fault, and are collectively referred to here as the 'West Yilgarn' superblock. The

Youanmi Terrane is further subdivided into the Murchison and Southern Cross Domains (Fig. 1a).

A summary of the preserved granite–greenstone geology of the Yilgarn Craton is presented in Cassidy *et al.* (2006), Wyche *et al.* (2012*b*), Table 1 and Figure 2.

The Yilgarn Craton has been the subject of numerous Sm–Nd isotopic studies, for example McCulloch & Compston (1981), Fletcher & Rosman (1982), McCulloch *et al.* (1983) Fletcher *et al.* (1984), McCulloch (1987), Fletcher *et al.* (1994), Champion & Sheraton (1997), Bateman *et al.* (2001), Cassidy *et al.* (2002), Barley *et al.* (2003), Griffin *et al.* (2004), Champion & Cassidy (2007) and Wyche *et al.* (2012*a*, *b*), that has led to a large body of spatially constrained data. Cassidy & Champion (2004) and Champion & Cassidy (2007) display this extensive isotopic dataset via contour mapping, demonstrating the significant spatial variation in the crustal history of the Yilgarn Craton. This map demonstrates that the Eastern Goldfields consist of much younger crust (*c.* 3000 Ma Nd model age) than the West Yilgarn (*c.* 3500–3300 Ma Nd model age). These two crustal domains are bounded by the Ida Fault, which is interpreted as a crustal-scale structure (Swager 1997; Drummond *et al.* 2000; Goleby *et al.* 2006; Dentith *et al.* 2012) representing the suture between two different lithospheric blocks.

Mole (2012), Ivanic *et al.* (2012) and Wyche *et al.* (2012*b*) took the isotopic study of the Yilgarn Craton further by using Lu–Hf isotopes from magmatic and inherited zircons. Wyche *et al.* (2012*b*) identified five crustal growth and recycling events at *c.* 4200, 3500, 3100, 2800 and 2700 Ma, and demonstrated shared, craton-wide magmatism and juvenile input after *c.* 3000 Ma. Mole (2012) confirmed the significant isotopic difference between the West Yilgarn and Eastern Goldfields Superterrane, and mapped the evolution of the craton from 3050 to 2600 Ma.

Cassidy & Champion (2004) and Champion & Cassidy (2007) used Sm–Nd data to produce a spatial analysis of crustal source regions for the entire Yilgarn Craton, although a number of areas had low sample density, particularly the southern Youanmi Terrane, which underwent targeted sampling for this work. Other isotopic studies (e.g. Griffin *et al.* 2004; Ivanic *et al.* 2012) focussed on smaller regions within the Yilgarn Craton. Such spatial isotopic work has also been performed in the Superior Craton (Boily *et al.* 2009) and Albany–Fraser Orogen (Kirkland *et al.* 2011). Griffin *et al.* (2004) used Lu–Hf analyses on detrital zircons from modern drainage systems to infer a series of crustal domains in the NW Yilgarn Craton. However, although the use of stream-sampled detrital zircons allows the analysis of a large area, the resolution of the spatial component is highly uncertain. Ivanic *et al.* (2012) used Lu–Hf isotopes on magmatic zircons from granites of the Murchison Domain to better understand the crustal history through time; however, samples from this study were focused within a narrow region.

Granites of the Yilgarn Craton

Geochronology shows that granites (*sensu lato*) were emplaced during several discrete episodes dating back to *c.* 3700 Ma (Cassidy *et al.* 1998, 2002; Mole *et al.* 2012), with the majority of preserved granites emplaced at *c.* 2680–2670, 2660–2650 and 2640–2620 Ma (Cassidy *et al.* 2002; Mole *et al.* 2012; Pawley *et al.* 2012). The 2660–2650 group is the most widespread and was broadly synchronous with late Archaean volcanism, deformation and metamorphism (Cassidy *et al.* 2002; Barley *et al.* 2003; Kositcin *et al.* 2008; Mole *et al.* 2012). The 2640–2620 Ma group is also common and appears to be the last magmatic event in the Yilgarn Craton, correlating with the craton-wide gold mineralization (Kent *et al.* 1996; Kent & McDougall 1995). This suggests that both events are intimately associated with final cratonization of the Yilgarn (Kent *et al.* 1996). Metamorphism throughout the craton is typically of prehnite–pumpellyite to upper amphibolite (Ahmat 1984; Cassidy *et al.* 2006; Goscombe *et al.* 2009), although granulite facies metamorphism, concurrent with emplacement of the *c.* 2640–2620 Ma charnockite granites, is found in the South West Terrane (Nemchin *et al.* 1994).

Compositionally, late Archaean granites across the craton belong to two primary groups, the High-Ca and Low-Ca granites, which account for *c.* 60 and 20% of the total surface area of Yilgarn granites, respectively (Champion & Sheraton 1997; Champion & Cassidy 2007; Czarnota *et al.* 2010). In addition, there are three minor groups: the Mafic, Syenitic and High-HFSE (high field strength element) groups. The Mafic granites are of particular interest here as they have been proposed as a source of gold in the Yilgarn, and also host gold mineralization at several deposits (e.g. Granny Smith, Great Eastern, Lady Bountiful and Porphyry; Cassidy *et al.* 1998). They comprise up to 10% by surface area of the granites in the craton, are typically located within or marginal to greenstone belts, and are characterized by their diverse form, mineralogy and geochemistry (Champion & Sheraton 1997).

The majority of Yilgarn granites are interpreted to have a low to mid-crustal derivation (Champion & Sheraton 1997; Cassidy *et al.* 2002; Barley *et al.* 2003; Champion & Cassidy 2007). Granites

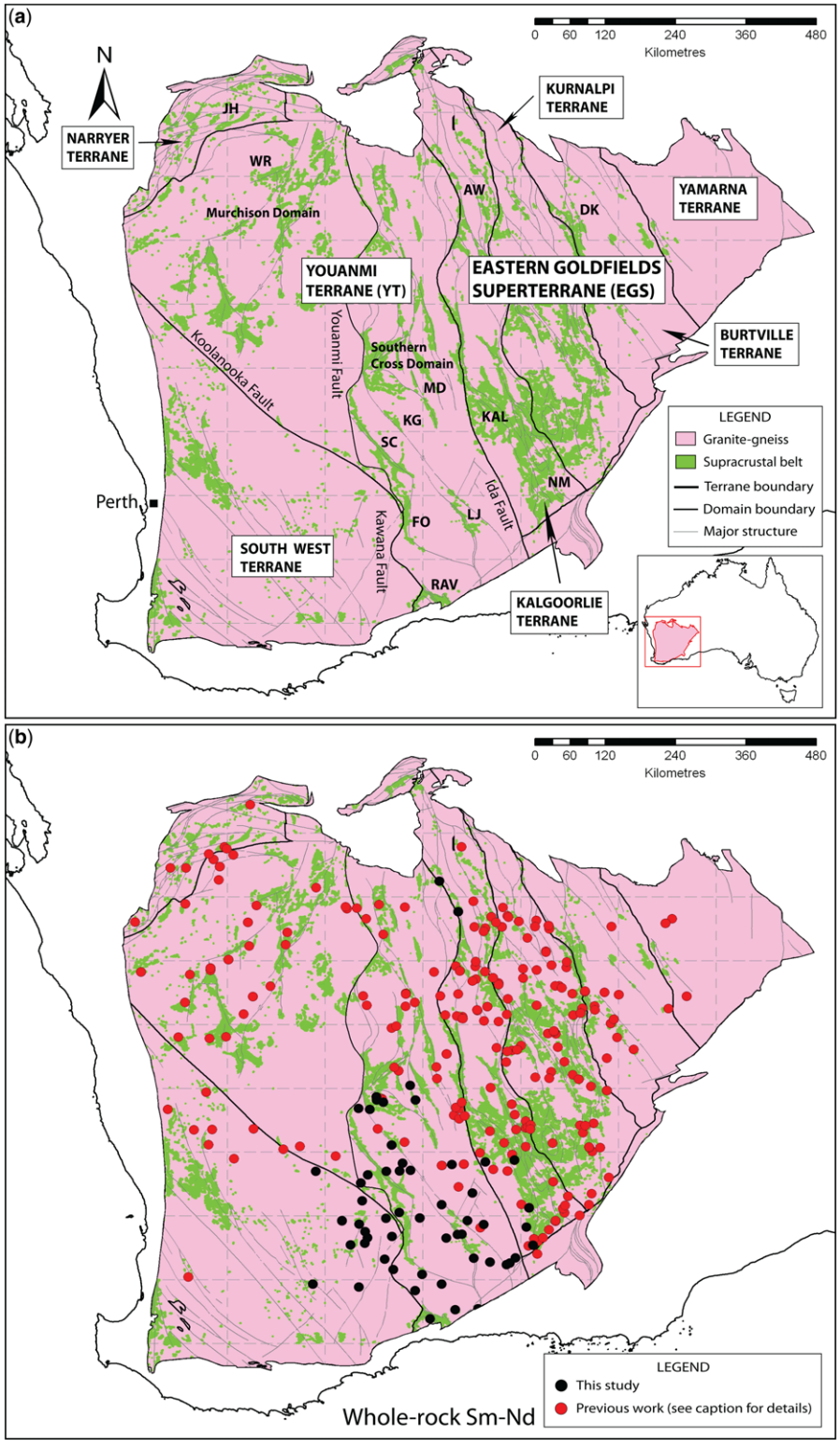

of the Low-Ca group typically have a rare-earth element (REE) pattern suggestive of a plagioclase-bearing source, while the High-Ca granites typically demonstrate a garnet-bearing source. This suggests that the High-Ca granites are from a deeper source (>35 km), while the Low-Ca granites originate from shallower crustal melting (Cassidy *et al.* 2002; Champion & Cassidy 2007; Mole 2012).

Mineral systems in the Yilgarn Craton

The Yilgarn Craton is one of the most endowed geological terranes on Earth (Fig. 3) and hosts a number of world-class orogenic gold (e.g. Golden Mile, Sons of Gwalia, Sunrise Dam) and komatiite-hosted nickel deposits (Mt Keith, Kambalda camp), as well as numerous large BIF-hosted iron deposits (Windarling, Koolyanobbing, Weld Range). These three commodities dominate the mineral systems of the craton; however, volcanic-hosted massive sulphide Cu–Zn (i.e. Golden Grove, Teutonic Bore/Jaguar), vanadium (i.e. Windimurra) and Sn–Ta deposits (i.e. Greenbushes) also occur, although not presently at camp scale.

Gold mineralization occurs in all terranes of the Yilgarn Craton (Fig. 3), with most deposits concentrated in number and resource size in the Eastern Goldfields Superterrane. Orogenic gold deposits are the most common type of gold system in the craton (Fig. 3), although there are rare exceptions such as the Boddington Cu–Au deposit (Archaean porphyry-type with an orogenic gold overprint; McCuaig *et al.* 2001; Stein *et al.* 2001). Gold deposits are hosted by a variety of rocks types, with variable structural setting, alteration and ore mineralogy (Witt & Vanderhor 1998; Duuring *et al.* 2007). However, common parameters suggest they represent a coherent group of epigenetic deposits that formed during a widespread (500 000 km^2) hydrothermal event at *c.* 2650–2630 Ma (Groves 1993; Kent & McDougall 1995; Kent *et al.* 1996; Witt & Vanderhor 1998; Robert *et al.* 2005; Duuring *et al.* 2007) during the closing stages of the late Archaean tectono-thermal evolution of the Yilgarn Craton. Gold deposits cluster in the Eastern Goldfields Superterrane as well as the north-central Murchison Domain and the central Southern Cross Domain in the Youanmi Terrane (Fig. 3). In the Eastern Goldfields Superterrane, deposits are concentrated in the Norseman–Wiluna Belt in the Kalgoorlie Terrane and the Laverton belt in the Kurnalpi Terrane, particularly along major regional structures and their subsidiary faults (e.g. Robert *et al.* 2005).

Iron deposits in the Yilgarn Craton are hosted by banded iron formation, which represents a widely distributed, but volumetrically minor, lithology in exposed greenstone belts (Gole 1981). Economic iron ore bodies are commonly the product of several superimposed early hypogene and late supergene hydrothermal alteration stages (Duuring & Hagemann 2013*a*). This study is not concerned with the supergene processes, as these are usually late, and unrelated to crustal evolution. To form hypogene BIF-hosted iron ore, BIF (*c.* 30 wt% Fe) is enriched in iron (>50% Fe) via the dissolution of primary quartz-, iron silicate- or carbonate-rich bands by fluids and the addition of iron oxides to BIF. As in gold deposits, structure plays an important role during the enrichment process, with enriched/upgraded BIF, now as iron ore, often concentrated in late shear zones (e.g. Koolyanobbing; Angerer & Hagemann 2010) and reactivated fault zones located along the margins of the BIF. The BIF sequences within the West Yilgarn are estimated at 3.0–2.8 Ga (Gole 1981; Angerer & Hagemann 2010); however, the fluids and localizing structures that upgrade BIF to iron ore are younger, possibly *c.* 2.7 Ga. Crustal architecture has the potential to control both these features. BIF-hosted iron deposits are concentrated in the central Southern Cross Domain, Murchison Domain (external to most gold occurrences) and the Narryer Terrane (within the Jack Hills metasedimentary gneiss belt).

Nickel deposits in the Yilgarn Craton are hosted by Archaean komatiites, which are characterized by extremely high eruption or emplacement temperatures (>1600 °C), high MgO (>18% MgO), turbulent magma flow and high-flux emplacement (Nisbet *et al.* 1993; Hill *et al.* 1995; Hill 2001; Barnes 2006*a*, *b*; Herzberg *et al.* 2007; Arndt *et al.* 2008). Typically, komatiite-hosted nickel deposits form through the addition of external sulphur (sediment or exhalative) to the ultramafic magma. This drives the system to sulphur saturation and the formation of an immiscible sulphide liquid, which subsequently concentrates chalcophile elements into ore-grade accumulations (Groves *et al.* 1986; Arndt *et al.* 2008).

Fig. 1. (**a**) Map of the Archaean Yilgarn Craton showing the basic granite–greenstone bedrock geology and major structures. Individual terranes/domains are labelled and taken from Cassidy *et al.* (2006) and Pawley *et al.* (2012). Important greenstone belts referred to in this study are labelled as follows: JH, Jack Hills; WR, Weld Range; MD, Marda–Diemals; SC, Southern Cross; KG, Koolyanobbing; FO, Forrestania; RAV, Ravensthorpe, LJ, Lake Johnston; AW, Agnew–Wiluna; KAL, Kalgoorlie/Kambalda; NM, Norseman and DK, Duketon. (**b**) Map showing the distribution of Sm–Nd samples throughout the Yilgarn Craton. Red points represent data collated from previous studies (see Table 2) and black points show primary data collected and analysed by this study.

Table 1. *Summary of the preserved geology of the Yilgarn Craton*

Terrane/ domain*	Age (Ma)	Supracrustal events†	Basic lithologies present‡	Komatiite events?	Age (Ma)	Granite events	Sm–Nd isotopes (T_{DM})§	Mineralization?‖	References
Yamarna Terrane	>2830	Dorothy Hills greenstone belt	Mafic volcanics Mafic intrusives Clastic sedimentary rocks	None known	*c.* 2832	Ziggy monzogranite	*c.* 3.1–2.9 Ga (very little data available)	Some small gold prospects, e.g. Dorothy Hills and Golden Sands	Pawley *et al.* (2012); Champion & Cassidy (2007); Wyche *et al.* (2012*a*, *b*)
	c. 2680	Yamarna–Mt Gill greenstone belt	Mafic volcanics Clastic sedimentary rocks Felsic volcanics Ultramafic rocks	Possibly at base of sequence? (poorly constrained at present)	*c.* 2775–2735	Ages from metagranitic and orthogneissic rocks			
					c. 2715–2705	2706 Rason gneiss 2711 Throssell orthogneiss			
					2681–2658	Widespread granitic magmatism across the NE Yilgarn			
					2650–2634	Post-tectonic, Low-Ca granites			
Burtville Terrane	2970–2910	Ulrich Range greenstone belt	Mafic volcanics Clastic sedimentary rocks Felsic volcanics BIF/chert Mafic intrusives		2970–2910	Inherited zircons from younger granites	*c.* 3.1–2.8 Ga	Ni–Cu–PGE e.g. Duketon Gold, e.g. Brightstar, McKenzie Well	Pawley *et al.* (2012); Champion & Cassidy (2007); Barley *et al.* (2003); Cassidy *et al.* (2006); Kositcin *et al.* (2008); Wyche *et al.* (2012*a*, *b*)
	c. 2810–2755	Lower Duketon and Mt Sefton greenstone belts	Clastic sedimentary rocks Undivided ultramafic rocks Mafic volcanics Mafic intrusives Felsic volcanics BIF/chert	*c.* 2.8 Ga Munro-type komatiite event hosts the Rosie and Buldge Ni–Cu–PGE prospects	2815–2800	Inherited group from Throssell orthogneiss			
	c. 2770–2720	Laverton, Irwin Hills–Stella Range and Mt Venn greenstone belts	Clastic sedimentary rocks Undivided ultramafic rocks Mafic volcanics Mafic intrusives Felsic volcanics	Possibly but poorly constrained at present	*c.* 2775–2760	Ages from metagranitic and orthogneissic rocks (e.g. Mt Sefton metagranite, Stella Range orthogneisses)			
	c. 2714–2704	Upper Duketon greenstone belt	Clastic sedimentary rocks Undivided ultramafic rocks Mafic volcanics Felsic volcanics	Possibly but poorly constrained at present	*c.* 2755	Ages from the Mapa Igneous Complex, plagiogranite and a meta-granite			
					2740–2735	Lightfoot orthogneiss Argus Igneous Complex			
					c. 2715	Granite veins in basalt of the Irwin Hills–Stella Range belt Burtville granodiorite			
					2681–2658	Widespread granitic magmatism across the NE Yilgarn			
					2650–2634	Post-tectonic, Low-Ca granites including the Wartu Monzogranite and Shay Cart monzogranite			

Kurnalpi Terrane	<2870	Dingo Range greenstone belt	Komatiites Mafic volcanics BIF	Possibly – poorly understood belt	<2750	Inherited zircons appear to be rarer than other terranes of the Eastern Goldfields	*c.* 2.9–2.8 Ga	Ni–Cu–PGE e.g. Windarra, Murrin Murrin Gold, e.g. Granny Smith	Cassidy *et al.* (2006); Swager (1997); Barley *et al.* (2003); Brown *et al.* (2001); Champion & Cassidy (2007); Wyche *et al.* (2012*a*, *b*); Kositcin *et al.* (2008)
	c. 2810	Laverton Domain greenstones (Margaret anticline)	Komatiites Mafic volcanics BIF Felsic volcaniclastics	*c.* 2.8 Ga komatiite event possibly coeval with the the Duketon event	2680–2660	High-Ca granite magmatism			
	2720–2700	Minerie greenstone belt	Mafic volcanics Calc-alkaline complexes Feldspathic sedimentary rocks Mafic intrusives	None known	2660–2630	Low-Ca granite magmatism			
	c. 2690–2680	Gindalbie Domain greenstone belts	Bimodal rhyolite–basalt and felsic calc-alkaline complexes	None known					
Kalgoorlie Terrane	*c.* 2950–2940	Norseman/ Penneshaw sequence	Basalts Felsic volcanics Sediments	None known	*c.* 3200–2700	Rare inherited zircons (i.e. Kamblada dome)	*c.* 3.1–2.85 Ga	Ni–Cu–PGE e.g. Kambalda, Mt Keith, Cosmos Gold, e.g. KCGM – superpit, Gwalia VMS, e.g. Jaguar	Kositcin *et al.* (2008); Swager (1997); Claoué-Long *et al.* (1988); Nelson (1997); Barley *et al.* (2003); Krapez *et al.* (2000); Champion & Sheraton (1997); Champion & Cassidy (2007); Wyche *et al.* (2012*a*, *b*); Krapez & Hand (2008)
	2710–2690	Kambalda Sequence	Komatiite Mafic volcanics	*c.* 2.7 Ga Munro-type komatiite event	2680–2660	High-Ca granite magmatism			
	2690–2660	Kalgoorlie Sequence	Andesite–rhyolite felsic volcanics and volcaniclastics	None known	2660–2630	Low-Ca granite magmatism			
	<2660	Synorogenic 'late-basin' siliciclastic sequences	Kurrawang and Merougil sequences consisting of multiple litho-facies	None known					
Southern Cross Domain	<3100	Basal quartzite units from the Marda, Illara and Maynard Hills greenstone belts (detrital grains up to *c.* 4400 Ma)	Quartzite metasedimentary rocks	None known	3670–3050	Rare inherited zircons from younger granites	Broadly 3.3–3.0 Ga; N.B. area south of Marda is unsampled	Ni–Cu–PGE, e.g. Spotted Quoll, Maggie Hays Gold e.g. Marvel Loch Iron, e.g. Koolyanobbing, Windarling	Wyche *et al.* (2004); Wang *et al.* (1996); Heggie *et al.* (2012*a*, *b*); Perring *et al.* (1995); Perring *et al.* (1996); Witt (1999); Chen *et al.* (2003); Thébaud & Miller (2009); Mole *et al.* (2012); Wyche *et al.* (2012*a*, *b*); this study

(*Continued*)

Table 1. *Summary of the preserved geology of the Yilgarn Craton (Continued)*

Terrane/ domain*	Age (Ma)	Supracrustal events†	Basic lithologies present‡	Komatiite events?	Age (Ma)	Granite events	Sm–Nd isotopes (T_{DM})§	Mineralization?‖	References
	3000–2900	Domain-wide event represented in the Marda, Southern Cross, Forrestania, Lake Johnston, Ravensthorpe greenstone belts and potentially more in the north of the domain	Komatiite (all belts) High-Mg and tholeiitic basalt (all belts) Felsic volcanics (Lake Johnston and Rav') BIF and chert	*c.* 2.9 Ga Barberton- and Munro-type komatiites	3050–2830	Inherited zircons from younger granites			
	c. 2800 Ma	Unclear at present, but isolated U–Pb ages from the Southern Cross, Marda and Forrestania belts suggest a younger volcano-sedimentary package	Uncertain, dated lihologies at present comprise gabbro, felsic volcanic and an intrusive felsic porphyry	Unknown	2805–2720	Inherited and magmatic zircons			
	2730	Marda Complex	Andesite–rhyolite volcanic complex	None known	2720–2600	Major events at 2700, 2680–2670, 2660, 2645 and 2635 Ma			
	<2720	Clastic sediment packages in the Marda (Diemals Formation) and Southern Cross belt	Siliciclastic packages with various facies	None known					
Murchison Domain	2960–2930	Golden Grove Group	Komatiite High-Mg to tholeiitic basalt Mafic rocks with interlayered BIF Felsic volcanics and volcaniclastics Epiclastic sediments		2950–2920	Unnamed event – Pegmatite banded gneiss – High-Ca, Mafic, High-HFSE	Domain margins are *c.* 3.2 Ma, with internal 'rift' area as young as *c.* 2.9 Ga	Vanadium, e.g. Windimurra PGEs, e.g. Gnanagooragoo Gold, e.g. Big Bell, Mt Magnet	Ivanic *et al.* (2012); Van Kranendonk & Ivanic (2008); Ivanic *et al.* (2010); Champion & Cassidy (2007); Wyche *et al.* (2012*a*, *b*); Wang *et al.* (1998); Barley *et al.* (2000); Wyman & Kerrich (2012)
	2825–2800	Norie Group	Felsic volcanics Komatiitic-basalt ± interbedded andesite–rhyolite Coarse clastic sedimentary rocks and felsic volcaniclastics	Ti-enriched, Karasjok-type Gabanintha komatiites	2815–2800	Mt Kenneth – High-Ca, Mafic, High-HFSE			

	2810–2800	Mafic–ultramafic intrusions, i.e. Windimurra, Lady Alma	Peridotite–gabbro-anorthosite cycles		2785–2735	Cullculli – Mafic, High-Ca			
	2800–2735	Polelle Group	Tholeiitic basalt Komatiitic–basalt Komatiite ± thin interflow felsic volcaniclastic rocks Andesitic volcanics and volcaniclastics	Komatiite (no detailed information)	2750–2735	Eelya – High-HFSE			
	2735–2710	Glen Group	Felsic volcanics Komatiitic-basalt ± interbedded andesite–rhyolite Coarse clastic sedimentary rocks and felsic volcaniclastics	Komatiitic basalt	2720–2690	Big Bell – High-Ca			
	2735–2710	Mafic–ultramafic intrusions i.e. Yalgowra Suite, Gnanagooragoo Igneous Complex	Thick, layered mafic–ultramafic sills – thick gabbro with basal peridotite and pyroxenite and leucogabbro-anorthosite tops		2690–2670	Tuckanarra – High-Ca			
					2665–2640	Jungar – Low-Ca, High-Ca, High-HFSE			
					2640–2610	Walganna – Low-Ca			
					2610–2600	Wogala – Low-Ca			
South West Terrane	3200–3100	Chittering, Jimperding and Balingup metamorphic/quartzite belts (detrital zircons >3730–3170 Ma)	Meta-sedimentary rocks	None known	3240–2920	Inherited zircons from younger granites	Broadly *c.* 3.5–3.0 Ga	Gold, e.g. Boddington and Griffins Find	Wyche *et al.* (2012*a*, *b*); Champion & Cassidy (2007); Allibone *et al.* (1998); Wilde *et al.* (1996); Pidgeon *et al.* (2010); Wilde & Pidgeon (1986); Pidgeon & Wilde (1990); Mole *et al.* (2012); Nemchin *et al.* (1994)
	3010	Wongan Hills greenstone belt	Mafic and felsic volcanics Chert and BIF Small ultramafic intrusions	None known	2880–2820	Mostly inherited zircons from younger granites, some magmatic			
	2715–2675	Saddleback greenstone belt	Metasedimentary rocks Felsic-intermediate volcanic and volcaniclastic rocks Mafic ± felsic volcanics and sediments	None known	2805–2720	Mostly inherited zircons from younger granites, some magmatic			
					2720–2600	Most granites occur at 2680–2660, 2650–2630 and <2620 Ma			
					c. 2640	Granulite facies metamorphism, charnokite granite formation			

(*Continued*)

Table 1. *Summary of the preserved geology of the Yilgarn Craton (Continued)*

Terrane/ domain*	Age (Ma)	Supracrustal events†	Basic lithologies present‡	Komatiite events?	Age (Ma)	Granite events	Sm–Nd isotopes (T_{DM})§	Mineralization?‖	References
Narryer Terrane	4400–3750	Age of detrital zircons in Narryer and Jack Hills metasediments	Meta-sedimentary rocks	None known	3730	Manfred Compex tonalite–granodiorite Meeberrie Gneiss	Dominantly 3.8–3.3 Ga	BIF-hosted iron prospects	Wyche *et al.* (2012*a*, *b*); Myers (1997); Nutman *et al.* (1991); Wilde *et al.* (2001); Kinny *et al.* (1988); Myers & Williams (1985); Occhipinti *et al.* (2001)
	No zircons	Metasediments – including Mindle metasedimentary rocks	Meta-sedimentary rocks	None known	3650–3620	Monzogranite Meeberrie Gneiss			
	3280–2700	Metasediments – including Narryer and Jack Hills	Meta-sedimentary rocks BIF	None known	3385	Syenogranite and monzogranite Dugel Gneiss			
					3300	Monzogranite Dugel Gneiss			
					2750–2650	Granite and gabbro sheets			
					2650–2600	Granite sheets			

*Terrane/domains after Cassidy *et al.* (2006) and Pawley *et al.* (2012).

†Broad greenstone-forming events (timing in adjacent column).

‡Broad volcanic and sedimentary lithologies present in each event.

§Broad Sm–Nd model ages (depleted mantle) primarily from Champion & Cassidy (2007) and Wyche *et al.* (2012*a*, *b*).

‖Examples of major mineral deposits or prospects within the specific terrane/domain.

Major komatiite sequences of the Yilgarn Craton are clustered into two distinct temporal and spatial groups or 'camps' (Barnes 2006*a*; Mamuse *et al.* 2010; Barnes & Fiorentini 2012). The 2.9 Ga komatiites occur in the Southern Cross Domain of the Youanmi Terrane (Fig. 3). The majority of the high MgO, channelized, cumulate-rich flows, and corresponding nickel sulphide deposits, occur in the Lake Johnston (Maggie Hays; Heggie *et al.* 2012*a*, *b*), Forrestania (Flying Fox; Perring *et al.* 1995, 1996) and Ravensthorpe (RAV-8) greenstone belts (Figs 3, 10, 11 & 13) in the Southern Cross Domain.

The 2.7 Ga komatiites form an almost continuous *c.* 700 km belt of high MgO, adcumulate-rich ultramafic lava flows and sills within the Norseman–Wiluna greenstone belt in the Eastern Goldfields Superterrane (Fig. 3). This belt represents the greatest outpouring of komatiite magma and some of the hottest melts preserved on Earth (Arndt *et al.* 2008; Barnes 2006*b*; Barnes & Fiorentini 2012). In accordance with these features, the belt hosts two world-class nickel sulphide camps (Hoatson *et al.* 2006): (1) the Agnew–Wiluna belt in the northern Kalgoorlie Terrane, hosting numerous deposits such as Mt Keith, Cliffs, Perseverance, Honeymoon Well and Cosmos (Barnes 2006*a*; Fiorentini *et al.* 2010, 2012); and (2) the Kambalda camp in the south Kalgoorlie Terrane (Gresham & Loftus-Hills 1981; Beresford *et al.* 2002) containing many relatively small, high-grade (*c.* 30–10% Ni) deposits, such as Long, Victor and Lunnon (Gresham & Loftus-Hills 1981).

Methodology

In this study, the Sm–Nd isotopic technique was used to evaluate crustal evolution through time, with age constraints based on U–Pb secondary ion mass spectrometry (SIMS; using sensitive high-resolution mass spectrometry or SHRIMP) zircon geochronology where available (some collated samples from other studies use approximate ages based on regional stratigraphy and/or cross-cutting relationships; see Table 2). Previously published Sm–Nd isotope data (259 samples: Table 2) were augmented with new data from 60 samples for this study. The isotopic data (Table 2, Fig. 1) were investigated in space and time to constrain regions of crust with a common history. The result of the new dataset is a spatially diverse, high-resolution, isotopic understanding of the Archaean crust of the Yilgarn Craton.

Sm–Nd isotope analysis

The new Sm–Nd data acquired for this study were obtained on samples that were pulverized to X-ray fluorescence (XRF) grade and subsequently analysed at two laboratories (Table 2): (1) the University of Melbourne, (Victoria, Australia); and (2) Geosciences Rennes Laboratory (Rennes, France).

At the University of Melbourne, Sm–Nd isotopic data were obtained on sample powders spiked with a $^{149}Sm-^{150}Nd$ tracer and dissolved in Krogh-type high-pressure vessels. Subsequently, Sm and Nd were extracted using EICHROM^{TM} RE- and LN-resin (Maas *et al.* 2005). Total analytical blanks were well below 100 pg and negligible compared with the amounts of sample analyte. Isotopic analyses were carried out on an NU Instruments multicollector inductively-coupled plasma mass spectrometer with sample introduction via a CETAC Aridus desolvation system. The Nd isotope ratios were measured with signals of 12–20 V total Nd and corrected for mass bias and spike impurities using an online iterative procedure involving internal normalization to $^{146}Nd/^{145}Nd = 2.0719425$ (equivalent to $^{146}Nd/^{144}Nd = 0.7219$; Vance & Thirlwall 2002) with the exponential law. Typical in-run precision for $^{143}Nd/^{144}Nd$ is ± 0.000010 (2σ). Data are reported relative to the La Jolla standard ($Nd = 0.511850$). External precision, or reproducibility, is *c.* ± 0.000020 (2σ). US Geological Survey basalt standard BCR-2 yielded average $^{147}Sm/^{144}Nd$ and $^{143}Nd/^{144}Nd$ of 0.1383 ± 0.0002 and 0.512640 ± 20, respectively (2σ, $n = 10$, analyses from 2009–2010), consistent with thermal ionisation mass spectrometry (TIMS) reference values (Raczek *et al.* 2003).

At the Geosciences Rennes Laboratory, samples were spiked with a $^{149}Sm-^{150}Nd$ mixed solution and dissolved in $HF-HNO_3$. Rare-earth elements were separated using BioRad AG $50W \times 8H + 200–400$ mesh cationic resin. Subsequently, Sm and Nd were separated and collected by passing the solution through a further set of ion exchange columns loaded with LN spec EICHROM^{TM} resin. The Sm and Nd were loaded onto double Re filaments with HNO_3 reagent and analysed in a Finnigan MAT262 multicollector mass spectrometer in static mode. In each analytical session, the unknowns were analysed together with the Ames *n*Nd−1 Nd standard, which yielded an average of 0.511965 during the course of this study. All analyses of the unknowns are adjusted to a nominal $^{143}Nd/^{144}Nd$ value of 0.511850 for the La Jolla standard. Mass fractionation was monitored and corrected using the value $^{146}Nd/^{144}Nd = 0.7219$. Procedural blanks analysed during the period of these analyses were *c.* 190 pg and are considered to be negligible compared with the total quantity of Nd in the samples.

All εNd values reported in this paper are calculated for a modern chondritic uniform (bulk silicate Earth) reservoir (CHUR) with $^{147}Sm/^{144}Nd$

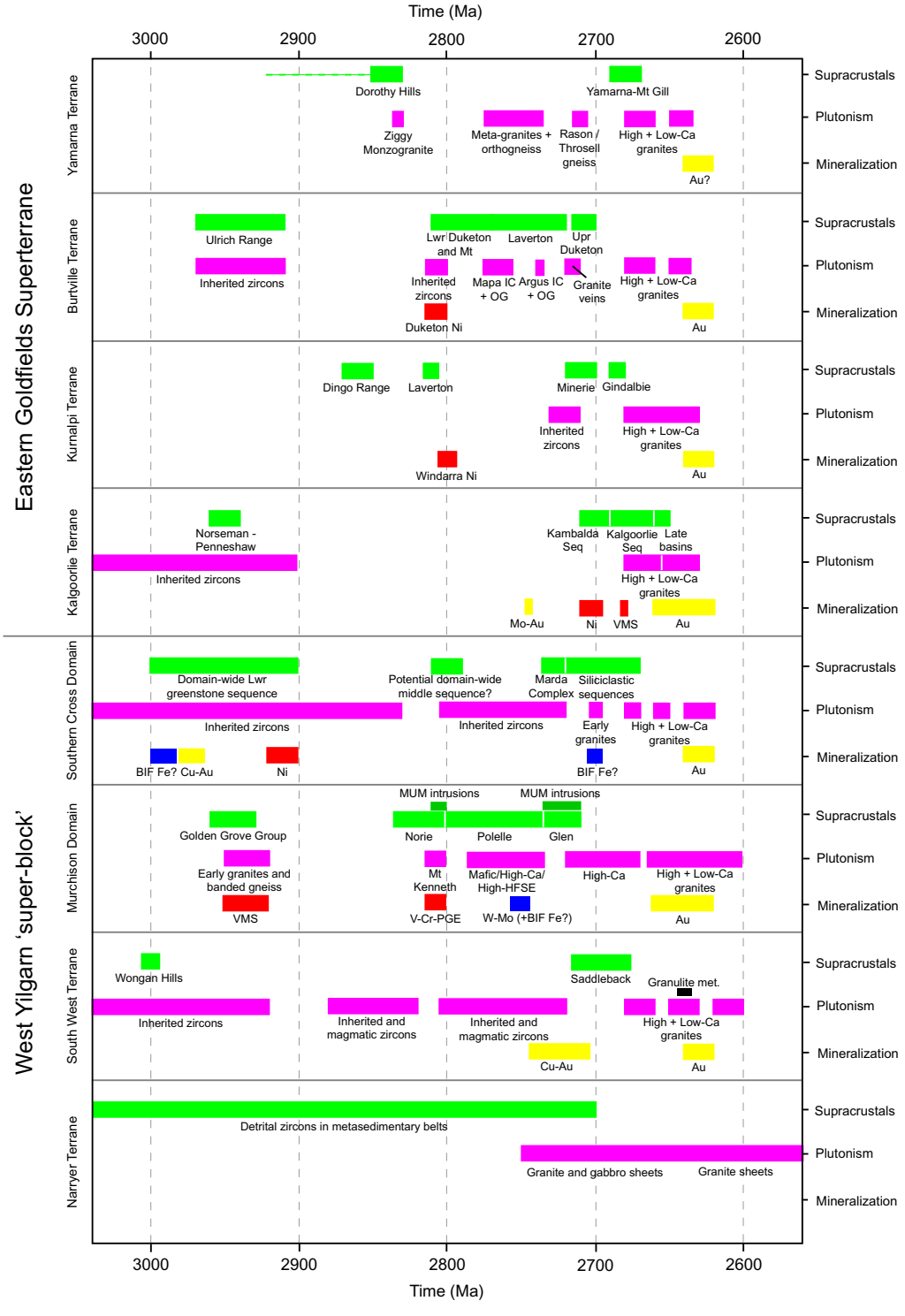

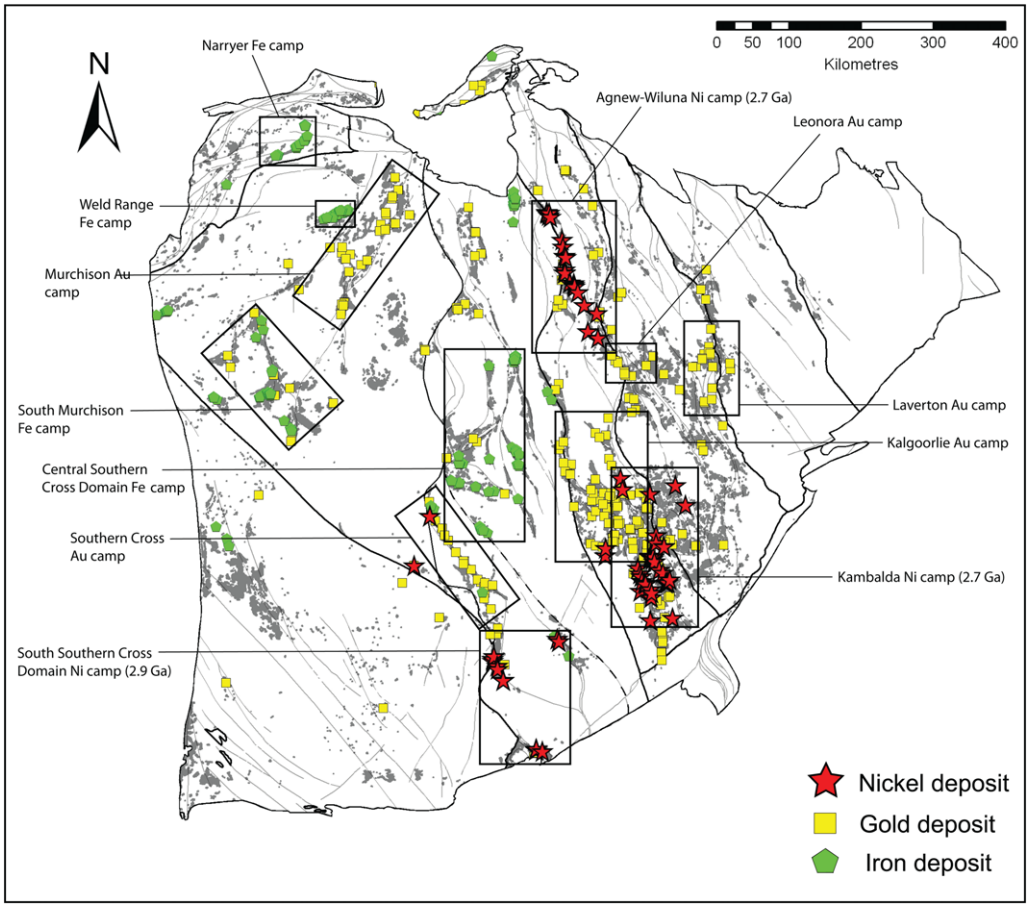

Fig. 3. Map of the Yilgarn Craton showing the locations of komatiite-hosted nickel, orogenic gold and BIF-hosted iron deposits. The location of Ni, Au and Fe camps referred to in the text are also shown.

0.1967 and $^{143}Nd/^{144}Nd_{CHUR}$ 0.512650 (Wyborn *et al.* 1988; NWA502 Chondrite). Depleted mantle model ages are two-stage model ages (T_{DM}^{2})-based on the depleted mantle model of Goldstein *et al.* (1984), with $^{147}Sm/^{144}Nd$ 0.2136, $^{143}Nd/^{144}Nd$ 0.513163 and a default average crustal $^{147}Sm/^{144}Nd_{CC}$ of 0.11 (Taylor & McLennan 1985); the ^{147}Sm decay constant is 6.54×10^{-12}/year.

Interpreting Sm–Nd data

When interpreting Nd isotopic data that are referenced to models of depleted mantle (DePaolo 1981; Goldstein *et al.* 1984) there are often multiple possibilities regarding the crust formation age (e.g. the model age in many cases could reflect a mixture; Arndt & Goldstein 1987; DePaolo *et al.* 1991). Only when initial Nd isotopic data plot

Fig. 2. Summary of geochronological events in the Yilgarn Craton for the 3000–2600 Ma period (adapted and extended after Duuring *et al.* 2007). References are documented by terrane/domain in Table 1. References for multiterrane features and events include Nelson (1995), Kent & McDougall (1995), Kent & Hagemann (1996), Schiotte & Campbell (1996), Yeats *et al.* (1996), (Nelson 1997), Krapez *et al.* (2000), Pidgeon & Hallberg (2000), Witt *et al.* (2001), Chen *et al.* (2001*a*), Chen *et al.* (2003), Van Kranendonk & Ivanic (2008), Ivanic *et al.* (2010), Pawley *et al.* (2012) and Mole (2012). The geological features/processes active at a given time are shown by different colours, where green represents supracrustal activity/formation; pink represents plutonism (mainly granitic); yellow represents gold-forming events (all types, i.e. gold only, Au–Mo etc.); red represents base-metal mineralization events (see accompanying description for specific type); and blue represents BIF-hosted iron ore mineralization.

(1) directly on depleted mantle or (2) as a well-constrained evolution line defined by a series of data points, is it possible to be certain of a singular source for that sample, and that the calculated model age is representative of crust formation. However, most Nd datasets for evolved crustal rocks do not plot near the depleted mantle evolution line (DePaolo *et al.* 1991; Taylor & McLennan 1985, 1995; Fletcher *et al.* 1994). The possible significance of such data is explored in schematic form in Figure 4.

In Figure 4a, a granite sample (green square) has a geological age T_2 with associated εNd well below the depleted mantle curve. This can be explained if the granitic magma is derived from older, felsic, light REE-enriched (low-Sm/Nd) crust. Extrapolation from the sample data-point to the depleted mantle curve using an average crustal Sm/Nd ratio will then yield an age T_1, the Nd model age or 'crustal extraction' age (T_{DM}^2). The situation in Figure 4a is complicated if the magma source of the sample is a mixed source, or if a mafic magma with juvenile εNd assimilates older, low-εNd crust to form a granitic body (Fig. 4b). As a result, the εNd and model age of the sample are not representative of the new crust (depleted mantle) or the old crust, but represent a mixture between the two sources. However, complete mixing very rarely occurs, and as a result, when multiple analyses are performed from an area, arrays of data (Fig. 4b) will often link the original sources involved with the final, mixed source (Arndt & Goldstein 1987; DePaolo *et al.* 1991). This is important as it allows the estimation of the age and character of the mixing components.

Results

To complement the existing Sm–Nd dataset, this study collected 36 field samples, together with 10 samples from the Geological Survey of Western Australia and 14 from the PhD study of Qiu (1997), for a targeted Nd isotope programme across the SW-central Yilgarn Craton. Previously published Sm–Nd data from 259 samples (Fletcher & Rosman 1982; McCulloch *et al.* 1983; McCulloch 1987; Watkins *et al.* 1991; Nutman *et al.* 1993; Fletcher *et al.* 1994; Champion & Sheraton 1997; Cassidy *et al.* 2002) were collated, resulting in a craton-wide database of 319 Sm–Nd analyses of granites and felsic volcanic rocks (see Table 2). Using this information, it is possible to investigate the spatial variation in lithospheric architecture of the Yilgarn Craton. First, the Nd isotopic data are examined through time (Figs 5–9) to establish the source character and age of the Yilgarn crust. These data are then plotted as maps (Figs 10–11) to understand the spatial distribution of those features. Data are presented as two-stage model ages (T_{DM}^2; Liew & Hofmann 1988) and εNd values. The T_{DM}^2 is preferred over depleted mantle model ages as this method uses the Sm/Nd ratio of the continental crust (0.11) rather than that of the sample. This produces more realistic model ages regarding crustal rocks.

Temporal analysis of Sm–Nd isotope data

Eastern Goldfields Superterrane: Yamarna Terrane. The Yamarna Terrane (Figs 5a, b & 8a; Pawley *et al.* 2012) is under-sampled relative to the other terranes of the Yilgarn Craton primarily because it is mostly covered by the sedimentary rocks of the Neoproterozoic Officer and Palaeozoic Gunbarrel Basins (Grey *et al.* 2005). Five samples from the western part of this terrane (Table 2, Fig. 1b) have U–Pb ages between 2711 and 2645 Ma. These samples have fairly homogenous εNd values ranging from 0.7 to 1.4 (Fig. 5a) and T_{DM}^2 of 2970–2860 Ma, peaking at *c.* 2900 Ma (Fig. 5a), indicating a relatively homogenous crustal magma source (Fig. 8a).

Eastern Goldfields Superterrane: Burtville Terrane. The Burtville Terrane is represented by 19 samples with U–Pb ages ranging from 2940 to 2638 Ma. The εNd (−1.2 to 2.2, Fig. 5c) and T_{DM}^2 (3130–2830 Ma, peak at *c.* 2900 Ma, Fig. 5d) data display some heterogeneity as illustrated by the εNd distribution (Fig. 5c).

Samples from this terrane, particularly those with U–Pb ages from 2681 to 2638 Ma, show a range of Nd isotope compositions that form an array between T_{DM}^2 ages of *c.* 3100 and 2850 Ma. Three samples with U–Pb ages of *c.* 2670, 2715 and 2940 Ma have T_{DM}^2 ages close to *c.* 3100 Ma, confirming the presence of older crust. This Nd data array suggests a heterogeneous crustal source for the Burtville Terrane (Fig. 8b).

Eastern Goldfields Superterrane: Kurnalpi Terrane. The Kurnalpi Terrane (Fig. 8c) is represented by 64 samples with U–Pb ages in a narrow range from 2714 to 2632 Ma. The T_{DM}^2 ages show a *c.* 500 myr range (3230–2710 Ma, peaking at *c.* 2900 Ma) and the probability density curve (Fig. 5f) tapers towards older T_{DM}^2 values. The εNd values mirror these observations, ranging from −3.2 to 3.6, peaking at 1.6 and tapering towards negative values (Fig. 5e), suggesting that this terrane, while dominated by a juvenile crustal component, also contains some older, reworked material with T_{DM}^2 ages of *c.* 3200–3100 Ma.

The U–Pb geochronology histogram for this terrane (Fig. 8c) displays four overlapping felsic magmatic events. The first, at 2715–2700 Ma, has

a juvenile source, with T_{DM}^2 of *c.* 2850 Ma and εNd of *c.* 2.0. At 2680–2670 Ma, the Nd isotopes demonstrate a more evolved signature with T_{DM}^2 ranging from *c.* 3200 to 2800 Ma and εNd values from *c.* −3.2 to 1.8. The third event at *c.* 2666–2660 Ma displays T_{DM}^2 of *c.* 2900 Ma and εNd of 1.0–2.0 (two points have $T_{DM}^2 < 2800$ Ma and εNd > 2.0), indicating an increase in radiogenic component and/or reduced interaction with an older crustal reservoir. The final 2650–2640 Ma event appears to represent reworking of this source. Hence, this terrane displays evidence for potentially three sources, a dominant *c.* 2900–2850 Ma source with εNd 1.6, an older, relatively minor *c.* 3200 Ma source with εNd of *c.* −3.0, and a highly juvenile source with T_{DM}^2 2800–2700 Ma and εNd of *c.* 2.0–4.0.

Eastern Goldfields Superterrane: Kalgoorlie Terrane. Seventy-seven samples with U–Pb ages ranging from 2801 to 2620 Ma are available for the Kalgoorlie Terrane (Fig. 1b & 8d). The T_{DM}^2 values for this terrane range from *c.* 3300 to 2700 Ma, peaking at *c.* 2900 Ma (Fig. 5h), with εNd values from −4.2 to 3.6, peaking at 1.1 (Fig. 5g). As in the Kurnalpi Terrane, the T_{DM}^2 and εNd probability density curves taper towards older and more reworked values, respectively (Fig. 5g), suggesting a dominantly juvenile crust with a minor reworked component.

The >2700 Ma samples (2760, 2800, 2801 Ma), which form a minor component of the dataset, have a T_{DM}^2 of *c.* 3000 Ma and fairly consistent εNd of 0.8–1.7. For samples with U–Pb ages <2700 Ma, four main felsic magmatic events can be defined (Fig. 8d). The 2685–2680 Ma group displays a heterogeneous source with T_{DM}^2 and εNd values defining an array from *c.* 3300 to 2900 Ma and from −3.5 to 1.7, respectively. The 2670–2660 Ma group displays significantly less reworking, and a more substantial juvenile component, with T_{DM}^2 and εNd clustered at *c.* 2900 Ma and 1.0, respectively. In addition, four samples have more juvenile T_{DM}^2 and εNd at 2800–2700 Ma and 2.6–3.4, respectively. The 2655–2650 Ma group shows a similarly heterogeneous crustal source to that of the 2685–2680 Ma group, with T_{DM}^2 values *c.* 3300–2900 Ma and εNd of −4.2 to 2.1. The youngest event at *c.* 2635–2620 Ma has a similar source to the 2685–2680 and 2655–2650 Ma events, showing T_{DM}^2 values of *c.* 3200–2850 Ma and εNd of −3.9 to 1.3.

Youanmi Terrane: Southern Cross Domain. Samarium–Nd data are available for 72 samples from the Southern Cross Domain, with U–Pb ages ranging from 2983 to 2615 Ma (Fig. 8e). The T_{DM}^2 ages from this domain range from *c.* 3500 to 2750 Ma, peaking at 3100 Ma, with εNd values between −6.9 and 3.9, peaking at −2.0 (Fig. 6a, b). This distribution indicates that, while old, reworked crust dominates this domain, a minor juvenile component is also present (Fig. 8e).

A small number of samples have U–Pb ages >2750 Ma; the 2983 Ma sample has a T_{DM}^2 of 3150 Ma (εNd of 1.8), while the 2813 Ma sample has a T_{DM}^2 of 2810 Ma (εNd of 3.9), suggesting that relatively juvenile crust was present at 2983 Ma, with the addition of mantle-derived material at *c.* 2810 Ma. Most samples younger than 2750 Ma fall into two groups with T_{DM}^2 ages of *c.* 3300 and 3100 Ma, with a lesser number overlapping with T_{DM}^2 ages *c.* 3200 Ma. Two samples with T_{DM}^2 *c.* 3500 Ma (εNd of −6.5) indicate the presence of a minor, older component (Palaeoarchaean crust) (Fig. 8e).

The Southern Cross Domain displays four distinct but overlapping felsic magmatic events younger than 2750 Ma (Fig. 8e). The first event, at 2750–2700 Ma, shows a heterogeneous crustal source with T_{DM}^2 ages of 3300–3000 Ma. The second, at 2690–2680 Ma, consists of crustal sources with T_{DM}^2 ages of 3300 (εNd −4.5 to −3.5) and 3100 Ma (εNd −0.9 to −0.5). The *c.* 2665–2650 Ma group consists of two very similar subgroups: (1) a dominant subgroup at T_{DM}^2 3100 Ma and εNd −2.0 to −1.0; and (2) a relatively minor subgroup at T_{DM}^2 3300 Ma and εNd *c.* −4.5. The final *c.* 2640–2630 Ma event dominantly displays a heterogeneous crustal source with T_{DM}^2 ages of 3300–2900 Ma (εNd −4.2 to 0.5), and a more continuous Nd 'array' than the previous two events.

Youanmi Terrane: Murchison Domain. Thirty-six samples with U–Pb ages ranging from 2950 to 2602 Ma are available from the Murchison Domain. The T_{DM}^2 values from this domain range from *c.* 3660 to 2950 Ma (peak at *c.* 3200 Ma), with εNd values between −7.2 and 2.9, peaking at −3.2 (subordinate peaks at −1.3 and 0.5; Fig. 6c). The wide range of the T_{DM}^2 and εNd probability density curves (Fig. 6c, d) demonstrates the heterogeneous nature of crustal sources in this domain.

Samples with U–Pb ages >2750 Ma demonstrate a wide range of source compositions, from a reworked source at *c.* 2950 Ma (T_{DM}^2 values of *c.* 3700–3300 Ma, εNd −5.9 to −0.9) to a juvenile source at *c.* 2920 Ma (T_{DM}^2 values of *c.* 3010–2980 Ma, εNd 1.7 and 2.9). After 2750 Ma, three broad, overlapping T_{DM}^2 groups occur at *c.* 3400–3300, 3200 and 3000 Ma (Fig. 8f).

The Murchison Domain displays three well-defined felsic magmatic events younger than 2760 Ma (Fig. 8f). The first, at *c.* 2760–2740 Ma, consists of the three main T_{DM}^2 groups at *c.* 3300, 3200–3100 and 3000 Ma, with corresponding εNd values of *c.* −4.4 to −3.7, −1.6 to −1.0 and

Table 2. *Sm–Nd data used in this study from the Yilgarn Craton, including new and collated data (sorted by terrane/domain)*

Sample ID	Data source	Longitude[1]	Latitude[1]	Terrane[2]	Domain[2]	LITH CODE[3]	Age, t (Ma)[4]	2σ Error (Ma)
98967051	Champion (2013)	123.8228	−27.3387	EGST	Yamarna	G	2645	3
98967052A	Champion (2013)	123.7221	−27.4103	EGST	Yamarna	G	2652	3
98967050A	Champion (2013)	124.0464	−28.5536	EGST	Yamarna	G	2672	12
98967050B	Champion (2013)	124.0464	−28.5536	EGST	Yamarna	G	2711	
98967052B	Champion (2013)	123.7221	−27.4103	EGST	Yamarna	G	2711	6
2001969019B	Champion (2013)	122.9297	−28.9127	EGST	Burtville	G	2638	2
99967004	Champion (2013)	123.2349	−29.3889	EGST	Burtville	G	2640	
99967018	Champion (2013)	122.8214	−29.5233	EGST	Burtville	G	2640	
2001967053B	Champion (2013)	122.8837	−28.9821	EGST	Burtville	G	2640	
92969124	Champion & Sheraton (1997)	122.4898	−28.4758	EGST	Burtville	G	2645	
96969046	AMIRA P482	121.9297	−27.4455	EGST	Burtville	G	2647	3
93969049	Champion & Sheraton (1997)	122.8918	−27.4611	EGST	Burtville	G	2650	
99967009	Champion (2013)	122.9825	−29.1977	EGST	Burtville	G	2650	
2001967039	Champion (2013)	122.6338	−28.7064	EGST	Burtville	G	2657	4
93969030C	Champion & Sheraton (1997)	123.0050	−28.5289	EGST	Burtville	G	2660	
92963431	Champion & Sheraton (1997)	122.4853	−28.4809	EGST	Burtville	G	2665	
2001967053A	Champion (2013)	122.8837	−28.9821	EGST	Burtville	G	2667	
2001969019A	Champion (2013)	122.9297	−28.9127	EGST	Burtville	G	2668	4
96969080A	AMIRA P482	122.7887	−28.4928	EGST	Burtville	G	2671	2
40597A	Fletcher *et al.* (1994)	123.7695	−28.7473	EGST	Burtville	G	2681	4
40597F	Fletcher *et al.* (1994)	123.7695	−28.7473	EGST	Burtville	G	2681	4
2001969033A	Champion (2013)	122.6406	−28.7680	EGST	Burtville	G	2716	3
96969055	Champion (2013)	121.9384	−27.4984	EGST	Burtville	G	2755	4
2001969122	Champion (2013)	121.9530	−27.4147	EGST	Burtville	G	2940	
2001969001	Champion (2013)	121.9876	−30.8542	EGST	Kurnalpi	G	2632	4
71–742	McCulloch (1987)	122.5500	−30.9189	EGST	Kurnalpi	G	2638	
2001969039	Champion (2013)	121.7281	−29.8266	EGST	Kurnalpi	G	2640	
59047	Fletcher *et al.* (1994)	121.2125	−27.4695	EGST	Kurnalpi	G	2645	
92969111	Champion & Sheraton (1997)	122.2009	−28.1035	EGST	Kurnalpi	G	2645	
92969115	Champion & Sheraton (1997)	121.9727	−28.0678	EGST	Kurnalpi	G	2645	
2001969103	Champion (2013)	121.2265	−27.1603	EGST	Kurnalpi	G	2645	
2001969108	Champion (2013)	121.3007	−27.2960	EGST	Kurnalpi	G	2645	
2001969113	Champion (2013)	121.7432	−27.3665	EGST	Kurnalpi	G	2645	
59046A	Fletcher *et al.* (1994)	121.2125	−27.4695	EGST	Kurnalpi	G	2645	
59046C	Fletcher *et al.* (1994)	121.2125	−27.4695	EGST	Kurnalpi	G	2645	
2001967045	Champion (2013)	121.2804	−29.5870	EGST	Kurnalpi	G	2649	7
92969022	Champion & Sheraton (1997)	121.2947	−29.4185	EGST	Kurnalpi	G	2650	
115559	Champion (2013)	122.5535	−30.9274	EGST	Kurnalpi	G	2650	
115587	Champion (2013)	122.4556	−30.6932	EGST	Kurnalpi	G	2650	
92969091	Champion & Sheraton (1997)	121.7455	−28.1431	EGST	Kurnalpi	G	2650	
94969608	Champion (2013)	121.3153	−27.3147	EGST	Kurnalpi	G	2650	
2001969058	Champion (2013)	122.1310	−28.4208	EGST	Kurnalpi	G	2650	
40591A	Fletcher *et al.* (1994)	121.8875	−27.8473	EGST	Kurnalpi	G	2650	
40592A	Fletcher *et al.* (1994)	121.8875	−27.8639	EGST	Kurnalpi	G	2650	
99967174A	AMIRA P482	122.3068	−28.8516	EGST	Kurnalpi	G	2657	25
99967176	AMIRA P482	122.3084	−28.8514	EGST	Kurnalpi	G	2657	25
98969003	AMIRA P482	122.8525	−31.3935	EGST	Kurnalpi	G	2659	11
97967150	AMIRA P482	122.5497	−31.8185	EGST	Kurnalpi	G	2660	25
97967152	AMIRA P482	122.5907	−31.6502	EGST	Kurnalpi	G	2660	25
92969087	Champion & Sheraton (1997)	121.5397	−28.1218	EGST	Kurnalpi	G	2660	
96969087	AMIRA P482	121.9173	−29.1369	EGST	Kurnalpi	G	2660	5
98967008	AMIRA P482	122.5998	−30.9864	EGST	Kurnalpi	G	2660	5
2001969007	Champion (2013)	121.7436	−28.6988	EGST	Kurnalpi	G	2660	
92969105	Champion & Sheraton (1997)	122.0925	−28.3939	EGST	Kurnalpi	G	2660	
115571	Champion (2013)	122.7204	−30.9270	EGST	Kurnalpi	G	2665	
94969580	Champion & Sheraton (1997)	122.4480	−28.7443	EGST	Kurnalpi	G	2665	

Sm (ppm)	Nd (ppm)	$^{147}Sm/^{144}Nd$	$^{143}Nd/^{144}Nd_m$[5]	2σ Error (10^{-6})	$^{143}Nd/^{144}Nd_i$[6]	$^{143}Nd/^{144}Nd_{CHUR}$[7]	$^{143}Nd/^{144}Nd_{DM}$[8]	εNd[15]	T_{DM} (Ga)[9]	$T_{DM}{}^2$ (Ga)[10]	Error (5%SE)[11]
3.34	21.01	0.0962	0.510941		0.509262	0.509218	0.509436	0.87	2.87	2.90	0.15
6.48	64.32	0.0609	0.510347		0.509282	0.509209	0.509426	1.44	2.79	2.86	0.14
1.91	12.02	0.0962	0.510892		0.509196	0.509182	0.509398	0.26	2.93	2.97	0.15
1.27	8.07	0.0948	0.510901		0.509205	0.509131	0.509342	1.44	2.88	2.91	0.15
0.81	7.02	0.0696	0.510414		0.509169	0.509131	0.509342	0.73	2.89	2.97	0.15
11.200	94.340	0.0718	0.510469		0.509219	0.509227	0.509446	−0.15	2.88	2.97	0.15
9.820	83.420	0.0712	0.510519		0.509279	0.509224	0.509443	1.07	2.81	2.88	0.14
6.330	58.700	0.0652	0.510383		0.509247	0.509224	0.509443	0.45	2.84	2.93	0.15
3.410	29.450	0.0701	0.510438		0.509217	0.509224	0.509443	−0.14	2.88	2.97	0.15
3.810	31.740	0.0725	0.510501	9	0.509235	0.509218	0.509436	0.34	2.86	2.94	0.15
4.420	33.600	0.0794	0.510674	16	0.509288	0.509215	0.509433	1.42	2.81	2.86	0.14
6.543	37.187	0.1064	0.511165	9	0.509306	0.509211	0.509429	1.85	2.82	2.83	0.14
5.790	44.740	0.0783	0.510647		0.509278	0.509211	0.509429	1.31	2.82	2.87	0.14
3.340	26.560	0.0761	0.510540		0.509206	0.509202	0.509419	0.08	2.89	2.97	0.15
5.829	41.723	0.0844	0.510770	11	0.509288	0.509198	0.509415	1.77	2.81	2.85	0.14
15.413	113.281	0.0822	0.510722	12	0.509276	0.509192	0.509408	1.66	2.82	2.86	0.14
2.000	12.840	0.0941	0.510782		0.509126	0.509189	0.509405	−1.23	3.02	3.08	0.15
3.610	27.040	0.0807	0.510660		0.509240	0.509188	0.509403	1.02	2.85	2.91	0.15
3.220	19.600	0.0995	0.510924	17	0.509171	0.509184	0.509399	−0.26	2.97	3.01	0.15
5.500	40.000	0.0829	0.510685	25	0.509219	0.509171	0.509385	0.94	2.87	2.93	0.15
1.800	5.500	0.2009	0.512818	25	0.509264	0.509171	0.509385	1.84	4.10	2.86	0.14
3.770	21.560	0.1057	0.510997		0.509103	0.509125	0.509335	−0.44	3.04	3.06	0.15
13.420	45.350	0.1789	0.512437	0	0.509184	0.509074	0.509280	2.17	3.17	2.90	0.14
1.300	7.810	0.1004	0.510835		0.508886	0.508831	0.509016	1.07	3.11	3.13	0.16
4.080	25.480	0.0969	0.510926		0.509244	0.509235	0.509454	0.17	2.90	2.94	0.15
1.600	9.400	0.1013	0.511041	20	0.509278	0.509227	0.509446	1.01	2.86	2.88	0.14
2.640	13.030	0.1224	0.511386		0.509254	0.509224	0.509443	0.59	2.95	2.92	0.15
13.400	82.000	0.0992	0.511036	25	0.509305	0.509218	0.509436	1.71	2.82	2.84	0.14
4.485	33.450	0.0810	0.510666	11	0.509252	0.509218	0.509436	0.67	2.85	2.92	0.15
6.499	40.451	0.0971	0.510975	10	0.509281	0.509218	0.509436	1.23	2.85	2.87	0.14
10.960	69.950	0.0948	0.510990		0.509336	0.509218	0.509436	2.32	2.77	2.79	0.14
6.540	55.550	0.0711	0.510519		0.509278	0.509218	0.509436	1.19	2.81	2.88	0.14
4.240	31.300	0.0819	0.510708		0.509279	0.509218	0.509436	1.20	2.82	2.88	0.14
3.800	27.000	0.0858	0.510822	25	0.509325	0.509218	0.509436	2.10	2.78	2.81	0.14
12.600	95.000	0.0807	0.510702	25	0.509294	0.509218	0.509436	1.49	2.81	2.85	0.14
5.620	43.030	0.0790	0.510616		0.509235	0.509213	0.509430	0.45	2.87	2.94	0.15
5.809	26.309	0.1335	0.511458	10	0.509125	0.509211	0.509429	−1.70	3.22	3.10	0.15
1.640	10.570	0.0940	0.510896		0.509253	0.509211	0.509429	0.81	2.87	2.91	0.15
4.190	23.750	0.1066	0.511151		0.509287	0.509211	0.509429	1.49	2.85	2.86	0.14
8.480	70.059	0.0732	0.510548	12	0.509269	0.509211	0.509429	1.14	2.82	2.89	0.14
6.790	49.900	0.0823	0.510718	20	0.509279	0.509211	0.509429	1.33	2.82	2.87	0.14
4.350	30.940	0.0849	0.510774		0.509290	0.509211	0.509429	1.54	2.81	2.86	0.14
12.800	109.000	0.0708	0.510493	25	0.509255	0.509211	0.509429	0.86	2.83	2.91	0.15
14.100	117.000	0.0727	0.510497	25	0.509226	0.509211	0.509429	0.29	2.87	2.95	0.15
19.860	138.000	0.0870	0.510825	19	0.509300	0.509202	0.509419	1.92	2.80	2.83	0.14
85.180	574.300	0.0896	0.510838	19	0.509267	0.509202	0.509419	1.28	2.84	2.88	0.14
1.870	11.800	0.0956	0.510884	11	0.509207	0.509199	0.509416	0.15	2.92	2.97	0.15
6.200	35.300	0.1062	0.511137	10	0.509273	0.509198	0.509415	1.48	2.86	2.87	0.14
4.430	26.500	0.1010	0.511048	10	0.509276	0.509198	0.509415	1.52	2.85	2.87	0.14
1.613	9.643	0.1011	0.511080	7	0.509306	0.509198	0.509415	2.12	2.81	2.82	0.14
3.340	22.500	0.0899	0.510836	19	0.509258	0.509198	0.509415	1.18	2.85	2.89	0.14
7.700	49.200	0.0946	0.510912	18	0.509252	0.509198	0.509415	1.05	2.87	2.90	0.14
4.580	31.130	0.0889	0.510823	0	0.509263	0.509198	0.509415	1.27	2.84	2.88	0.14
0.769	4.737	0.0982	0.510893	8	0.509170	0.509198	0.509415	−0.55	2.98	3.02	0.15
5.540	41.320	0.0810	0.510666		0.509242	0.509192	0.509408	0.99	2.85	2.91	0.15
2.738	16.980	0.0974	0.510957	8	0.509244	0.509192	0.509408	1.03	2.88	2.91	0.15

(*Continued*)

Table 2. *Sm–Nd data used in this study from the Yilgarn Craton, including new and collated data (sorted by terrane/domain) (Continued)*

Sample ID	Data source	Longitude[1]	Latitude[1]	Terrane[2]	Domain[2]	LITH CODE[3]	Age, t (Ma)[4]	2σ Error (Ma)
94969584B	Champion & Sheraton (1997)	122.4220	−28.8166	EGST	Kurnalpi	G	2665	
115542	Champion (2013)	122.5811	−29.9682	EGST	Kurnalpi	G	2665	
115552	Champion (2013)	122.4112	−30.5745	EGST	Kurnalpi	G	2665	
115595	Champion (2013)	122.6181	−30.5475	EGST	Kurnalpi	G	2665	
2000969006	Champion (2013)	122.0695	−29.3524	EGST	Kurnalpi	G	2665	5
2001969005	Champion (2013)	122.4914	−30.5840	EGST	Kurnalpi	G	2665	
Maas-1	Champion (2013)	122.3014	−29.7820	EGST	Kurnalpi	G	2665	
93969021	Champion & Sheraton (1997)	121.6034	−27.6400	EGST	Kurnalpi	G	2665	
96969044	AMIRA P482	121.4729	−27.3830	EGST	Kurnalpi	G	2665	3
92969113A	Champion & Sheraton (1997)	122.2073	−28.0164	EGST	Kurnalpi	G	2670	
2001969035	Champion (2013)	121.9403	−29.8383	EGST	Kurnalpi	G	2671	4
77–53	McCulloch *et al.* (1983)	122.8241	−30.0338	EGST	Kurnalpi	G	2675	
77–54	McCulloch *et al.* (1983)	122.8241	−30.0338	EGST	Kurnalpi	G	2675	
77–55	McCulloch *et al.* (1983)	122.8241	−30.0338	EGST	Kurnalpi	G	2675	
101381	Champion (2013)	121.9673	−29.7393	EGST	Kurnalpi	G	2675	
92969004	Champion & Sheraton (1997)	121.3690	−29.4025	EGST	Kurnalpi	G	2680	
92969015	Champion & Sheraton (1997)	121.5096	−29.3281	EGST	Kurnalpi	G	2680	
92969084	Champion & Sheraton (1997)	121.3060	−28.5930	EGST	Kurnalpi	G	2680	
92969101	Champion & Sheraton (1997)	121.5369	−28.2705	EGST	Kurnalpi	G	2680	
99967170A	AMIRA P482	121.1627	−28.3486	EGST	Kurnalpi	G	2680	50
92969104B	Champion & Sheraton (1997)	122.0303	−28.3935	EGST	Kurnalpi	G	2680	
92969122	Champion & Sheraton (1997)	122.2963	−28.5128	EGST	Kurnalpi	G	2680	
96969076	Champion (2013)	121.0779	−28.2641	EGST	Kurnalpi	G	2686	7
92969016B	Champion & Sheraton (1997)	121.4442	−29.3925	EGST	Kurnalpi	G	2690	
99969014A	Champion (2013)	121.1632	−28.3742	EGST	Kurnalpi	G	2693	3
99969014B	Champion (2013)	121.1632	−28.3742	EGST	Kurnalpi	G	2693	3
2000969004	Champion (2013)	122.0097	−29.0956	EGST	Kurnalpi	G	2703	4
92967064	Champion & Sheraton (1997)	122.0389	−29.1459	EGST	Kurnalpi	G	2704	
2000969003	Champion (2013)	122.0163	−29.1097	EGST	Kurnalpi	G	2704	5
96969022	Champion (2013)	122.1749	−29.5832	EGST	Kurnalpi	G	2710	6
2001969111B	Champion (2013)	121.7213	−27.4632	EGST	Kurnalpi	G	2711	3
96969019	Champion (2013)	122.3889	−29.8541	EGST	Kurnalpi	G	2714	
97969209	AMIRA P482	121.7648	−32.3947	EGST	Kalgoorlie	G	2620	25
ARC69[14]	This study	120.96	−31.15	EGST	Kalgoorlie		2621	4
97969201	AMIRA P482	121.7579	−32.5938	EGST	Kalgoorlie	G	2623	7
97969237	AMIRA P482	121.8439	−32.3417	EGST	Kalgoorlie	G	2625	25
97967153	AMIRA P482	122.2266	−31.6898	EGST	Kalgoorlie	G	2630	25
98967116D	Champion (2013)	121.5115	−31.8145	EGST	Kalgoorlie	G	2630	
97969044	AMIRA P482	121.2473	−30.8504	EGST	Kalgoorlie	G	2640	25
97969245	AMIRA P482	122.1718	−31.9468	EGST	Kalgoorlie	G	2640	25
94962355	Champion (2013)	120.7763	−27.0682	EGST	Kalgoorlie	G	2645	
92969080A	Champion & Sheraton (1997)	120.7598	−28.3183	EGST	Kalgoorlie	G	2648	
2001969044	Champion (2013)	120.5220	−28.8652	EGST	Kalgoorlie	G	2648	3
97969256B	AMIRA P482	122.4076	−31.9867	EGST	Kalgoorlie	G	2650	25
92969052	Champion & Sheraton (1997)	120.9369	−28.9409	EGST	Kalgoorlie	G	2650	
92969054	Champion & Sheraton (1997)	120.3441	−28.8512	EGST	Kalgoorlie	G	2650	
92969071	Champion & Sheraton (1997)	120.8104	−28.0095	EGST	Kalgoorlie	G	2650	
97969248	AMIRA P482	122.1482	−31.8844	EGST	Kalgoorlie	G	2650	9
98969144	Champion (2013)	120.8756	−31.0103	EGST	Kalgoorlie	G	2650	
71–736	McCulloch (1987)	121.3681	−31.0320	EGST	Kalgoorlie	G	2650	

Sm (ppm)	Nd (ppm)	$^{147}Sm/^{144}Nd$	$^{143}Nd/^{144}Nd_m$[5]	2σ Error (10^{-6})	$^{143}Nd/^{144}Nd_i$[6]	$^{143}Nd/^{144}Nd_{CHUR}$[7]	$^{143}Nd/^{144}Nd_{DM}$[8]	εNd[15]	T_{DM} (Ga)[9]	$T_{DM}{}^{2}$ (Ga)[10]	Error (5%SE)[11]
4.571	30.423	0.0908	0.510868	9	0.509271	0.509192	0.509408	1.57	2.83	2.87	0.14
6.050	39.780	0.0919	0.510914		0.509298	0.509192	0.509408	2.09	2.80	2.83	0.14
4.870	26.560	0.1109	0.511249		0.509299	0.509192	0.509408	2.11	2.82	2.82	0.14
4.180	22.890	0.1104	0.511158		0.509217	0.509192	0.509408	0.50	2.94	2.95	0.15
2.430	10.640	0.1380	0.511768	0	0.509342	0.509192	0.509408	2.95	2.80	2.76	0.14
4.080	23.920	0.1031	0.511187		0.509374	0.509192	0.509408	3.59	2.71	2.71	0.14
8.570	54.110	0.0958	0.510945	0	0.509261	0.509192	0.509408	1.35	2.85	2.88	0.14
3.267	20.470	0.0965	0.510957	9	0.509261	0.509192	0.509408	1.36	2.85	2.88	0.14
4.190	26.900	0.0942	0.510949	18	0.509293	0.509192	0.509408	1.99	2.81	2.83	0.14
1.210	6.705	0.1091	0.511090	9	0.509168	0.509185	0.509400	−0.33	3.00	3.01	0.15
2.000	13.000	0.0926	0.510901		0.509269	0.509184	0.509399	1.68	2.83	2.86	0.14
2.090	14.100	0.0896	0.510701	40	0.509119	0.509179	0.509393	−1.16	3.01	3.08	0.15
2.420	16.400	0.0891	0.510621	30	0.509048	0.509179	0.509393	−2.56	3.09	3.18	0.16
1.240	8.340	0.0897	0.510601	20	0.509018	0.509179	0.509393	−3.16	3.13	3.23	0.16
4.310	24.230	0.1076	0.511178		0.509279	0.509179	0.509393	1.97	2.84	2.84	0.14
1.777	7.489	0.1434	0.511662	8	0.509126	0.509172	0.509386	−0.91	3.24	3.06	0.15
6.392	33.203	0.1164	0.511295	8	0.509237	0.509172	0.509386	1.28	2.91	2.90	0.14
2.514	12.790	0.1188	0.511225	8	0.509124	0.509172	0.509386	−0.94	3.09	3.07	0.15
2.297	12.510	0.1110	0.511258	10	0.509296	0.509172	0.509386	2.43	2.81	2.81	0.14
8.320	34.800	0.1445	0.511821	18	0.509266	0.509172	0.509386	1.85	2.94	2.86	0.14
1.809	12.235	0.0894	0.510799	7	0.509219	0.509172	0.509386	0.91	2.88	2.93	0.15
2.551	15.487	0.0995	0.510941	7	0.509181	0.509172	0.509386	0.17	2.95	2.98	0.15
8.510	38.180	0.1347	0.511648	20	0.509261	0.509164	0.509378	1.90	2.91	2.86	0.14
4.858	27.263	0.1077	0.511112	9	0.509200	0.509159	0.509372	0.81	2.93	2.94	0.15
34.670	146.300	0.1433	0.511648	0	0.509102	0.509155	0.509368	−1.04	3.26	3.08	0.15
6.800	28.450	0.1445	0.511873	0	0.509305	0.509155	0.509368	2.96	2.83	2.78	0.14
7.690	34.870	0.1333	0.511631	0	0.509254	0.509142	0.509353	2.19	2.89	2.85	0.14
2.959	15.010	0.1192	0.511353	7	0.509227	0.509141	0.509352	1.69	2.90	2.89	0.14
2.870	14.970	0.1158	0.511336	0	0.509270	0.509141	0.509352	2.54	2.83	2.83	0.14
7.040	36.590	0.1163	0.511323	0	0.509243	0.509133	0.509344	2.17	2.86	2.86	0.14
2.020	12.340	0.0991	0.511016		0.509243	0.509131	0.509342	2.20	2.84	2.86	0.14
3.110	11.660	0.1613	0.512116	20	0.509227	0.509127	0.509338	1.96	3.03	2.88	0.14
6.910	31.800	0.1314	0.511460	10	0.509189	0.509251	0.509471	−1.21	3.14	3.04	0.15
3.9	25.4	0.092255	0.510642	6	0.509047	0.509249	0.509470	−3.97	3.14	3.24	0.16
18.510	117.800	0.0950	0.510710	10	0.509066	0.509247	0.509467	−3.54	3.13	3.21	0.16
4.850	27.200	0.1079	0.511079	10	0.509211	0.509244	0.509464	−0.66	2.99	3.00	0.15
4.180	23.400	0.1081	0.511131	10	0.509256	0.509237	0.509457	0.36	2.92	2.93	0.15
5.980	38.930	0.0929	0.510917		0.509305	0.509237	0.509457	1.33	2.82	2.85	0.14
4.470	25.100	0.1076	0.511046	10	0.509172	0.509224	0.509443	−1.03	3.02	3.04	0.15
4.460	28.200	0.0958	0.510906	10	0.509238	0.509224	0.509443	0.26	2.90	2.94	0.15
7.280	52.980	0.0831	0.510725	20	0.509275	0.509218	0.509436	1.12	2.83	2.88	0.14
2.280	14.897	0.0925	0.510855	11	0.509239	0.509214	0.509432	0.50	2.89	2.93	0.15
5.390	37.810	0.0862	0.510640		0.509134	0.509214	0.509432	−1.57	3.00	3.09	0.15
12.450	83.200	0.0904	0.510841	10	0.509261	0.509211	0.509429	0.97	2.86	2.90	0.14
5.381	45.913	0.0708	0.510392	9	0.509154	0.509211	0.509429	−1.13	2.94	3.06	0.15
6.693	49.591	0.0816	0.510559	9	0.509133	0.509211	0.509429	−1.54	2.99	3.09	0.15
6.801	17.564	0.2342	0.513207	8	0.509113	0.509211	0.509429	−1.93	0.33	3.12	0.16
3.890	22.800	0.1031	0.511067	10	0.509265	0.509211	0.509429	1.05	2.87	2.89	0.14
10.870	89.710	0.0733	0.510353		0.509072	0.509211	0.509429	−2.74	3.03	3.18	0.16
13.300	88.200	0.0911	0.510791	30	0.509198	0.509211	0.509429	−0.26	2.93	2.99	0.15

(*Continued*)

Table 2. *Sm–Nd data used in this study from the Yilgarn Craton, including new and collated data (sorted by terrane/domain) (Continued)*

Sample ID	Data source	Longitude[1]	Latitude[1]	Terrane[2]	Domain[2]	LITH CODE[3]	Age, t (Ma)[4]	2σ Error (Ma)
96969025	Champion (2013)	121.1219	−27.3941	EGST	Kalgoorlie	G	2650	
99969017	Champion (2013)	120.9528	−28.1687	EGST	Kalgoorlie	G	2650	
92969068	Champion & Sheraton (1997)	120.2702	−28.5471	EGST	Kalgoorlie	G	2650	
96969034	Champion (2013)	120.7932	−27.4689	EGST	Kalgoorlie	G	2652	
97969243	AMIRA P482	121.9315	−32.2127	EGST	Kalgoorlie	G	2655	6
97969249	AMIRA P482	122.1837	−31.8288	EGST	Kalgoorlie	G	2655	10
97967038G	AMIRA P482	121.4111	−30.4089	EGST	Kalgoorlie	G	2656	3
97969202	AMIRA P482	121.6207	−32.4674	EGST	Kalgoorlie	G	2656	10
93901	Champion & Sheraton (1997)	121.3665	−30.2475	EGST	Kalgoorlie	G	2657	
92969032	Champion & Sheraton (1997)	120.8301	−28.7703	EGST	Kalgoorlie	G	2660	
92969051	Champion & Sheraton (1997)	121.1596	−28.9516	EGST	Kalgoorlie	G	2660	
97969223	AMIRA P482	122.0355	−32.0827	EGST	Kalgoorlie	G	2660	9
97967069A	AMIRA P482	121.0516	−27.3099	EGST	Kalgoorlie	G	2660	25
104964[13]	This Study	121.6309740	−31.87	EGST	Kalgoorlie	G	2664	
93906	Champion & Sheraton (1997)	121.0423	−29.9860	EGST	Kalgoorlie	G	2665	
98276	Champion (2013)	121.4073	−31.1241	EGST	Kalgoorlie	G	2665	
92963318	Champion & Sheraton (1997)	120.5052	−28.0846	EGST	Kalgoorlie	G	2665	
92969031	Champion & Sheraton (1997)	120.8387	−28.7777	EGST	Kalgoorlie	G	2665	
92969082	Champion & Sheraton (1997)	120.5674	−28.1565	EGST	Kalgoorlie	G	2665	
95969716B	Champion & Sheraton (1997)	121.6400	−30.6217	EGST	Kalgoorlie	G	2665	
95969725B	Champion & Sheraton (1997)	121.5801	−30.5110	EGST	Kalgoorlie	G	2665	
95969727B	Champion & Sheraton (1997)	121.6086	−30.6094	EGST	Kalgoorlie	G	2665	
98967124	Champion (2013)	121.9979	−31.4609	EGST	Kalgoorlie	G	2665	
2000969007	Champion (2013)	121.5783	−30.9117	EGST	Kalgoorlie	G	2665	
2001969055B	Champion (2013)	121.1332	−29.3647	EGST	Kalgoorlie	G	2665	
77–41	McCulloch *et al.* (1983)	121.6304	−31.8664	EGST	Kalgoorlie	G	2665	
77–42	McCulloch *et al.* (1983)	121.6304	−31.8664	EGST	Kalgoorlie	G	2665	
77–43	McCulloch *et al.* (1983)	121.6304	−31.8664	EGST	Kalgoorlie	G	2665	
2001967017A	Champion (2013)	121.0315	−30.6703	EGST	Kalgoorlie	G	2666	3
94962258A	AMIRA P482	120.9567	−27.4887	EGST	Kalgoorlie	G	2667	3
2001969053C	Champion (2013)	120.6120	−28.9039	EGST	Kalgoorlie	G	2670	
96969038	Champion (2013)	120.5908	−26.2102	EGST	Kalgoorlie	G	2673	
ARC35[13]	This study	121.59	−32.17	EGST	Kalgoorlie	G	2673	8
92969038	Champion & Sheraton (1997)	120.6067	−28.8767	EGST	Kalgoorlie	G	2676	
142803[13]	This Study	120.4478690	−31.19	EGST	Kalgoorlie	G	2676	
92969067	Champion & Sheraton (1997)	120.5408	−28.5204	EGST	Kalgoorlie	G	2678	
63202	Fletcher & Rosman (1982)	121.6542	−30.5708	EGST	Kalgoorlie	F	2680	
63206	Fletcher & Rosman (1982)	121.6472	−30.6389	EGST	Kalgoorlie	F	2680	
63217	Fletcher & Rosman (1982)	121.4333	−30.6417	EGST	Kalgoorlie	F	2680	
92963213	Champion & Sheraton (1997)	120.8053	−28.0861	EGST	Kalgoorlie	G	2680	
92969024	Champion & Sheraton (1997)	120.9895	−28.7195	EGST	Kalgoorlie	G	2680	
92969025	Champion & Sheraton (1997)	120.9895	−28.7195	EGST	Kalgoorlie	G	2680	
92969073	Champion & Sheraton (1997)	120.8165	−28.2839	EGST	Kalgoorlie	G	2680	
77–45	McCulloch *et al.* (1983)	121.3015	−31.2941	EGST	Kalgoorlie	G	2680	

Sm (ppm)	Nd (ppm)	$^{147}Sm/^{144}Nd$	$^{143}Nd/^{144}Nd_m$[5]	2σ Error (10^{-6})	$^{143}Nd/^{144}Nd_i$[6]	$^{143}Nd/^{144}Nd_{CHUR}$[7]	$^{143}Nd/^{144}Nd_{DM}$[8]	εNd[15]	T_{DM} (Ga)[9]	$T_{DM}{}^{2}$ (Ga)[10]	Error (5%SE)[11]
5.040	33.140	0.0919	0.510869	20	0.509262	0.509211	0.509429	1.00	2.86	2.90	0.14
5.150	39.130	0.0795	0.510688		0.509298	0.509211	0.509429	1.71	2.80	2.84	0.14
9.182	70.982	0.0782	0.510366	8	0.508999	0.509211	0.509429	−4.16	3.13	3.28	0.16
6.370	52.100	0.0739	0.510606	20	0.509313	0.509209	0.509426	2.05	2.77	2.82	0.14
7.550	51.100	0.0893	0.510804	10	0.509240	0.509205	0.509422	0.69	2.87	2.92	0.15
2.850	18.900	0.0910	0.510984	10	0.509390	0.509205	0.509422	3.64	2.69	2.70	0.14
5.650	34.700	0.0983	0.510985	10	0.509263	0.509203	0.509420	1.16	2.86	2.89	0.14
1.970	14.400	0.0827	0.510629	10	0.509180	0.509203	0.509420	−0.46	2.93	3.01	0.15
7.152	45.686	0.0946	0.511046	18	0.509387	0.509202	0.509419	3.64	2.70	2.70	0.14
3.917	32.799	0.0722	0.510475	11	0.509208	0.509198	0.509415	0.20	2.88	2.96	0.15
0.847	2.931	0.1746	0.512348	7	0.509284	0.509198	0.509415	1.68	3.16	2.85	0.14
2.710	17.600	0.0930	0.510857	12	0.509225	0.509198	0.509415	0.53	2.90	2.94	0.15
4.310	26.200	0.0994	0.510999	15	0.509255	0.509198	0.509415	1.11	2.87	2.90	0.14
1.09	6.54	0.1006	0.510981		0.509212	0.509193	0.509409	0.37	2.93	2.95	0.15
2.714	22.042	0.0744	0.510555	13	0.509247	0.509192	0.509408	1.08	2.84	2.90	0.15
4.320	28.140	0.0927	0.510964		0.509334	0.509192	0.509408	2.80	2.76	2.77	0.14
2.056	11.911	0.1043	0.511118	9	0.509284	0.509192	0.509408	1.81	2.84	2.85	0.14
2.623	15.159	0.1046	0.511059	10	0.509220	0.509192	0.509408	0.56	2.92	2.94	0.15
3.006	21.723	0.0836	0.510704	9	0.509234	0.509192	0.509408	0.82	2.87	2.92	0.15
3.810	24.462	0.0941	0.510980	7	0.509325	0.509192	0.509408	2.62	2.77	2.79	0.14
2.013	12.001	0.1014	0.511019	9	0.509237	0.509192	0.509408	0.88	2.89	2.92	0.15
7.170	45.964	0.0944	0.510950	10	0.509290	0.509192	0.509408	1.93	2.81	2.84	0.14
2.090	12.160	0.1041	0.511073		0.509243	0.509192	0.509408	1.00	2.89	2.91	0.15
7.790	45.540	0.1034	0.511103	0	0.509285	0.509192	0.509408	1.83	2.83	2.85	0.14
4.420	32.180	0.0830	0.510665		0.509206	0.509192	0.509408	0.28	2.90	2.96	0.15
2.440	19.660	0.0749	0.510581	30	0.509264	0.509192	0.509408	1.41	2.82	2.88	0.14
4.650	23.840	0.1179	0.511362	20	0.509289	0.509192	0.509408	1.91	2.85	2.84	0.14
2.500	16.340	0.0925	0.510871	30	0.509245	0.509192	0.509408	1.04	2.87	2.91	0.15
1.670	10.980	0.0917	0.510830		0.509217	0.509190	0.509406	0.53	2.90	2.94	0.15
3.650	23.900	0.0924	0.510878	15	0.509252	0.509189	0.509405	1.24	2.86	2.89	0.14
1.910	13.960	0.0829	0.510684		0.509224	0.509185	0.509400	0.76	2.87	2.93	0.15
2.090	13.940	0.0906	0.510877	0	0.509279	0.509181	0.509396	1.93	2.82	2.85	0.14
4.00	29.85	0.0809	0.510729		0.509302	0.509181	0.509396	2.37	2.78	2.81	0.14
2.914	22.523	0.0782	0.510614	22	0.509234	0.509177	0.509392	1.11	2.85	2.91	0.15
1.27	7.38	0.1036	0.510902		0.509073	0.509177	0.509392	−2.06	3.11	3.15	0.16
2.543	15.204	0.1011	0.511013	8	0.509227	0.509175	0.509389	1.02	2.89	2.92	0.15
4.000	15.300	0.1606	0.512088	25	0.509249	0.509172	0.509386	1.50	3.07	2.88	0.14
3.300	12.700	0.1565	0.511977	30	0.509211	0.509172	0.509386	0.76	3.14	2.94	0.15
4.800	30.300	0.0964	0.510947	25	0.509243	0.509172	0.509386	1.40	2.86	2.89	0.14
1.917	12.284	0.0943	0.510774	7	0.509106	0.509172	0.509386	−1.30	3.03	3.09	0.15
2.307	16.615	0.0839	0.510689	9	0.509205	0.509172	0.509386	0.66	2.89	2.95	0.15
1.551	5.437	0.1724	0.512275	10	0.509226	0.509172	0.509386	1.06	3.26	2.92	0.15
2.478	17.928	0.0835	0.510719	10	0.509242	0.509172	0.509386	1.37	2.85	2.89	0.14
1.330	9.520	0.0844	0.510540	40	0.509048	0.509172	0.509386	−2.43	3.07	3.18	0.16

(*Continued*)

Table 2. *Sm–Nd data used in this study from the Yilgarn Craton, including new and collated data (sorted by terrane/domain) (Continued)*

Sample ID	Data source	Longitude[1]	Latitude[1]	Terrane[2]	Domain[2]	LITH CODE[3]	Age, t (Ma)[4]	2σ Error (Ma)
77–47	McCulloch *et al.* (1983)	121.3015	−31.2941	EGST	Kalgoorlie	G	2680	
92963013A	Champion & Sheraton (1997)	120.5976	−28.9006	EGST	Kalgoorlie	G	2680	
2001967019A	Champion (2013)	121.0805	−31.2650	EGST	Kalgoorlie	G	2680	
MKTD584W.1434[13]	This study	120.5430310	−27.23	EGST	Kalgoorlie	F	2680	
MKTD617W2.1114[13]	This study	120.5430310	−27.23	EGST	Kalgoorlie	F	2680	
ARC67[14]	This study	121.4	−31.12	EGST	Kalgoorlie	G	2684	6
MKD1-180[13]	This study	120.2499880	−26.75	EGST	Kalgoorlie	F	2684	
97969212	AMIRA P482	121.7049	−32.3567	EGST	Kalgoorlie	G	2685	25
71–909	McCulloch (1987)	122.0333	−32.0686	EGST	Kalgoorlie	G	2686	
95969704K	Champion & Sheraton (1997)	121.5805	−30.6156	EGST	Kalgoorlie	G	2687	
94969596	Champion (2013)	120.9312	−27.5389	EGST	Kalgoorlie	G	2690	
ARC32[13]	This study	121.6880680	−32.46	EGST	Kalgoorlie	G	2691	9
97969225A	Champion (2013)	121.2886	−28.8405	EGST	Kalgoorlie	G	2760	
2001967041A	Champion (2013)	121.1013	−29.4275	EGST	Kalgoorlie	G	2800	
142802[13]	This study	121.3055310	−31.3	EGST	Kalgoorlie	G	2801	
ARC94[14]	This study	120.108980	−33.611150	Youanmi	Southern Cross	G	2983	8
ARC98[14]	This study	120.497460	−33.464880	Youanmi	Southern Cross	G	2688	8
83691[13]	This study	120.8469300	−33.45	Youanmi	Southern Cross	G	2631	
ARC87[14]	This study	119.881880	−33.165660	Youanmi	Southern Cross	G	2686	8
ARC90[14]	This study	120.287330	−33.067230	Youanmi	Southern Cross	G	2646	5
ARC80[14]	This study	119.990590	−32.911940	Youanmi	Southern Cross	G	2663	9
ARC81[14]	This study	119.545550	−32.838840	Youanmi	Southern Cross	G	2663	10
ARC29[13]	This study	121.2859250	−32.76	Youanmi	Southern Cross	G	2639	6
ARC30[13]	This study	121.3332270	−32.74	Youanmi	Southern Cross	G	2653	13
ARC28[13]	This study	121.0283740	−32.72	Youanmi	Southern Cross	G	2720	10
ARC27[13]	This study	120.7825150	−32.66	Youanmi	Southern Cross	G	2708	8
ARC31[13]	This study	121.4217930	−32.65	Youanmi	Southern Cross	G	2656	9
ARC118[14]	This study	120.36	−32.35	Youanmi	Southern Cross	G	2699	8
ARC23[13]	This study	120.5321720	−32.29	Youanmi	Southern Cross	G	2774	6
ARC24[13]	This study	120.5988870	−32.28	Youanmi	Southern Cross	G	2696	14
72–864	McCulloch (1987)	120.8847	−32.1839	Youanmi	Southern Cross	G	2661	
ARC34[13]	This study	120.93	−32.13	Youanmi	Southern Cross	G	2653	7
ARC33[13]	This study	120.69	−32.07	Youanmi	Southern Cross	G	2658	5
ARC100[14]	This study	119.954550	−32.028690	Youanmi	Southern Cross	G	2705	6
ARC77[14]	This study	119.640080	−31.943110	Youanmi	Southern Cross	G	2685	5
ARC101[14]	This study	120.286510	−31.823560	Youanmi	Southern Cross	G	2639	6
ARC71[14]	This study	120.76	−31.64	Youanmi	Southern Cross	G	2635	5
56478	Fletcher *et al.* (1994)	120.5459	−31.5404	Youanmi	Southern Cross	G	2660	
YQ46[13]	This study	119.05	−31.48	Youanmi	Southern Cross	G	2632	
YQ45[13]	This study	119.16	−31.35	Youanmi	Southern Cross	G	2637	
YQ38[13]	This study	119.44	−31.3	Youanmi	Southern Cross	G	2615	
ARC22[13]	This study	119.6418040	−31.2947130	Youanmi	Southern Cross	G	2746	8
ARC21[13]	This study	119.8119770	−31.2841270	Youanmi	Southern Cross	G	2661	9
56477	Fletcher *et al.* (1994)	120.2904	−31.2070	Youanmi	Southern Cross	G	2640	
98967100A	AMIRA P482	120.2906	−31.2045	Youanmi	Southern Cross	G	2630	25
97969034	AMIRA P482	120.6298	−31.1872	Youanmi	Southern Cross	G	2640	25
ARC20[13]	This study	119.6868790	−31.1705610	Youanmi	Southern Cross	G	2626	11
ARC19[13]	This study	119.5213250	−30.8863660	Youanmi	Southern Cross	G	2665	17
97969090	AMIRA P482	119.5231	−30.8845	Youanmi	Southern Cross	G	2656	25
81884	Fletcher *et al.* (1994)	119.7207	−30.8425	Youanmi	Southern Cross	G	2680	
98967102E	AMIRA P482	119.3093	−30.6333	Youanmi	Southern Cross	G	2699	10
2001967009	Champion (2013)	120.5594	−30.4767	Youanmi	Southern Cross	G	2640	
2001967014	Champion (2013)	120.6411	−30.4283	Youanmi	Southern Cross	G	2700	
97969023	AMIRA P482	120.4761	−30.4189	Youanmi	Southern Cross	G	2640	25
ARC1A[13]	This study	119.1876080	−30.3282860	Youanmi	Southern Cross	G	2695	10
97969045	Champion (2013)	120.5598	−30.3153	Youanmi	Southern Cross	G	2630	
168956[13]	This study	119.0137960	−30.3146500	Youanmi	Southern Cross	G	2711	
97969049	Champion (2013)	120.5089	−30.2948	Youanmi	Southern Cross	G	2630	
168959[13]	This study	119.3922120	−30.2182530	Youanmi	Southern Cross	G	2730	
2001967013	Champion (2013)	120.5987	−30.2165	Youanmi	Southern Cross	G	2640	
168960[13]	This study	119.2924360	−30.1797140	Youanmi	Southern Cross	F	2732	
168976[13]	This study	119.8843670	−30.1783990	Youanmi	Southern Cross	G	2723	
71179	Fletcher & Rosman (1982)	119.3639	−30.1658	Youanmi	Southern Cross	F	2750	

Sm (ppm)	Nd (ppm)	$^{147}Sm/^{144}Nd$	$^{143}Nd/^{144}Nd_m$[5]	2σ Error (10^{-6})	$^{143}Nd/^{144}Nd_i$[6]	$^{143}Nd/^{144}Nd_{CHUR}$[7]	$^{143}Nd/^{144}Nd_{DM}$[8]	εNd[15]	T_{DM} (Ga)[9]	$T_{DM}{}^2$ (Ga)[10]	Error (5%SE)[11]
1.070	7.130	0.0906	0.510731	30	0.509129	0.509172	0.509386	−0.85	2.99	3.06	0.15
0.479	1.214	0.2387	0.513246	7	0.509025	0.509172	0.509386	−2.90	0.50	3.21	0.16
1.570	9.960	0.0955	0.510884		0.509195	0.509172	0.509386	0.46	2.92	2.96	0.15
4.73	26.56	0.1076	0.511045		0.509141	0.509172	0.509386	−0.60	3.03	3.04	0.15
3.51	11.68	0.1813	0.512451		0.509245	0.509172	0.509386	1.44	3.33	2.89	0.14
3.3	17.6	0.114141	0.511080	9	0.509059	0.509167	0.509381	−2.12	3.17	3.16	0.16
4.22	22.15	0.1149	0.511168		0.509133	0.509167	0.509381	−0.66	3.06	3.05	0.15
2.740	14.400	0.1153	0.511226	10	0.509183	0.509165	0.509379	0.35	2.98	2.97	0.15
2.400	18.100	0.0807	0.510641	20	0.509210	0.509164	0.509378	0.91	2.87	2.93	0.15
3.345	21.225	0.0953	0.510936	7	0.509247	0.509163	0.509376	1.66	2.85	2.88	0.14
5.010	25.590	0.1182	0.511261	20	0.509163	0.509159	0.509372	0.08	3.02	3.00	0.15
5.63	31.93	0.1064	0.510870		0.508982	0.509158	0.509371	−3.45	3.23	3.26	0.16
2.070	12.130	0.1030	0.511002		0.509126	0.509067	0.509272	1.15	2.96	2.98	0.15
2.430	13.340	0.1099	0.511088		0.509057	0.509015	0.509216	0.83	3.03	3.03	0.15
1.85	11.16	0.1003	0.510951		0.509098	0.509014	0.509214	1.65	2.96	2.97	0.15
2.0	8.8	0.133262	0.511492	7	0.508867	0.508775	0.508955	1.81	3.15	3.11	0.16
1.8	11.4	0.093577	0.510784	6	0.509124	0.509162	0.509375	−0.74	3.00	3.06	0.15
1.16	8.47	0.0830	0.510613		0.509173	0.509236	0.509456	−1.24	2.96	3.05	0.15
3.4	20.7	0.098837	0.510869	5	0.509118	0.509164	0.509378	−0.91	3.03	3.07	0.15
4.3	39.4	0.066589	0.510523	4	0.509361	0.509217	0.509435	2.84	2.72	2.75	0.14
3.7	26.7	0.082687	0.510555	5	0.509102	0.509194	0.509410	−1.81	3.02	3.12	0.16
9.3	80.9	0.069238	0.510304	4	0.509087	0.509194	0.509410	−2.10	3.00	3.14	0.16
8.00	67.52	0.0715	0.510368		0.509124	0.509226	0.509444	−2.00	2.98	3.11	0.16
3.75	34.72	0.0653	0.510266		0.509123	0.509207	0.509425	−1.65	2.96	3.10	0.15
1.82	11.85	0.0930	0.510729		0.509061	0.509120	0.509329	−1.16	3.05	3.12	0.16
2.24	10.72	0.1259	0.511373		0.509123	0.509135	0.509346	−0.24	3.09	3.04	0.15
4.71	34.61	0.0821	0.510580		0.509141	0.509203	0.509420	−1.22	2.97	3.07	0.15
0.4	2.2	0.111179	0.510772	5	0.508792	0.509147	0.509359	−6.97	3.53	3.53	0.18
1.05	5.21	0.1214	0.511281		0.509059	0.509049	0.509253	0.20	3.09	3.06	0.15
2.96	15.91	0.1124	0.511025		0.509026	0.509151	0.509363	−2.46	3.20	3.19	0.16
3.600	28.000	0.0773	0.510480	30	0.509123	0.509197	0.509413	−1.44	2.98	3.09	0.15
11.20	85.05	0.0795	0.510509		0.509118	0.509207	0.509425	−1.75	3.00	3.10	0.16
3.17	21.20	0.0903	0.510681		0.509097	0.509201	0.509417	−2.05	3.05	3.13	0.16
2.2	17.5	0.074732	0.510415	6	0.509081	0.509139	0.509351	−1.14	3.00	3.10	0.16
1.3	10.3	0.078556	0.510534	8	0.509143	0.509165	0.509379	−0.45	2.95	3.03	0.15
6.9	46.8	0.088557	0.510660	4	0.509118	0.509226	0.509444	−2.11	3.03	3.12	0.16
4.6	33.2	0.083344	0.510626	4	0.509177	0.509231	0.509450	−1.06	2.95	3.04	0.15
4.600	31.800	0.0866	0.510623	25	0.509103	0.509198	0.509415	−1.87	3.03	3.12	0.16
15.36	77.60	0.1195	0.511150		0.509075	0.509235	0.509454	−3.14	3.24	3.19	0.16
20.27	122.35	0.1000	0.510738		0.508998	0.509228	0.509447	−4.52	3.23	3.30	0.16
2.60	15.96	0.0984	0.510858		0.509162	0.509257	0.509479	−1.88	3.03	3.08	0.15
0.81	5.04	0.0976	0.510868		0.509100	0.509086	0.509292	0.29	2.99	3.03	0.15
2.93	22.47	0.0788	0.510507		0.509124	0.509197	0.509413	−1.44	2.98	3.09	0.15
4.600	29.300	0.0949	0.510744	25	0.509091	0.509224	0.509443	−2.62	3.08	3.16	0.16
5.860	39.400	0.0900	0.510632	22	0.509071	0.509237	0.509457	−3.28	3.10	3.20	0.16
5.120	43.200	0.0717	0.510436	10	0.509187	0.509224	0.509443	−0.73	2.91	3.02	0.15
4.19	21.75	0.1162	0.511118		0.509105	0.509243	0.509463	−2.71	3.18	3.15	0.16
3.16	20.83	0.0916	0.510709		0.509099	0.509192	0.509408	−1.82	3.04	3.12	0.16
2.650	17.400	0.0922	0.510768	10	0.509152	0.509203	0.509420	−1.00	2.99	3.05	0.15
2.800	20.600	0.0815	0.510514	25	0.509073	0.509172	0.509386	−1.95	3.04	3.14	0.16
13.700	49.700	0.1666	0.511978	15	0.509011	0.509147	0.509359	−2.67	3.81	3.21	0.16
6.840	48.970	0.0845	0.510720		0.509248	0.509224	0.509443	0.47	2.87	2.93	0.15
5.120	31.950	0.0970	0.510547		0.508819	0.509146	0.509358	−6.42	3.39	3.49	0.17
3.810	20.600	0.1118	0.511048	10	0.509101	0.509224	0.509443	−2.42	3.14	3.14	0.16
0.64	4.84	0.0794	0.510431		0.509020	0.509152	0.509365	−2.61	3.08	3.20	0.16
3.230	25.570	0.0763	0.510522		0.509198	0.509237	0.509457	−0.77	2.91	3.01	0.15
2.72	17.90	0.0918	0.510682		0.509039	0.509131	0.509342	−1.82	3.08	3.16	0.16
11.860	83.460	0.0859	0.510594		0.509104	0.509237	0.509457	−2.63	3.05	3.15	0.16
6.75	38.28	0.1064	0.510860		0.508943	0.509107	0.509315	−3.21	3.25	3.28	0.16
6.740	44.060	0.0925	0.510723		0.509112	0.509224	0.509443	−2.21	3.05	3.13	0.16
6.29	35.51	0.1069	0.510869		0.508942	0.509104	0.509312	−3.18	3.25	3.28	0.16
3.94	21.26	0.1118	0.510925		0.508916	0.509116	0.509325	−3.93	3.33	3.33	0.17
6.700	38.000	0.1074	0.510867	25	0.508917	0.509080	0.509287	−3.21	3.27	3.29	0.16

(*Continued*)

Table 2. *Sm–Nd data used in this study from the Yilgarn Craton, including new and collated data (sorted by terrane/domain) (Continued)*

Sample ID	Data source	Longitude[1]	Latitude[1]	Terrane[2]	Domain[2]	LITH CODE[3]	Age, t (Ma)[4]	2σ Error (Ma)
71180	Fletcher & Rosman (1982)	119.3750	−30.1583	Youanmi	Southern Cross	G	2750	
71178	Fletcher & Rosman (1982)	119.3208	−30.1444	Youanmi	Southern Cross	F	2750	
168961[13]	This study	119.2889320	−30.1314240	Youanmi	Southern Cross	F	2734	
169064[13]	This study	119.8036880	−29.9534090	Youanmi	Southern Cross	G	2685	
96969002	Champion (2013)	120.2172	−29.8445	Youanmi	Southern Cross	G	2630	
87955	Fletcher *et al.* (1994)	119.6282	−29.7208	Youanmi	Southern Cross	G	2660	
87975	Fletcher *et al.* (1994)	119.5620	−29.6656	Youanmi	Southern Cross	G	2640	
96969010	Champion (2013)	120.2056	−29.6612	Youanmi	Southern Cross	G	2660	
96969012	AMIRA P482	120.3633	−29.4586	Youanmi	Southern Cross	G	2633	2
97969104	AMIRA P482	119.5204	−29.0515	Youanmi	Southern Cross	G	2682	6
97969102B	AMIRA P482	119.5918	−29.0244	Youanmi	Southern Cross	G	2737	25
97969082A	AMIRA P482	119.7326	−28.7103	Youanmi	Southern Cross	G	2682	5
71124	Fletcher *et al.* (1994)	119.1375	−28.6987	Youanmi	Southern Cross	G	2680	
71123	Fletcher *et al.* (1994)	119.8779	−28.6529	Youanmi	Southern Cross	G	2680	
98968104	AMIRA P482	118.8916	−28.5741	Youanmi	Southern Cross	G	2813	5
71125	Fletcher *et al.* (1994)	119.0847	−28.5487	Youanmi	Southern Cross	G	2660	
71122	Fletcher *et al.* (1994)	119.7389	−28.5181	Youanmi	Southern Cross	G	2640	
97969063	AMIRA P482	119.7385	−28.5107	Youanmi	Southern Cross	G	2684	8
92964658	Champion & Sheraton (1997)	120.1699	−28.1737	Youanmi	Southern Cross	G	2653	
98969055	AMIRA P482	119.3954	−27.5856	Youanmi	Southern Cross	G	2712	6
98969033	AMIRA P482	119.1284	−27.3390	Youanmi	Southern Cross	G	2671	3
98969045	AMIRA P482	118.9864	−27.1706	Youanmi	Southern Cross	G	2700	25
98969019	AMIRA P482	119.7234	−27.1557	Youanmi	Southern Cross	G	2640	50
98969025	AMIRA P482	119.3254	−27.1168	Youanmi	Southern Cross	G	2661	7
83551	Watkins *et al.* (1991)	116.2516	−29.1943	Youanmi	Murchison	G	2602	
97969125	AMIRA P482	118.6631	−31.0587	Youanmi	Murchison	G	2617	3
88–195	Nutman *et al.* (1993)	116.8667	−26.7333	Youanmi	Murchison	G	2620	
99967114	AMIRA P482	117.4501	−27.1326	Youanmi	Murchison	G	2630	50
98969042	AMIRA P482	118.8374	−27.1815	Youanmi	Murchison	G	2630	50
83407	Watkins *et al.* (1991)	116.7247	−29.2169	Youanmi	Murchison	G	2640	
99969049	AMIRA P482	118.1124	−30.9082	Youanmi	Murchison	G	2640	5
98969044	AMIRA P482	118.8164	−27.1530	Youanmi	Murchison	G	2650	10
88–186	Nutman *et al.* (1993)	117.0917	−26.3417	Youanmi	Murchison	G	2672	
88–189	Nutman *et al.* (1993)	116.3567	−27.1083	Youanmi	Murchison	G	2679	
74459	Watkins *et al.* (1991)	117.8943	−27.7484	Youanmi	Murchison	G	2681	
83524	Watkins *et al.* (1991)	117.6629	−28.3960	Youanmi	Murchison	G	2690^{+}	
77334	Fletcher *et al.* (1994)	116.8819	−26.5245	Youanmi	Murchison	G	2690^{+}	
77391	Fletcher *et al.* (1994)	116.7861	−26.4126	Youanmi	Murchison	G	2690^{+}	
77392	Fletcher *et al.* (1994)	116.7861	−26.4126	Youanmi	Murchison	F	2690^{+}	
77337A	Fletcher *et al.* (1994)	116.8819	−26.5245	Youanmi	Murchison	G	2690^{+}	
17808	Fletcher *et al.* (1994)	117.3181	−27.3987	Youanmi	Murchison	G	2700^{+}	
83474	Watkins *et al.* (1991)	117.2515	−28.8324	Youanmi	Murchison	G	2700^{+}	
83478	Watkins *et al.* (1991)	117.3930	−28.5613	Youanmi	Murchison	G	2700^{+}	
77362	Fletcher *et al.* (1994)	115.6736	−28.1751	Youanmi	Murchison	G	2700^{+}	
77366	Fletcher *et al.* (1994)	115.6736	−28.1751	Youanmi	Murchison	G	2700^{+}	
17810	Fletcher *et al.* (1994)	117.0181	−27.9821	Youanmi	Murchison	G	2720^{+}	
99969164A	AMIRA P482	116.4262	−28.2138	Youanmi	Murchison	G	2742	7
99964100	AMIRA P482	116.7434	−28.1490	Youanmi	Murchison	G	2743	4
99964003	AMIRA P482	116.7408	−28.1146	Youanmi	Murchison	G	2745	10
99967141	AMIRA P482	117.3383	−27.7655	Youanmi	Murchison	G	2745	25
99969142	AMIRA P482	116.3510	−28.6497	Youanmi	Murchison	G	2747	3
99964016C	AMIRA P482	116.9789	−29.1887	Youanmi	Murchison	G	2756	20
74474	Watkins *et al.* (1991)	117.9221	−27.5550	Youanmi	Murchison	G	2760^{+}	
81711A	Watkins *et al.* (1991)	118.3623	−26.8545	Youanmi	Murchison	G	2760	
83305	Watkins *et al.* (1991)	117.0085	−27.4497	Youanmi	Murchison	G	2920	
83399	Watkins *et al.* (1991)	116.6182	−28.7762	Youanmi	Murchison	G	2920	
88–183	Nutman *et al.* (1993)	116.6667	−28.7000	Youanmi	Murchison	G	2920	
77346	Fletcher *et al.* (1994)	116.3944	−27.1223	Youanmi	Murchison	G	2950^{+}	
77350	Fletcher *et al.* (1994)	116.3944	−27.1223	Youanmi	Murchison	G	2950^{+}	
77353	Fletcher *et al.* (1994)	116.3917	−27.1543	Youanmi	Murchison	G	2950^{+}	
97969138	AMIRA P482	117.8597	−30.9514	South West	South West	G	2627	3
99969063	AMIRA P482	116.7697	−30.6420	South West	South West	G	2630	6
YQ13[13]	This study	118.89	−32.45	South West	South West	G	2631	
YQ10[13]	This study	118.31	−33.07	South West	South West	G	2636	
YQ11[13]	This study	118.31	−33.07	South West	South West	G	2636	

Sm (ppm)	Nd (ppm)	$^{147}Sm/^{144}Nd$	$^{143}Nd/^{144}Nd_m$[5]	2σ Error (10^{-6})	$^{143}Nd/^{144}Nd_i$[6]	$^{143}Nd/^{144}Nd_{CHUR}$[7]	$^{143}Nd/^{144}Nd_{DM}$[8]	εNd[15]	T_{DM} (Ga)[9]	$T_{DM}{}^2$ (Ga)[10]	Error (5%SE)[11]
6.600	37.000	0.1078	0.510882	25	0.508926	0.509080	0.509287	−3.03	3.26	3.28	0.16
7.200	32.000	0.1056	0.510844	25	0.508927	0.509080	0.509287	−3.02	3.25	3.28	0.16
7.26	37.92	0.1155	0.511020		0.508936	0.509101	0.509309	−3.25	3.31	3.28	0.16
5.53	35.54	0.0940	0.510601		0.508937	0.509165	0.509379	−4.49	3.24	3.34	0.17
10.160	72.630	0.0845	0.510531	20	0.509065	0.509237	0.509457	−3.39	3.09	3.21	0.16
6.100	37.000	0.0995	0.510710	25	0.508964	0.509198	0.509415	−4.60	3.25	3.32	0.17
8.600	67.000	0.0779	0.510504	25	0.509147	0.509224	0.509443	−1.52	2.97	3.08	0.15
5.210	35.280	0.0892	0.510688	20	0.509123	0.509198	0.509415	−1.48	3.01	3.09	0.15
8.870	58.700	0.0913	0.510605	15	0.509019	0.509234	0.509453	−4.21	3.17	3.27	0.16
2.260	14.100	0.0972	0.510690	11	0.508970	0.509169	0.509383	−3.92	3.21	3.29	0.16
1.830	13.500	0.0818	0.510539	11	0.509062	0.509097	0.509305	−0.70	3.01	3.10	0.15
4.730	27.600	0.1038	0.510793	10	0.508956	0.509169	0.509383	−4.19	3.27	3.31	0.17
3.600	23.300	0.0926	0.510708	25	0.509071	0.509172	0.509386	−1.99	3.07	3.15	0.16
3.300	24.000	0.0827	0.510410	25	0.508948	0.509172	0.509386	−4.41	3.18	3.33	0.17
11.520	45.700	0.1524	0.512026	16	0.509196	0.508998	0.509197	3.90	2.81	2.81	0.14
3.100	21.900	0.0867	0.510613	25	0.509091	0.509198	0.509415	−2.10	3.04	3.14	0.16
2.900	21.300	0.0821	0.510399	20	0.508969	0.509224	0.509443	−5.01	3.18	3.34	0.17
3.060	23.200	0.0796	0.510399	10	0.508989	0.509167	0.509381	−3.48	3.12	3.26	0.16
7.470	52.709	0.0857	0.510479	6	0.508980	0.509207	0.509425	−4.47	3.17	3.31	0.17
0.880	4.900	0.1093	0.510942	14	0.508986	0.509130	0.509341	−2.83	3.22	3.23	0.16
2.230	19.600	0.0688	0.510197	15	0.508985	0.509184	0.509399	−3.91	3.10	3.28	0.16
1.360	7.900	0.1043	0.511043	13	0.509185	0.509146	0.509358	0.77	2.94	2.95	0.15
5.160	27.800	0.1122	0.511045	15	0.509091	0.509224	0.509443	−2.62	3.16	3.16	0.16
3.510	26.800	0.0792	0.510479	15	0.509089	0.509197	0.509413	−2.13	3.02	3.14	0.16
11.400	53.000	0.1300	0.511262	11	0.509031	0.509274	0.509497	−4.77	3.44	3.29	0.16
4.300	25.900	0.1005	0.510850	11	0.509115	0.509254	0.509476	−2.74	3.10	3.15	0.16
		0.1104	0.510985	7	0.509077	0.509251	0.509471	−3.41	3.19	3.20	0.16
9.670	65.600	0.0890	0.510611	18	0.509067	0.509237	0.509457	−3.35	3.10	3.20	0.16
2.240	13.700	0.0985	0.510804	11	0.509095	0.509237	0.509457	−2.79	3.10	3.16	0.16
12.500	68.000	0.1122	0.510967	13	0.509014	0.509224	0.509443	−4.13	3.27	3.27	0.16
3.260	18.800	0.1047	0.510841	10	0.509018	0.509224	0.509443	−4.06	3.23	3.27	0.16
2.400	14.900	0.0976	0.510933	18	0.509227	0.509211	0.509429	0.30	2.91	2.95	0.15
		0.0800	0.510224	5	0.508814	0.509182	0.509398	−7.24	3.33	3.53	0.18
		0.1079	0.510864	5	0.508957	0.509173	0.509388	−4.25	3.29	3.31	0.17
3.700	25.000	0.0905	0.510764	18	0.509163	0.509171	0.509385	−0.15	2.95	3.01	0.15
2.700	24.000	0.0679	0.510381	13	0.509176	0.509159	0.509372	0.34	2.89	2.98	0.15
3.200	22.500	0.0871	0.510564	10	0.509018	0.509159	0.509372	−2.77	3.11	3.21	0.16
7.100	42.000	0.1030	0.510887	10	0.509058	0.509159	0.509372	−1.97	3.12	3.15	0.16
7.400	36.000	0.1225	0.511083	10	0.508909	0.509159	0.509372	−4.90	3.45	3.37	0.17
10.700	72.000	0.0898	0.510661	10	0.509067	0.509159	0.509372	−1.80	3.06	3.14	0.16
4.700	31.300	0.0910	0.510688	21	0.509067	0.509146	0.509358	−1.55	3.06	3.13	0.16
3.200	29.000	0.0660	0.510297	12	0.509121	0.509146	0.509358	−0.49	2.94	3.05	0.15
5.500	43.000	0.0679	0.510356	12	0.509146	0.509146	0.509358	0.01	2.92	3.01	0.15
1.500	12.800	0.0730	0.510269	10	0.508969	0.509146	0.509358	−3.48	3.11	3.27	0.16
3.000	22.600	0.0791	0.510393	10	0.508983	0.509146	0.509358	−3.19	3.12	3.25	0.16
2.200	13.700	0.0970	0.510908	11	0.509167	0.509120	0.509329	0.92	2.93	2.96	0.15
2.810	22.600	0.0750	0.510492	16	0.509135	0.509091	0.509298	0.87	2.92	2.98	0.15
2.780	19.800	0.0850	0.510578	12	0.509039	0.509090	0.509297	−0.98	3.04	3.12	0.16
11.900	79.200	0.0908	0.510507	10	0.508862	0.509087	0.509294	−4.41	3.27	3.38	0.17
5.940	25.400	0.1413	0.511458	30	0.508898	0.509087	0.509294	−3.70	3.56	3.33	0.17
8.110	48.400	0.1012	0.510836	15	0.509001	0.509084	0.509291	−1.63	3.13	3.17	0.16
2.070	13.400	0.0932	0.510700	11	0.509005	0.509072	0.509278	−1.33	3.10	3.16	0.16
2.200	11.800	0.1120	0.511176	14	0.509137	0.509067	0.509272	1.36	2.96	2.96	0.15
3.900	22.000	0.1076	0.511061	10	0.509102	0.509067	0.509272	0.68	3.00	3.01	0.15
4.600	33.000	0.0852	0.510585	16	0.508943	0.508858	0.509045	1.67	3.04	3.07	0.15
3.300	26.000	0.0782	0.510453	11	0.508946	0.508858	0.509045	1.74	3.03	3.07	0.15
		0.0728	0.510407	11	0.509003	0.508858	0.509045	2.87	2.96	2.98	0.15
4.300	35.000	0.1483	0.511410	10	0.508520	0.508818	0.509002	−5.86	4.05	3.66	0.18
14.300	116.000	0.0744	0.510110	10	0.508661	0.508818	0.509002	−3.09	3.32	3.45	0.17
4.900	16.900	0.0876	0.510482	10	0.508775	0.508818	0.509002	−0.85	3.22	3.29	0.16
7.480	44.900	0.1008	0.510816	11	0.509069	0.509241	0.509462	−3.38	3.15	3.20	0.16
16.660	85.300	0.1180	0.511103	14	0.509056	0.509237	0.509457	−3.57	3.26	3.22	0.16
12.63	94.50	0.0806	0.510444		0.509045	0.509236	0.509456	−3.75	3.09	3.24	0.16
3.27	9.21	0.2142	0.512772		0.509047	0.509230	0.509449	−3.58	−155.24	3.23	0.16
2.90	8.95	0.1957	0.512355		0.508952	0.509230	0.509449	−5.45	6.75	3.37	0.17

(*Continued*)

Table 2. *Sm–Nd data used in this study from the Yilgarn Craton, including new and collated data (sorted by terrane/domain) (Continued)*

Sample ID	Data source	Longitude[1]	Latitude[1]	Terrane[2]	Domain[2]	LITH CODE[3]	Age, t (Ma)[4]	2σ Error (Ma)
YQ21[13]	This study	118.76	−32.07	South West	South West	G	2638	
99969096	AMIRA P482	116.6770	−30.0570	South West	South West	G	2639	6
YQ17[13]	This study	119.15	−32.34	South West	South West	G	2639	
YQ22[13]	This study	118.76	−32.08	South West	South West	G	2640	
99967055	AMIRA P482	117.4022	−30.6317	South West	South West	G	2641	5
99967066	AMIRA P482	116.0854	−30.3261	South West	South West	G	2645	5
ARC99[14]	This study	119.523740	−32.321120	South West	South West	G	2654	6
YQ14[13]	This study	119.11	−32.43	South West	South West	G	2654	
YQ18[13]	This study	119.12	−32.24	South West	South West	G	2663	
ARC82[14]	This study	119.415530	−32.676030	South West	South West	G	2664	7
ARC84[14]	This study	119.015750	−33.113200	South West	South West	G	2670	11
ARC76[14]	This study	119.437040	−32.035420	South West	South West	G	2671	7
YQ19[13]	This study	119.02	−32.12	South West	South West	G	2691	
Fletcher	Fletcher *et al.* (1994)	116.7100	−30.8800	South West	South West	G	2700+	
Fletcher	Fletcher *et al.* (1994)	116.4014	−32.9528	South West	South West	G	2700+	
99969066	AMIRA P482	116.4898	−30.6497	South West	South West	G	2730	75
95YQ120[13]	This study	118.36	−31.3	South West	South West	G	2781	
99967049A	AMIRA P482	117.1021	−31.0992	South West	South West	G	2787	4
95YQ70[13]	This study	118.5	−32.78	South West	South West	G	2851	
99967082C	AMIRA P482	116.4627	−30.4651	South West	South West	G	2940	25
99967082C	AMIRA P482	116.46	−30.47	South West	South West	G	2940	
59925	Fletcher *et al.* (1994)	117.2487	−32.6779	South West	South West	G	3000+	
59926	Fletcher *et al.* (1994)	117.5932	−32.7391	South West	South West	G	3000+	
99969093B	AMIRA P482	116.7501	−30.1629	South West	South West	G	3007	3
99969093B	AMIRA P482	116.75	−30.16	South West	South West	G	3007	
87–305	Nutman *et al.* (1993)	117.3500	−25.5500	Narryer	Narryer	G	2620	
84–97	Nutman *et al.* (1993)	116.3639	−26.5417	Narryer	Narryer	G	2638	
88–179	Nutman *et al.* (1993)	115.5839	−27.3894	Narryer	Narryer	G	2643	
88–196	Nutman *et al.* (1993)	116.7150	−26.3250	Narryer	Narryer	G	2648	
88–188	Nutman *et al.* (1993)	116.9533	−26.2133	Narryer	Narryer	G	2654	
88–192	Nutman *et al.* (1993)	116.9889	−26.2444	Narryer	Narryer	G	2685	
88–182	Nutman *et al.* (1993)	116.1250	−26.5417	Narryer	Narryer	G	2748	
88–22	Nutman *et al.* (1993)	116.8222	−26.2667	Narryer	Narryer	G	2994	
91–615	Nutman *et al.* (1993)	116.8833	−26.2917	Narryer	Narryer	G	2994	
77270	Fletcher *et al.* (1994)	115.6931	−27.4140	Narryer	Narryer	G	3000+	
77272	Fletcher *et al.* (1994)	115.6931	−27.4140	Narryer	Narryer	G	3000+	
80309	Fletcher *et al.* (1994)	116.3542	−26.3332	Narryer	Narryer	G	3000+	
80313	Fletcher *et al.* (1994)	116.3819	−26.3209	Narryer	Narryer	G	3000+	
80316	Fletcher *et al.* (1994)	116.4014	−26.0793	Narryer	Narryer	G	3000+	
80322	Fletcher *et al.* (1994)	116.4194	−26.0765	Narryer	Narryer	G	3000+	
88–169	Nutman *et al.* (1993)	115.5839	−27.3894	Narryer	Narryer	G	3005	

[1]Latitude and longitude are shown in the Geocentric Datum of Australia 1994 (GDA 1994) coordinate system.
[2]Terranes/domains taken from Cassidy *et al.* (2006): EGST, Eastern Goldfields Superterrane.
[3]Basic lithology code: G, granite; F, felsic volcanic; F–P, felsic porphyry; G–Mig, granite–migmatite.
[4]All ages from this study and the majority of collated data are U–Pb SHRIMP ages. However, some ages (shown by +) are estimates based on stratigraphic and geochemical relationships.
[5]Measured $^{143}Nd/^{144}Nd$ ratios.
[6]Initial $^{143}Nd/^{144}Nd$ ratios at time, t.
[7]The $^{143}Nd/^{144}Nd$ ratio of the chondritic uniform reservoir (CHUR) at time, t.
[8]The $^{143}Nd/^{144}Nd$ ratio of the depleted mantle (DM) at time, t.

0.7 to 1.4. The magmas with positive εNd may represent reworking of the *c.* 2920 Ma juvenile source (Fig. 8f). The second event at 2700–2680 Ma displays an array of Nd values, with T_{DM}^2 of *c.* 3300–3000 Ma and εNd of −4.9 to 0.3, representing reworking of the sources identified at *c.* 2760–2740 Ma. The final group, at 2640–2620 Ma, displays more homogenous source with T_{DM}^2 ages of 3200–3100 Ma (εNd of −3.4 to −2.7).

South West Terrane. Thirty samples from the South West Terrane have U–Pb ages from 3007 to 2627 Ma, with T_{DM}^2 ages from *c.* 3400 to 3000 Ma, peaking at *c.* 3200 Ma (Fig. 6e, f), and εNd values between −5.5 and 2.6, with the major peak at −1.6. Additional subordinate peaks occur at −3.4 and 2.5 (Fig. 6e). Samples with U–Pb ages of *c.* 3000 Ma have two apparent sources with T_{DM}^2 of *c.* 3250 and 3100 Ma and εNd of 0.2 and 2.5, respectively (Fig. 8g). Felsic magmatism after 3000 Ma appears to represent reworking of this heterogeneous *c.* 3200 Ma source, including the major *c.* 2645–2630 Ma magmatic event. Data from this group form an array with T_{DM}^2 ages

Sm (ppm)	Nd (ppm)	$^{147}Sm/^{144}Nd$	$^{143}Nd/^{144}Nd_m$[5]	2σ Error (10^{-6})	$^{143}Nd/^{144}Nd_i$[6]	$^{143}Nd/^{144}Nd_{CHUR}$[7]	$^{143}Nd/^{144}Nd_{DM}$[8]	εNd[15]	T_{DM} (Ga)[9]	T_{DM}^2 (Ga)[10]	Error (5%SE)[11]
2.82	17.57	0.0968	0.510862		0.509178	0.509227	0.509446	−0.96	2.98	3.03	0.15
13.190	81.000	0.0984	0.510713	10	0.509000	0.509226	0.509444	−4.43	3.22	3.29	0.16
3.99	28.17	0.0855	0.510617		0.509129	0.509226	0.509444	−1.91	3.01	3.10	0.16
2.26	15.05	0.0907	0.510791		0.509212	0.509224	0.509443	−0.25	2.92	2.98	0.15
11.460	76.300	0.0908	0.510626	10	0.509044	0.509223	0.509442	−3.52	3.13	3.23	0.16
8.460	60.200	0.0849	0.510499	17	0.509018	0.509218	0.509436	−3.93	3.13	3.26	0.16
1.8	12.9	0.084063	0.510581	5	0.509109	0.509206	0.509423	−1.91	3.02	3.12	0.16
7.57	48.91	0.0935	0.510728		0.509091	0.509206	0.509423	−2.25	3.07	3.14	0.16
3.25	21.53	0.0910	0.510623		0.509024	0.509194	0.509410	−3.35	3.14	3.23	0.16
2.5	18.4	0.080846	0.510521	10	0.509100	0.509193	0.509409	−1.83	3.01	3.12	0.16
2.1	13.2	0.097418	0.510866	5	0.509150	0.509185	0.509400	−0.69	2.99	3.04	0.15
3.6	26.1	0.082522	0.510540	4	0.509086	0.509184	0.509399	−1.93	3.03	3.13	0.16
2.46	16.05	0.0925	0.510706		0.509064	0.509158	0.509371	−1.85	3.07	3.14	0.16
7.300	47.000	0.0956	0.510732	22	0.509029	0.509146	0.509358	−2.30	3.12	3.18	0.16
3.500	18.100	0.1173	0.511270	22	0.509180	0.509146	0.509358	0.68	2.98	2.96	0.15
2.100	13.100	0.0967	0.510702	11	0.508960	0.509107	0.509315	−2.88	3.19	3.25	0.16
5.88	32.97	0.1076	0.510972		0.508996	0.509040	0.509243	−0.6	3.13	3.14	0.16
6.430	33.200	0.1168	0.511122	22	0.508974	0.509032	0.509234	−1.15	3.19	3.17	0.16
7.15	37.73	0.1144	0.511031		0.508878	0.508948	0.509143	−1.37	3.25	3.24	0.16
5.280	35.800	0.0891	0.510487	13	0.508757	0.508831	0.509016	−1.46	3.25	3.32	0.17
5.28	35.8	0.09	0.510487		0.508757	0.508831	0.509016	−1.46	3.25	3.32	0.17
5.900	34.000	0.1058	0.510967	20	0.508871	0.508753	0.508931	2.32	3.08	3.09	0.15
8.100	58.000	0.0846	0.510561	21	0.508885	0.508753	0.508931	2.60	3.05	3.07	0.15
1.570	14.100	0.0670	0.510082	15	0.508751	0.508743	0.508921	0.16	3.18	3.26	0.16
1.57	14.1	0.07	0.510082		0.508751	0.508743	0.508921	0.16	3.18	3.26	0.16
		0.0952	0.510541	8	0.508896	0.509251	0.509471	−6.97	3.35	3.47	0.17
		0.0692	0.510066	10	0.508862	0.509227	0.509446	−7.17	3.24	3.50	0.17
		0.0572	0.509999	5	0.509002	0.509220	0.509439	−4.30	3.06	3.29	0.16
		0.1146	0.510743	8	0.508741	0.509214	0.509432	−9.29	3.69	3.66	0.18
		0.0698	0.510109	5	0.508887	0.509206	0.509423	−6.27	3.21	3.44	0.17
		0.1069	0.510951	6	0.509057	0.509165	0.509379	−2.12	3.14	3.16	0.16
		0.0825	0.510230	12	0.508734	0.509083	0.509289	−6.86	3.38	3.57	0.18
		0.1063	0.510789	15	0.508687	0.508761	0.508939	−1.44	3.35	3.37	0.17
		0.1173	0.510997	5	0.508678	0.508761	0.508939	−1.63	3.40	3.38	0.17
1.700	9.800	0.1021	0.510823	10	0.508799	0.508753	0.508931	0.92	3.18	3.19	0.16
2.600	12.900	0.1213	0.511147	10	0.508743	0.508753	0.508931	−0.18	3.30	3.28	0.16
4.700	34.000	0.0832	0.510329	10	0.508680	0.508753	0.508931	−1.43	3.29	3.37	0.17
9.000	62.000	0.0882	0.510475	10	0.508728	0.508753	0.508931	−0.48	3.24	3.30	0.16
1.000	6.000	0.1021	0.510826	10	0.508803	0.508753	0.508931	0.99	3.17	3.19	0.16
1.400	6.900	0.1276	0.511138	10	0.508609	0.508753	0.508931	−2.82	3.56	3.47	0.17
		0.1049	0.510835	12	0.508753	0.508746	0.508924	0.14	3.24	3.26	0.16

[9]Depleted mantle model age using depleted mantle model of Goldstein *et al.* (1984); values below.
[10]Two-stage (crustal) model age using depleted mantle model of Goldstein *et al.* (1984): $^{147}Sm/^{144}Nd = 0.2136$, $^{143}Nd/^{144}Nd = 0.513163$ and average crustal $^{147}Sm/^{144}Nd$ of 0.11.
[11]The error on the crustal model age is calculated as 5% standard error (SE).
[12]Present day CHUR values taken from Wyborn *et al.* (1988): $^{147}Sm/^{144}Nd = 0.512650$ and $^{147}Sm/^{144}Nd$ 0.1967.
[13]Analysis performed at the University of Melbourne.
[14]Analysis performed at the Geosciences Rennes Laboratory.
[15]A standard error of 0.5 ε units is used for the εNd data as this corresponds to the average analytical error.

ranging from 3400 to 3000 Ma (εNd −5.5 and −0.3; Fig. 8g), clustering at a T_{DM}^2 ages of 3200 Ma (εNd −3.5).

Narryer Terrane. In the NW of the Yilgarn Craton, 16 samples aged between *c.* 3005 and 2620 Ma are available from the Narryer Terrane (Figs 6g, h & 8h). The T_{DM}^2 values for this terrane range from *c.* 3700 to 3150 Ma, peaking at *c.* 3400–3300 Ma (Fig. 6h). The εNd values for this area range from −9.0 to 1.0, and peak at −6.8 and −1.5, with relatively minor peaks at −9.2, −4.2 and 0 (Fig. 6g). Figure 8h suggests that at *c.* 3000 Ma the crustal source had T_{DM}^2 ages of 3500–3200 Ma, focused around the *c.* 3300 Ma crustal evolution line. Younger felsic magmatic events with U–Pb ages of 2750–2620 Ma appear to be reworking this source. Interaction with older crustal material at *c.* 2650 Ma may have led to the *c.* 3700 Ma T_{DM}^2 age. These data suggest that this terrane is very long lived, with isotopic evidence of crust formation as old as *c.* 3700 Ma. The εNd values decrease consistently through time (Fig. 8h) suggesting significant reworking of a 3500–3200 Ma source.

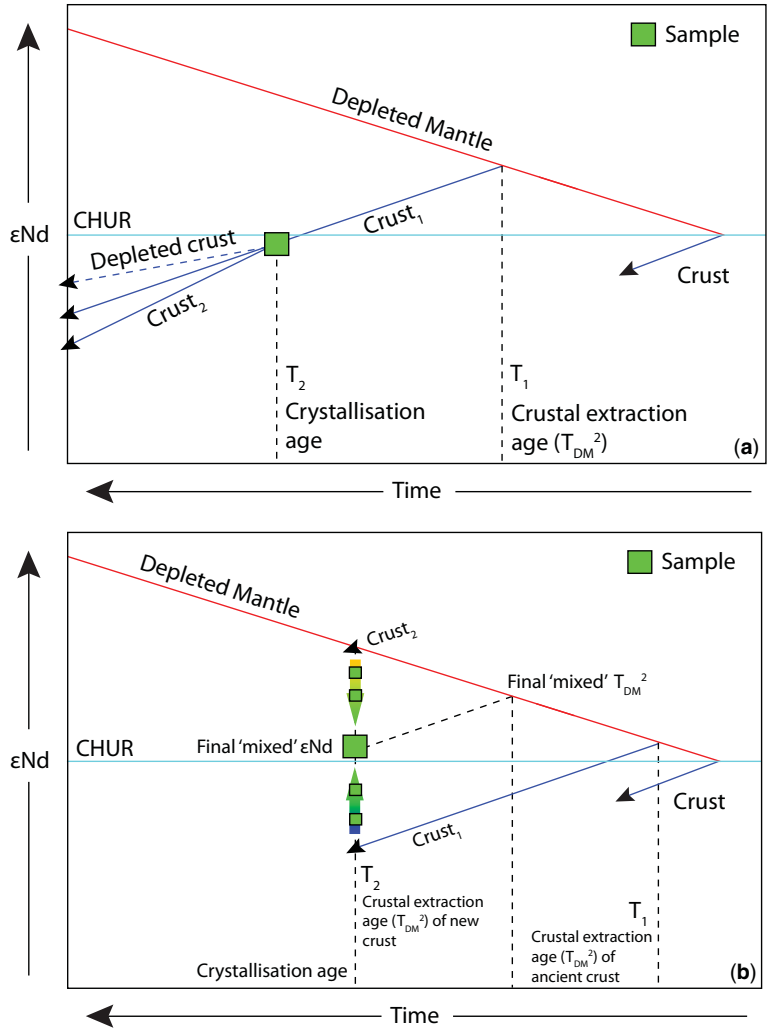

Fig. 4. Diagrams demonstrating the multiple interpretations of unradiogenic Sm–Nd data. (**a**) This εNd isotope plot demonstrates a potential interpretation for an isolated data-point crystallized at T_2, with no direct connection with the depleted mantle. Here, the sample is inferred to be the reworked product of precursor, juvenile crust that was extracted from the mantle at T_1. Hence this rock has a T_1 model age. (**b**) An alternative interpretation for this data-point is mixing of two contrasting Nd sources. Here, new, highly radiogenic mantle-derived crust is emplaced into older, precursor crustal material (model age T_1) at T_2. During emplacement, the juvenile magma assimilates and mixes with the precursor crust. This produces a rock with Nd systematics intermediate between the two components. As a result, the model age here is a mixed age, and does not represent a mantle extraction event. This produces a crustal source with a multistage isotopic history. In this situation, data 'arrays' often form between the two sources. These represent magmas with varying degrees of contamination. CHUR, chondritic uniform reservoir.

Spatial evaluation of Sm–Nd isotope data

The temporal analysis of regional Sm–Nd isotopic data presented above documents the crustal history of the individual terranes/domains of the Yilgarn Craton. However, the isotopic data are sorted using an independently derived terrane system (Cassidy *et al.* 2006), developed in conjunction with additional litho-stratigraphic and geochronological data. The use of these datasets, while beneficial in the understanding of the complete tectono-stratigraphic evolution of an area, also introduces an external level of interpretation that may not be truly representative of the isotopic

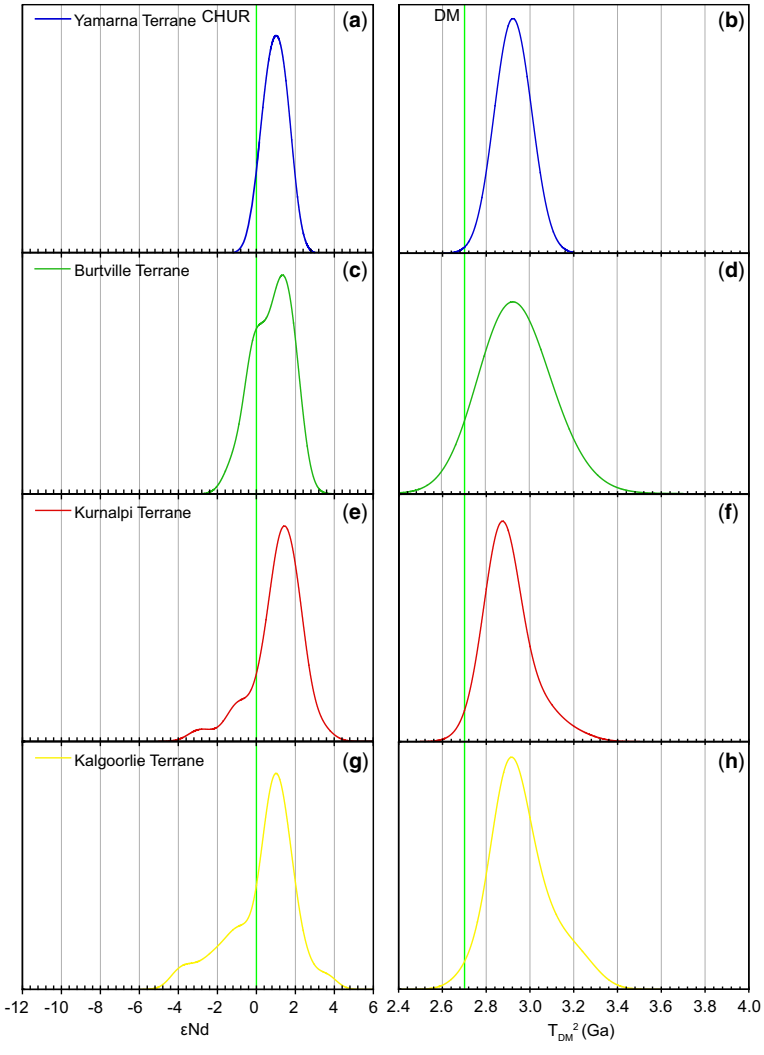

Fig. 5. Probability density plots of Sm–Nd data showing εNd (a, c, e, g) and T_{DM}^2 (b, d, f, h). Data are shown by terrane/domain: (**a**, **b**) Yamarna Terrane; (**c**, **d**) Burtville Terrane; (**e**, **f**) Kurnalpi Terrane; and (**g**, **h**) Kalgoorlie Terrane. The chondritic uniform reservoir (CHUR) and depleted mantle (DM) are shown by the green lines.

history of the crust alone. As a result, the Sm–Nd isotope characteristics (T_{DM}^2 and εNd) were plotted as contour maps (Figs 10 & 11) in order to constrain the spatial relationships in crustal evolution without the use of external datasets. Only granites and felsic volcanic rocks with U–Pb crystallization ages of 2800–2600 Ma were mapped in order to reduce potential mixing signatures between distinct events. As a result, this map represents a snapshot of the lithospheric architecture of the Yilgarn Craton at 2800–2600 Ma.

As well as the T_{DM}^2 and εNd contour maps (Fig. 10a, b), two key isotopic cross sections are plotted (Fig. 11b, c) to show the change in isotopic character of the crust across key sections of the craton. The T_{DM}^2 and εNd values presented in this section are broad regional approximations based on the maps of Figure 10a, b, used in conjunction with Figure 8. Individual sample sites are displayed on the maps, and it is important to account for the location and density of sampling, as they provide a fundamental first-order control on the precision of the contour mapping.

The most striking observation is that, as indicated by previous studies (Champion & Sheraton 1997; Cassidy *et al.* 2002; Champion & Cassidy

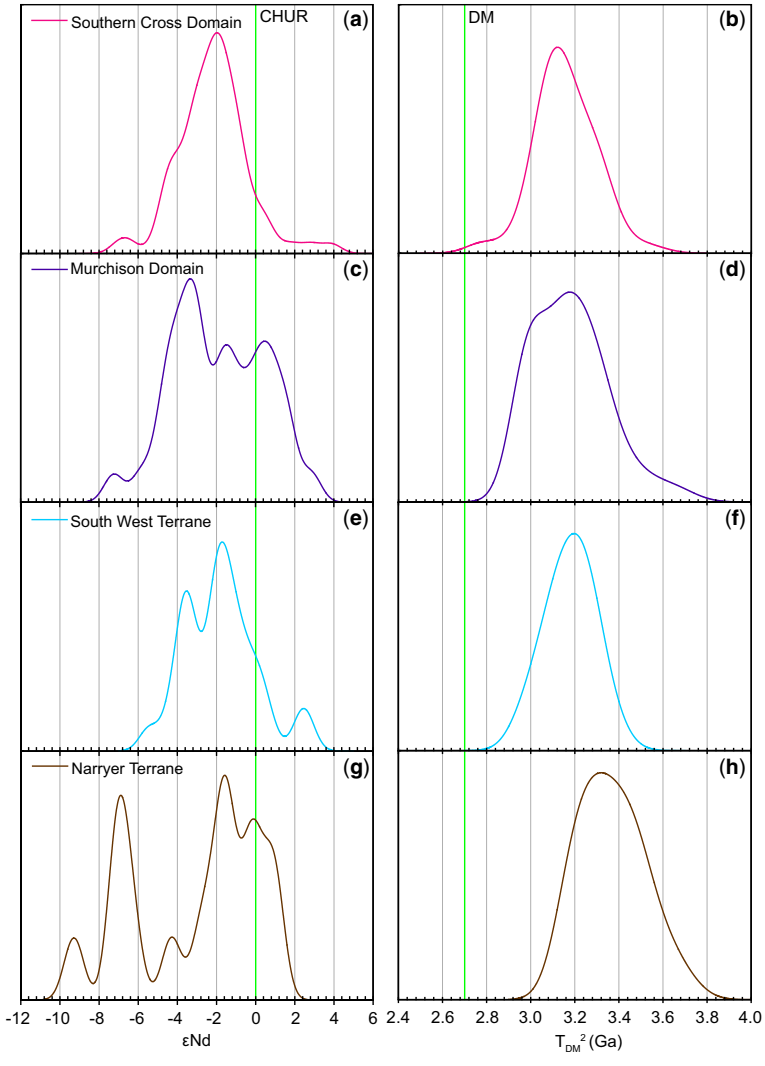

Fig. 6. Probability density plots of Sm–Nd data showing εNd (a, c, e, g) and T_{DM}^2 (b, d, f, h). Data are shown by terrane/domain: (**a**, **b**) Southern Cross Domain; (**c**, **d**) Murchison Domain; (**e**, **f**) South West Terrane; and (**g**, **h**) Narryer Terrane. The chondritic uniform reservoir (CHUR) and depleted mantle (DM) are shown by the green lines.

2007), the Eastern Goldfields Superterrane forms a distinct crustal block, with typical T_{DM}^2 values of *c.* 3000–2700 Ma (Fig. 10b) and εNd of *c.* −0.2 to 3.6 (Fig. 10a). This superterrane is younger and more juvenile than the West Yilgarn, which dominantly consists of crust with T_{DM}^2 of 3300–3000 Ma and εNd of −4.0 to −1.0. The margin between the isotopically distinct West Yilgarn and Eastern Goldfields Superterrane represents a lower crustal boundary between contrasting source regions at the time of granite magmatism. This boundary correlates with the surface expression of the Ida (south: Swager 1997; Drummond *et al.* 2000; Goleby *et al.* 2004, 2006) and Waroonga faults (north; Cassidy *et al.* 2006). This association empirically suggests that these major crustal faults (Drummond *et al.* 2000; Goleby *et al.* 2004, 2006) represent the contact between two proto-cratonic blocks (Cassidy & Champion 2004; Champion & Cassidy 2007), although at present this relationship is unconfirmed. Figure 11b illustrates the significant difference between the West Yilgarn and Eastern Goldfields Superterrane and demonstrates (1) the occurrence of the reworked Southern Cross Domain component within the Kalgoorlie Terrane and (2) the juvenile

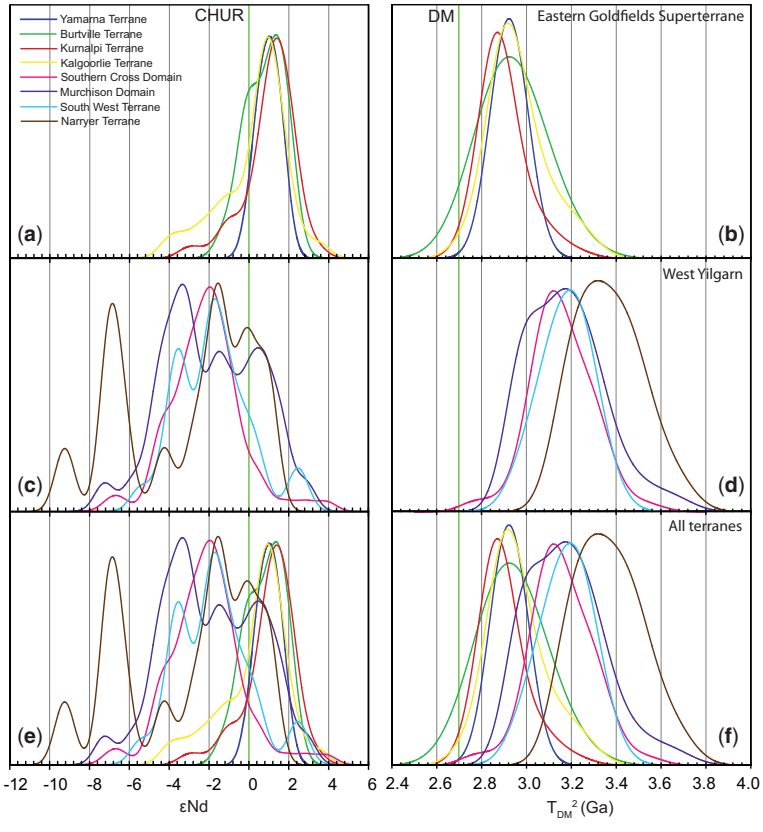

Fig. 7. Comparison of probability density plots of Sm–Nd data from (**a**, **b**) Eastern Goldfields Superterrane; (**c**, **d**) West Yilgarn; and (**e**, **f**) all terranes/domains. εNd (a, c, e) and T_{DM}^2 (b, d, f) are shown. The chondritic uniform reservoir (CHUR) and depleted mantle (DM) are shown by the green lines.

Eastern Goldfields component in the Southern Cross Domain.

As highlighted previously (Fig. 8c), the Kurnalpi Terrane has an older, reworked component at *c.* 2680–2670 Ma, which has a T_{DM}^2 of *c.* 3200–2800 Ma and εNd values from −3.2 to 1.8. Figure 10 shows that this older component forms a relatively old 'block' of crust at the margin between the Kurnalpi and Burtville Terranes, and may be the result of reworking associated with terrane amalgamation, or alternatively a small fragment/sliver of older crust sitting at the terrane boundary. To the west, the structural boundaries of the Kurnalpi Terrane (Cassidy *et al.* 2006) correlate with a north–south belt of young, relatively juvenile crust with T_{DM}^2 values of *c.* 2900–2700 Ma and εNd of *c.* 1.0 to 3.0.

In contrast, the Kalgoorlie Terrane demonstrates a mixed source as identified in the temporal analysis section (Fig. 8d). The eastern side of the terrane dominantly comprises young, juvenile material similar in age to that of the Kurnalpi Terrane. The T_{DM}^2 and εNd values increase and decrease, respectively, from east to west with the increasing interaction and addition of the older Southern Cross Domain component (Fig. 10a, b).

Furthermore, there is subtle variation along the north–south isotopic margin between the Kalgoorlie Terrane and Southern Cross Domain. In the south and north Kalgoorlie Terrane, the juvenile material extends close to the surface positions of the Ida and Waroonga faults, respectively, specifically in the areas underlying the Agnew–Wiluna and Kalgoorlie–Norseman greenstone belts. However, in the central Kalgoorlie Terrane, there is a 200–150 km embayment in this isotopic margin where older material extends further east into the Kalgoorlie Terrane, shifting the north–south-trending isotopic boundary eastward (see Figs 10–13). This feature correlates spatially with the poorly mineralized area between the gold–nickel-rich Agnew–Wiluna and Kalgoorlie–Norseman greenstone belts (Figs 3, 12 & 13; Thébaud *et al.* 2012). Unlike elsewhere in the Kalgoorlie Terrane,

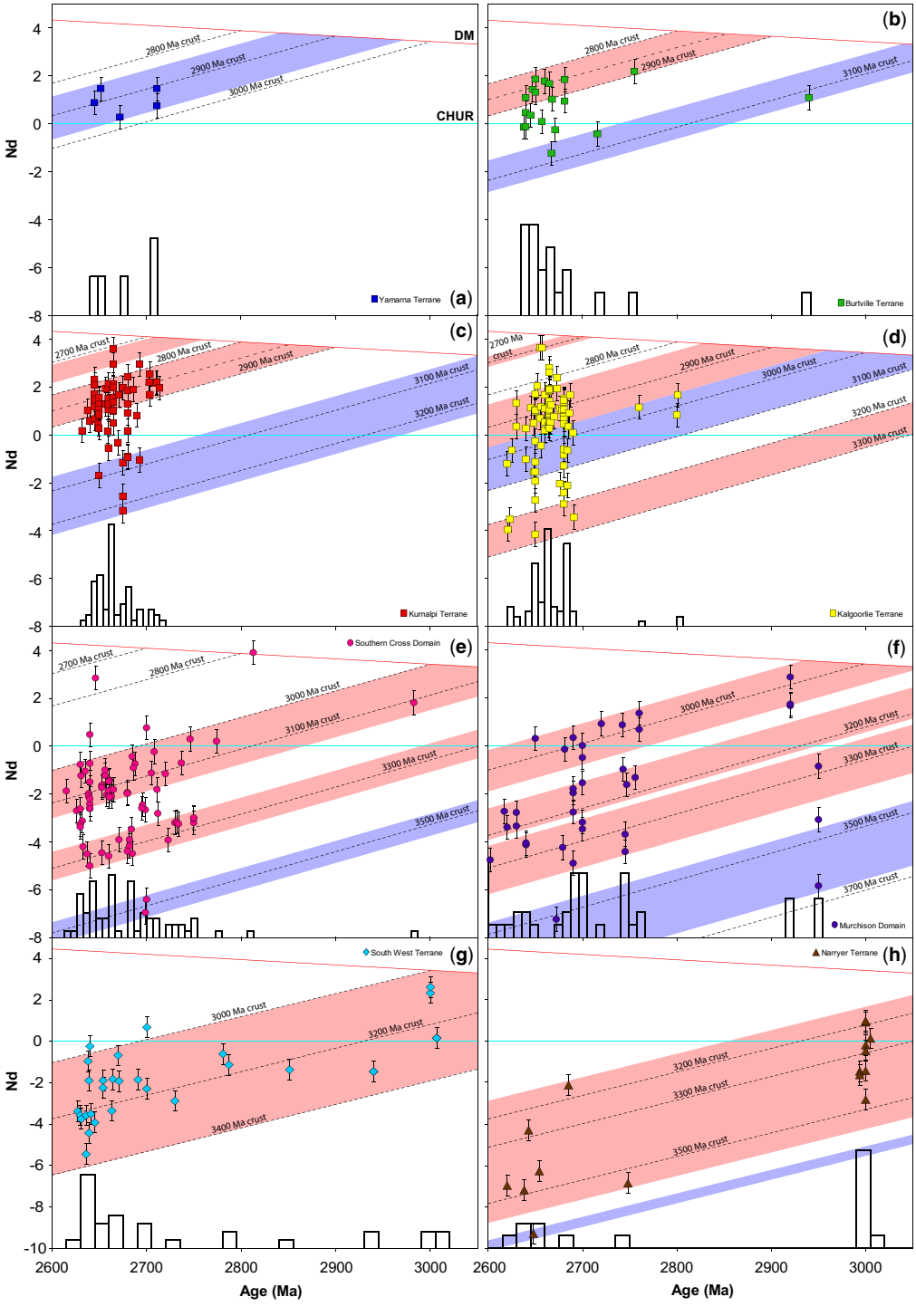

Fig. 8. Sm–Nd isotope data (as εNd) v. age for all samples from the Yilgarn Craton (see Table 2). The data are sorted by terrane/domain: (**a**) Yamarna Terrane; (**b**) Burtville Terrane; (**c**) Kurnalpi Terrane; (**d**) Kalgoorlie Terrane; (**e**) Southern Cross Domain; (**f**) Murchison Domain; (**g**) South West Terrane; and (**h**) Narryer Terrane. The chondritic uniform

this area does not contain high-MgO komatiites or associated nickel sulphide deposits (Fig. 13). As a result, this feature appears to have a significant physical control on geological processes and features of the terrane.

In contrast to the relatively homogenous isotopic character of the Eastern Goldfields Superterrane, the West Yilgarn is heterogeneous with respect to spatial variations in crustal source, creating a more complex, intra-cratonic lithospheric architecture. As a result, a number of discrete crustal blocks can be identified that do not generally match the terrane subdivision of Cassidy *et al.* (2006). This is probably because the current terrane structure was dominantly controlled by late, major tectono-thermal and structural events in the Yilgarn at *c.* 2680–2620 Ma (Cassidy *et al.* 2002, Champion & Cassidy 2007; Mole *et al.* 2012), whereas the Nd isotopic map contains time-resolved information that accounts for previous tectonic and magmatic events. The crustal blocks identified here (Figs 10 & 11) may represent preserved cratonic elements that collectively form the West Yilgarn proto-craton.

The Southern Cross Domain is characterized by a northern area with T_{DM}^2 values of *c.* 3400–3200 Ma and εNd of −6.0 to −1.0, and a less evolved southern region with T_{DM}^2 values of *c.* 3200–3000 Ma and εNd of −2.0 to 0. The northern, more reworked area is designated as the Marda block, and the southern area as the Lake Johnston block (Fig. 11a).

The north–south isotopic cross-section of the crust across the craton (Fig. 11c) displays similar features to that observed across the West Yilgarn–Eastern Goldfields Superterrane boundary (Fig. 11b). The crustal εNd values decrease significantly to the north of the Lake Johnston block margin, which occurs at the southern edge of the Marda greenstone belt. The Marda block contains a small component of the Lake Johnston block and vice versa, suggesting that their source regions interacted during tectono-thermal development of the region.

Available T_{DM}^2 and εNd data from the South West Terrane largely suggest it has a similar crustal history to the Lake Johnston block, although the northern boundary (around the Koolanooka fault; Fig. 10a, b) is more similar to the Marda block. This suggests that the reworked Marda block may extend west across the West Yilgarn into the South West Terrane (Figs 10 & 11), cross-cutting previously proposed terrane/domain boundaries including the Southern Cross–Murchison Domain and Youanmi–South West Terrane boundaries. This is in agreement with the assertion of Cassidy *et al.* (2006) that many of the domain/terrane boundaries are the structural expression of late tectono-thermal events in the Yilgarn Craton.

The crust of the Murchison Domain appears to have two spatially distinct crustal sources, which correlate with the T_{DM}^2 values of the *c.* 3400, 3200 and 3000 Ma groups identified previously (Fig. 8f). The *c.* 3400 group is very minor and spatially difficult to discriminate from the 3200 Ma (εNd −3.9 to −2.2) group, which is generally restricted to the margins of the domain. The T_{DM}^2 3000 Ma (εNd −1.0–1.6) source dominates the central to northern area of the domain and forms a band of relatively juvenile crust (Cue Domain of Cassidy & Champion 2004) previously identified by Cassidy *et al.* (2005), Champion & Cassidy (2007) and Ivanic *et al.* (2010, 2012), which is flanked by regional structures (i.e. Carbar, Big Bell, Cuddingwarra and Mt Magnet faults) of the same orientation (Spaggiari 2006; Van Kranendonk & Ivanic 2008). This NE to SW band of juvenile crust has been interpreted as a failed continental rift (Ivanic *et al.* 2010). It is unlikely to represent a back-arc rift formed during the docking of the Narryer Terrane, as this amalgamation probably occurred at 2750–2650 Ma, along the Balbalinga Fault (Occhipinti *et al.* 2001), which is later than the inferred age of the rift (*c.* 3000–2800 Ma). The majority of the greenstone sequences in this domain occur within this 'rift' zone (i.e. Meekatharra–Wydgee belt; Spaggiari 2006), and the large layered intrusions of the Murchison Domain (Ivanic *et al.* 2010) occur on its flanks (Figs 10 & 11). The rift may have been formed at *c.* 2810–2800 Ma during the emplacement of the mafic–ultramafic intrusions (e.g. Windimurra; Cassidy & Champion 2004; Ivanic *et al.* 2010), which would have required significant crustal thinning to create space for the large magma volumes as well as the ascent of mantle-derived magmas (Ivanic *et al.* 2010). Alternatively, this event may have

Fig. 8. (*Continued*) reservoir (CHUR) and depleted mantle (DM) are shown by the blue and red lines, respectively. Error bars are ±0.5 εNd units, calculated using the average available analytical error on the $^{143}Nd/^{144}Nd$ analysis. Histograms of U–Pb geochronology are also shown for each terrane/domain. Some ages used for these histograms were acquired using stratigraphic, cross-cutting and/or structural relationships; these are highlighted in Table 2. Hence, although most ages presented here are U–Pb SHRIMP on zircon and the age groups plotted agree with previous studies (Mole *et al.* 2012, Cassidy *et al.* 2002, Champion & Sheraton 1997), these groups should be used tentatively. Crustal reservoirs referred to in the text are shown, where blue indicates the initial crust in the terrane (where known) and red highlights later additions of juvenile or ancient crustal material and the subsequent mixed reservoirs.

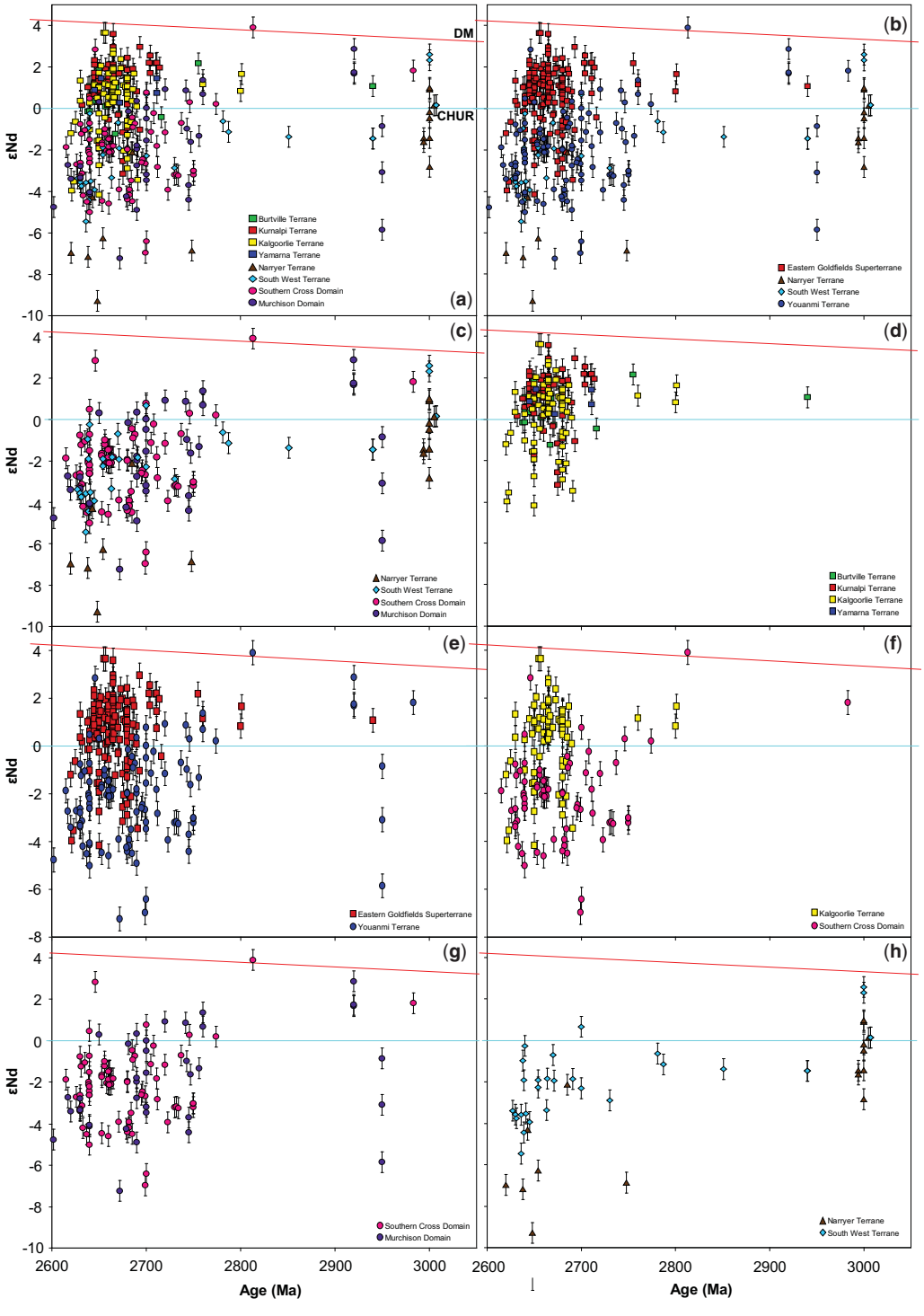

Fig. 9. Comparison of Sm–Nd isotope data (as εNd) between different terranes/domains of the Yilgarn Craton: (**a**) all terranes; (**b**) all Eastern Goldfields Superterrane, Narryer, South West and Youanmi Terranes; (**c**) Narryer, South West and Youanmi Terranes (Southern Cross and Murchison Domains); (**d**) all Eastern Goldfields terranes; (**e**) Eastern

reactivated a *c.* 3000 Ma rift, which created the *c.* 2940 Ma juvenile material (Fig. 8f). This scenario appears more likely, as the majority of the crust within the rift has a T_{DM}^2 of *c.* 3000 Ma (Figs 8f & 10b).

In the NW corner of the Yilgarn Craton, the Narryer Terrane is by far the oldest crustal block based on Nd isotope data, with T_{DM}^2 ages >3300 Ma and up to *c.* 3700 Ma (εNd −9.0 to −4.0) consistent with the occurrence of the oldest granites and mafic magmatic rocks in the Yilgarn Craton (Kinny *et al.* 1988; Nutman *et al.* 1993, 1991).

Discussion

Evaluation of Sm–Nd data in space and time

The data collected in this study and corresponding analysis presented in the results section can be used to evaluate the crustal history of the individual terranes that make up the Yilgarn Craton. The potential geodynamic settings driving this crustal evolution are suggested where possible. The Nd isotopic system differentiates between crust and mantle sources for magmas, and subsequently cannot uniquely discriminate between all tectonic settings, only those which require juvenile input (continental rift, island arc, back-arc, plume magmatism) or crustal melting (collisional orogenies, continental arcs).

Eastern Goldfields Superterrane: Yamarna Terrane. The Sm–Nd data from the Yamarna Terrane cluster relatively tightly above CHUR at 0.7 to 1.4 εNd and T_{DM}^2 of *c.* 2950–2850 Ma and shows little variation toward more juvenile or reworked ages. Based on this data distribution, it appears that the Yamarna Terrane was extracted from the mantle at *c.* 2950–2850 Ma. The possibility of crustal source mixing was disregarded based on the juvenile (εNd) and clustered nature of the data, together with the lack of any pre-existing >2900 Ma crust. This suggests that the model age represents a real crustal growth event. This theory could be further evaluated by collecting Sm–Nd and/or Lu–Hf isotopes from supracrustal rocks of this terrane, which span a considerable geological history (>2832–2630 Ma; Pawley *et al.* 2012). Understanding of this terrane is at an early stage, and as the available dataset is very small, the interpretation presented here should be considered speculative.

Eastern Goldfields Superterrane: Burtville Terrane. The Nd isotope distribution of the Burtville Terrane could be interpreted using a number of crustal evolution models:

(1) *Evolution of the crust from a single source*. This appears unlikely owing to the spread in Sm–Nd data and the observation of two sources prior to 2700 Ma with T_{DM}^2 2900 Ma (at 2755 Ma) and 3100 Ma (at 2940 Ma). In addition, if the crust of this terrane was derived from a mantle extraction event at the dominant T_{DM}^2 age of *c.* 2900–2850 Ma, the 2940 Ma sample should record a depleted mantle signature and represent the original crust, which is not the case (Fig. 8b).

(2) *Derivation of the crust of the Burtville Terrane from multiple crustal sources*. Initially, at *c.* 2940 Ma, the crust had a T_{DM}^2 of *c.* 3100 Ma and εNd 1.1 (Figure 8b). At some point between 2940 and 2755 Ma, this crust was rejuvenated by the addition of juvenile material, speculated here to occur at 2810–2750 Ma, corresponding with highly juvenile Lu–Hf data from the Mapa Igneous Complex and Swincer Dolerite (Wyche *et al.* 2012*b*; Pawley *et al.* 2012), as well as the juvenile sample at *c.* 2755 Ma in Figure 8b. The Hf data from the *c.* 2812 Ma Swincer Dolerite (Pawley *et al.* 2012) support the crustal mixing model suggested here, showing εNd values ranging from −2.9 to +6.3 (Wyche *et al.* 2012*b*). This mixed reservoir was later reworked during the <2755 Ma granite events. This model explains the range of T_{DM}^2 ages for these later granites. As a result, at <2700 Ma, the majority of granites were formed by reworking of a mixed 2950–2850 Ma reservoir.

If the crustal history presented above is accurate, it suggests that a tectono-thermal event at *c.* 2900–2800 Ma led to the input of juvenile material into older *c.* 3100 Ma crust. The Duketon komatiites (Duketon greenstone belt; Fig. 1a) are dated at *c.* 2805 Ma (Kositcin *et al.* 2008), and these ultramafic lavas may represent the surface manifestation of a mantle plume. Crustal attenuation and thinning associated with this plume may have led to intracontinental rifting at this time, and the addition of juvenile mantle material into the crust.

Eastern Goldfields Superterrane: Kurnalpi Terrane. The Kurnalpi Terrane has a less extensive magmatic

Fig. 9. (*Continued*) Goldfields Superterrane and Youanmi Terrane; (**f**) Kalgoorlie Terrane and Southern Cross Domain; (**g**) Youanmi Terrane; and (**h**) Narryer and South West Terranes. The chondritic uniform reservoir (CHUR) and depleted mantle (DM) are shown by the blue and red lines, respectively. Error bars are ±0.5 εNd units, calculated using the average available analytical error on the $^{143}Nd/^{144}Nd$ analysis.

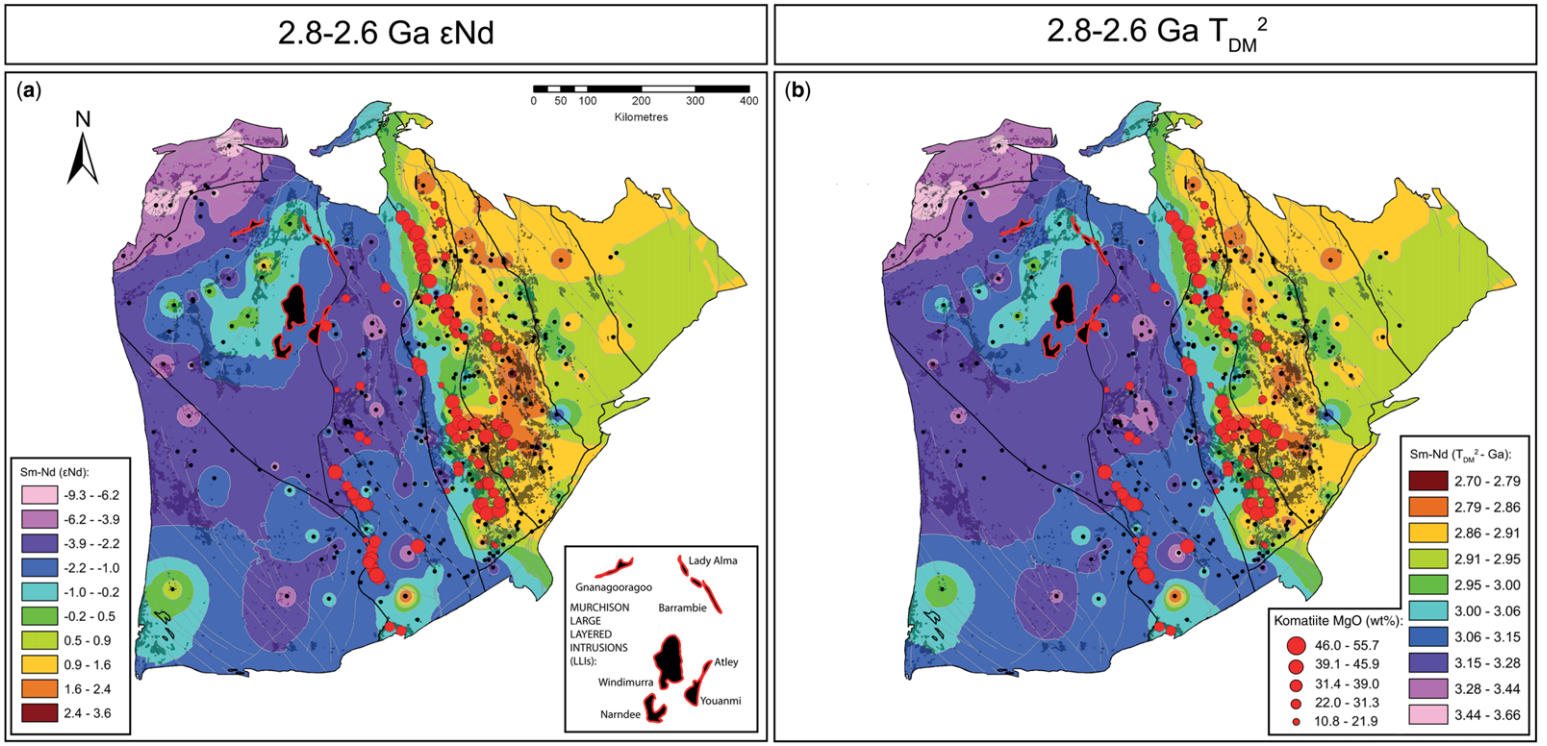

Fig. 10. Sm–Nd isotopic contour maps showing the spatial variation of εNd and T_{DM}^2 values from granitic (**a**) εNd data mapped using the geometric interval (GI) method, where all groups are sized using a geometric series that highlights the differences between areas and removes the effects of extreme values; (**b**) T_{DM}^2 data also mapped using the geometric interval (GI) method. The location and corresponding average MgO (plus standard deviation) content is shown for all komatiites (both *c.* 2.9 and 2.7 Ga), and the locations of the Murchison large layered intrusions are also plotted. Isotopic contour maps were produced using the inverse distance weighted interpolation method in ArcGIS®. This method, which used 15 nearest neighbours (minimum of 10) at a 'power' of 2, produced the most robust spatial representation of the isotopic dataset. Other methods, such as kriging, were not viable owing to the relatively small dataset. Data were grouped using the geometric interval method (a protocol built into ArcGIS®). This method designates class breaks based on intervals that have a geometrical series. This ensures that each class range has approximately the same number of values and that the change between intervals is fairly consistent. This algorithm, which was specifically designed to accommodate continuous data such as the isotope data, produces a result that minimizes variance within classes, and can even work reasonably well on data that are not normally distributed. As a result, this method enhances the contrast among different crustal regions as it accounts for extreme values and designates groups and group size accordingly.

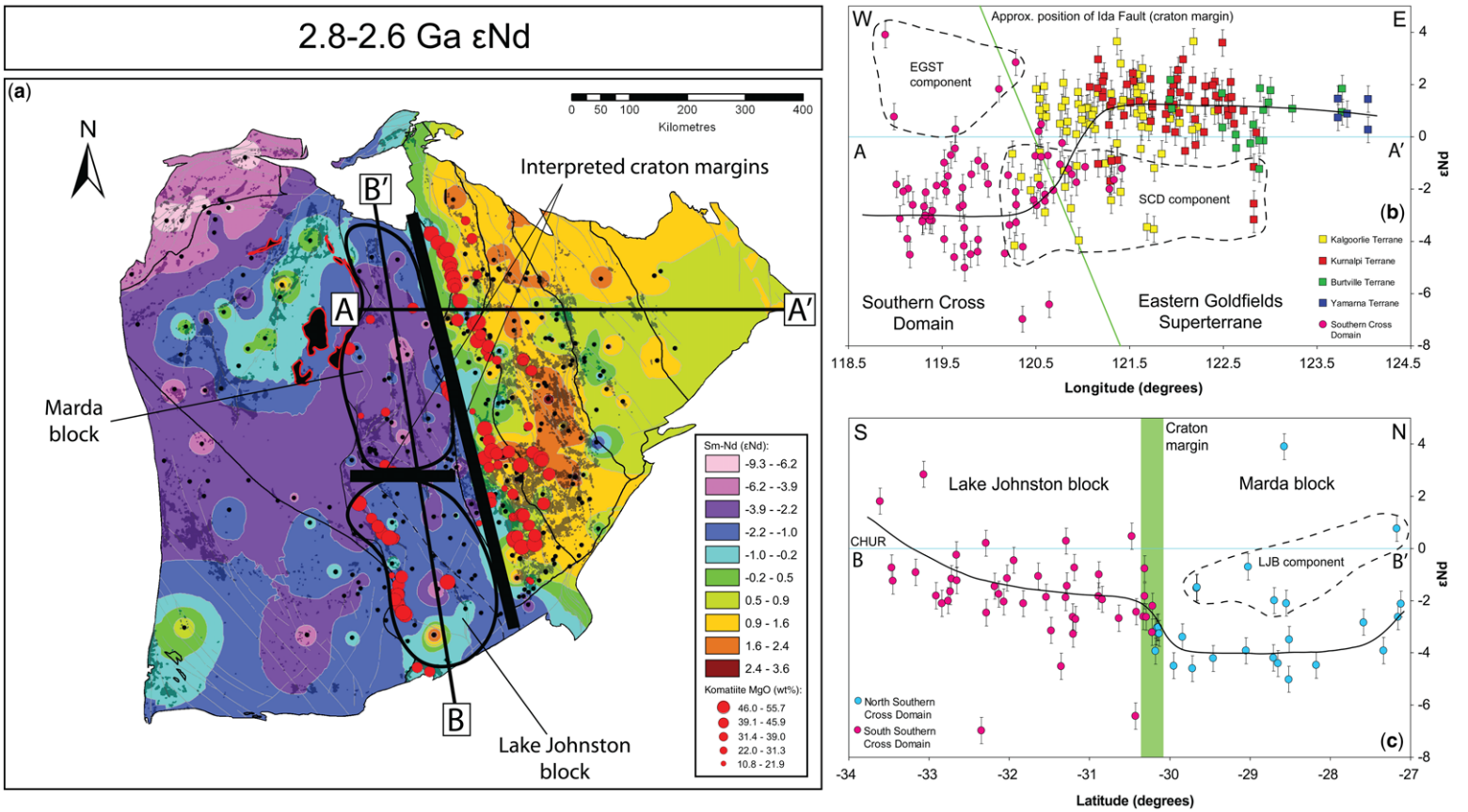

Fig. 11. This diagram illustrates how the spatial use of Sm–Nd can highlight the position and extent of craton margins within an area: (**a**) εNd contour map (geometric interval; 2.8–2.6 Ga) showing the position of inferred craton margins (thick black bars), the delineation of different crustal blocks (i.e. the Marda and Lake Johnston blocks of the Southern Cross Domain) and the orientation of isotopic cross sections through regions of crust shown by (b) and (c). The cross section lines are not typical in that they represent not only isotopic data along that line but also areas adjacent to the line, in order to constrain the full north–south or east–west variation in Sm–Nd isotopic values between different terranes/domains. (**b**) Diagram of an east–west isotopic section (A–A′) from the Yamarna Terrane in the east to the Southern Cross Domain in the west, as shown by (a). EGST, Eastern Goldfields Superterrane; SCD, Southern Cross Domain. (**c**) Diagram of a north–south isotopic section (B–B′) through the Southern Cross Domain. Both these sections highlight and constrain craton margins identified in the maps. LJB, Lake Johnston block.

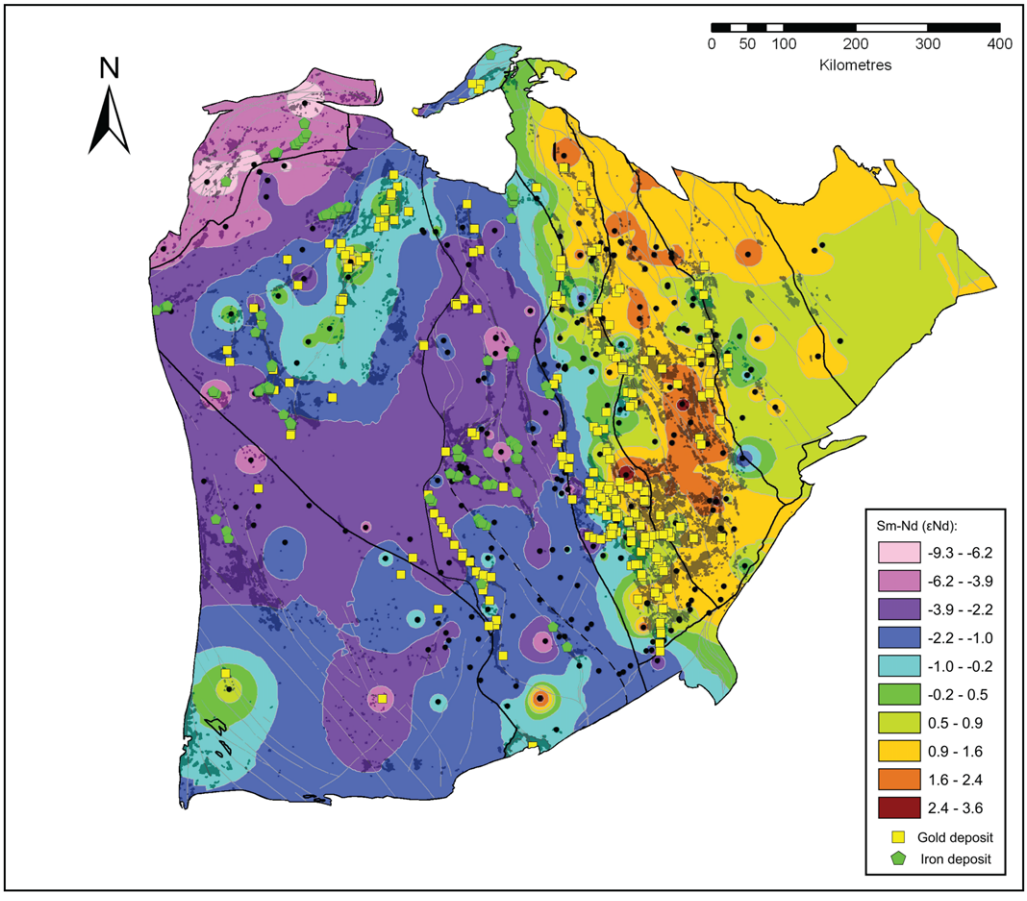

Fig. 12. Sm–Nd (εNd) isotopic map (geometric interval) showing the location of gold and iron deposits (see legend).

history than most other terranes, especially those of the West Yilgarn, with the oldest sample presented here dated at 2714 Ma. The evolution of this terrane occurred through a series of felsic magmatic events constrained by U–Pb data (Fig. 8c):

(1) The 2715–2700 Ma felsic magmatism has an εNd of 2.0 and was derived from reworking of a source with T_{DM}^2 *c.* 2850 Ma. Data from this event forms a tight cluster suggesting little to no mixing, possibly associated with the establishment of a rift between the Burtville and Youanmi Terranes. At the initiation of the extension, juvenile melts would be contaminated by *c.* 3100–2900 Ma Burtville crust; a feature not shown by the data in Figure 8c. However, Lu–Hf data for this >2700 Ma period (Mole 2012; Wyche *et al.* 2012b) demonstrate *c.* 3300–2900 Ma model ages. This suggests that the Sm–Nd samples presented here preserve the more juvenile component, and may have come from the rift axis rather than the margins.

(2) The 2680–2670 Ma magmatic event represents significant reworking and interaction with an older crustal component with T_{DM}^2 *c.* 3200 Ma. This reworked material is spatially localized at the margins of the Kurnalpi Terrane, suggesting it is sourced from the adjacent Burtville and Kalgoorlie Terranes. The >3100 Ma material is interpreted as 'initial crust' in Figure 8c, suggesting it may represent an older end member of Burtville Terrane crust. However, it may also have been sourced from the Southern Cross Domain (Fig. 11b). This suggests collisional tectonics and crustal thickening associated with the possible closure of a rift or rifts at these margins. This is supported by a transition in the composition of supracrustal rocks from mafic volcanics/intrusives, calc-alkaline complexes and feldspathic sedimentary rocks

at 2720–2700 Ma to bimodal rhyolite–basalt volcanism and felsic alkaline complexes at 2690–2680 Ma (Cassidy *et al.* 2006; Barley *et al.* 2008). This older, *c.* 3200 Ma component may represent thinned Burtville Terrane crust which has been overwhelmed with juvenile input at *c.* 2720 Ma.

(3) The 2666–2660 Ma event represents the resumed reworking of the 2900–2800 Ma (εNd 2.0 to 1.0) source. Older material present during the 2680–2670 Ma event is significantly less abundant, with only a minor T_{DM}^2 3000 Ma component observed. There is also evidence of a highly juvenile component with T_{DM}^2 *c.* 2700 Ma and εNd 3.6. The juvenile addition at this time, together with the reduced abundance of the older crustal component, suggests that collision/rift closure associated with the Burtville Terrane had ceased and that extension may have resumed.

(4) The final event, at 2650–2640 Ma, demonstrates reworking of the original *c.* 2900–2800 Ma source and represents the final cratonizing event in this terrane, 20–10 Ma earlier than in most other terranes (*c.* 2640–2620 Ma).

Eastern Goldfields Superterrane: Kalgoorlie Terrane. The oldest samples for the Kalgoorlie Terrane have U–Pb ages of 2801–2760 Ma, indicating a pre-2700 Ma crustal source of T_{DM}^2 3100–3000 Ma, similar to those of the Burtville Terrane and the older component of the Kurnalpi Terrane (Fig. 8c). This material may represent pre-existing Burtville Terrane crust which was thinned during extension at *c.* 2720 Ma. Felsic magmatism, while known to occur at 2720–2700 Ma in the Agnew–Wiluna belt (Barley *et al.* 2003; Kositcin *et al.* 2008), is relatively rare in comparison to the Kurnalpi Terrane, and is not represented in this dataset. This indicates the predominance of plume-derived mafic–ultramafic magmatism at this time (Claoué-Long *et al.* 1988; Nelson 1997; Barley *et al.* 2003; Cassidy *et al.* 2006). Subsequently, the felsic magmatic activity for this terrane occurs in four well-defined, overlapping events between 2690 and 2620 Ma:

(1) The first event occurs at *c.* 2685–2680 Ma and forms an array of T_{DM}^2 and εNd at *c.* 3300–2900 Ma and −2.9 to 1.7, respectively. This suggests that juvenile input, probably during the *c.* 2700 plume event, has occurred since 2760 Ma, reducing the T_{DM}^2 from *c.* 3100–3000 Ma. Despite this, significant reworking dominates this event, with the addition of an unradiogenic crustal component with T_{DM}^2 *c.* 3300 Ma. Based on Figures 10 and 11, it is likely that the juvenile addition and reworking signatures are spatially controlled, with the more juvenile source occurring in the east of the terrane and reworked magmas occurring in the west. The reworked areas are likely to be part of, or heavily contaminated by, the Southern Cross Domain (Champion & Sheraton 1997; Cassidy *et al.* 2002; Czarnota *et al.* 2010). In terms of geodynamics, the Sm–Nd array could represent crustally contaminated melts from the retreating or collapsing (Kumagai *et al.* 2007; Kumagai *et al.* 2008) *c.* 2700 Ma plume (Campbell & Hill 1988), or tectonic movement of the crust away from plume-sourced juvenile material. The process may have been coupled with the closure of the rift basin formed during komatiite emplacement and collision of the Eastern Goldfields and West Yilgarn proto-cratons.

(2) The second recorded magmatic event in the Kalgoorlie Terrane occurred at 2670–2660 Ma and appears to be more juvenile in nature, dominantly consisting of material with T_{DM}^2 3000–2800 Ma and εNd of 0.3 to 2.8. There is also a minor T_{DM}^2 *c.* 2700 Ma component which correlates with the *c.* 2700 Ma plume event, inferring crustal growth directly related to a mantle plume (Fig. 8d). The absence of the 3300–3200 Ma component indicates that the influence of the Southern Cross Domain waned during this period, possibly due to rifting of the Kalgoorlie Terrane away from the West Yilgarn. Alternatively, melting may have shifted to a deeper, more juvenile reservoir formed during previous plume magmatism. This scenario would correspond with deeper thermal effects of a retreating/collapsing plume.

(3) The third event occurred at 2655–2650 Ma and displays a similar Nd array to that of the 2685–2680 Ma event. While High-Ca granites are still abundant, the Low-Ca group begins to dominate at *c.* 2655 Ma (Cassidy *et al.* 2002) and felsic volcanism terminates (Kositcin *et al.* 2008), suggesting a major tectono-thermal change at this time (Cassidy *et al.* 2002, Champion & Cassidy 2007; Czarnota *et al.* 2007; Mole *et al.* 2012). In terms of geodynamics, this may be due to shallower melting of a more reworked source, as suggested by the chemistry of the Low-Ca granites (Champion & Sheraton 1997; Cassidy *et al.* 2002). Alternatively, reduced melt production and decreased mantle input associated with the 'retreat' of the mantle plume, together with crustal thickening associated with rift closure, may have led to an increase in crustal reworking.

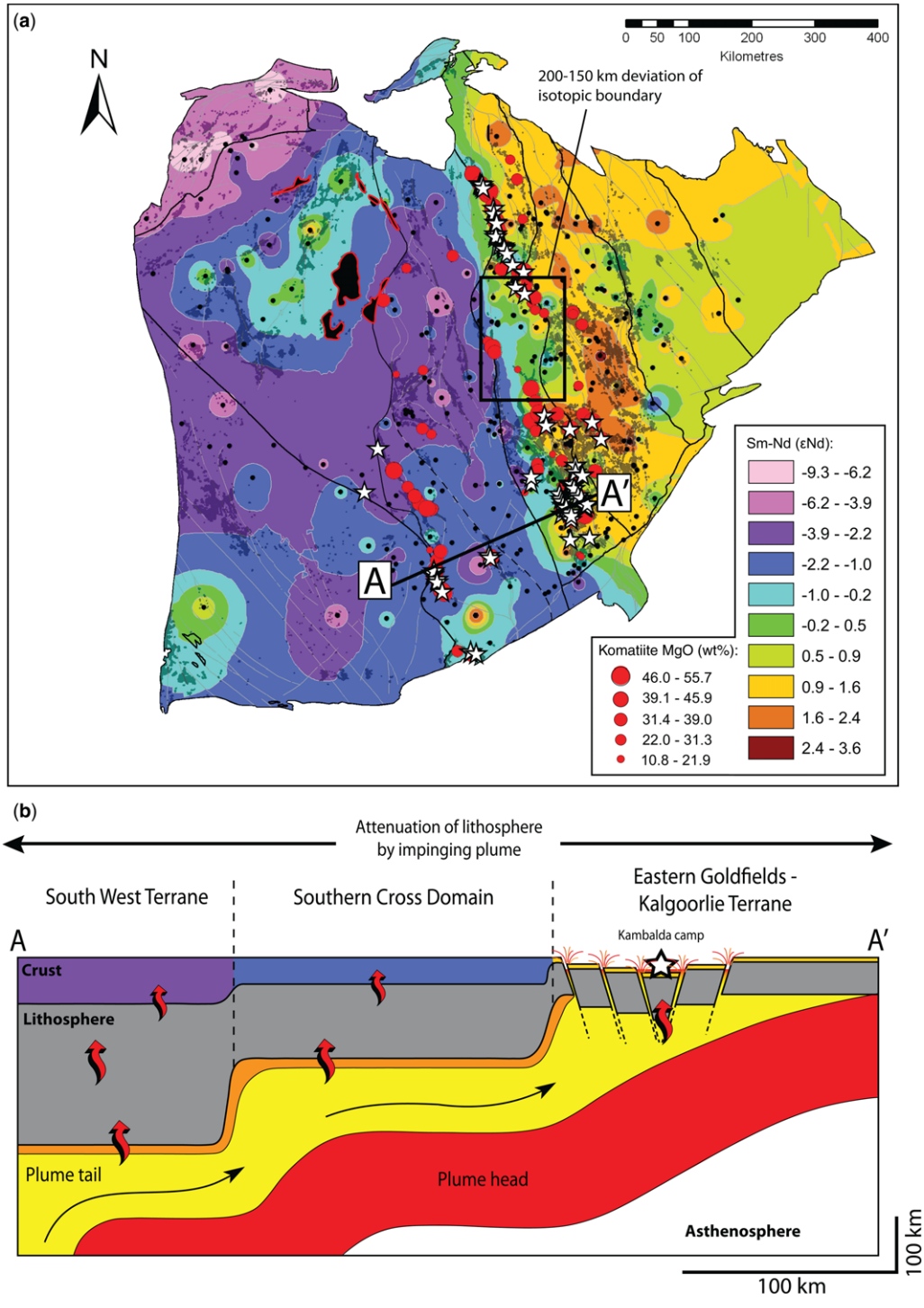

Fig. 13. (**a**) Sm–Nd (εNd) isotopic map (geometric interval) showing the location of komatiite-hosted nickel deposits (see legend). The *c.* 2.7 Ga komatiites occur to the east of the Ida Fault, whereas the *c.* 2.9 Ga komatiites and deposits occur to the west. Komatiite-hosted nickel deposits are also shown as white stars. (**b**) Interpreted lithospheric

(4) The fourth and final event at 2635–2620 Ma displays further reworking, with data clustered on the *c.* 3000 and 3200 Ma T_{DM}^2 lines. This event infers that the cratonizing granites of the Kalgoorlie Terrane intruded relatively late, *c.* 20–10 myr after those in the other terranes of the Yilgarn Craton with the exception of the South West Terrane, with which they are synchronous (Sircombe *et al.* 2007).

Although the Kalgoorlie Terrane appears to be more reworked than the Kurnalpi Terrane (Fig. 10), Figures 9d and 11b show that, if the contaminated material associated with the Southern Cross Domain is removed, the terranes have a similarly juvenile signature. This suggests that both terranes had similar juvenile histories prior to the contamination of the west Kalgoorlie Terrane with material from the Southern Cross Domain at *c.* 2685 Ma.

Youanmi Terrane: Southern Cross Domain. This domain is characterized by two spatially distinct crustal domains, with the T_{DM}^2 *c.* 3300 Ma Marda block in the central-north of the domain, and the T_{DM}^2 *c.* 3100 Ma Lake Johnston block in the south (Fig. 11a). This, together with the occurrence of younger T_{DM}^2 *c.* 2800 Ma (εNd 2.8 to 3.9) and older *c.* 3500 Ma (εNd −7.0) material, suggests that multiple crustal sources were involved during the evolution of this domain.

Despite these observations, the crustal reservoirs of the Southern Cross Domain remain fairly consistent through time, suggesting that the older 3500 Ma source was very minor and/or almost completely rejuvenated by the input of younger material. As the *c.* 3100 Ma source of the Lake Johnston block can be traced back to 2983 Ma (Fig. 8e), it appears that this T_{DM}^2 is representative of a crustal growth (mantle extraction) event, which may have assimilated the 3500 Ma component. In the Marda block, T_{DM}^2 ages of *c.* 3300 Ma suggest that either mantle input at 3100 Ma was less extensive in this area, or that this crust was extracted earlier.

These scenarios assume a pre-existing *c.* 3500 Ma crust in both blocks, as suggested by single data points (Figs 8e & 10) and >3400 Ma zircon xenocrysts found in granites from these blocks (Cassidy *et al.* 2002; Mole 2012; Mole *et al.* 2012). This is especially likely in the Marda block, where Lu–Hf data on zircon indicated model ages >4000 Ma (Wyche *et al.* 2012*b*), and detrital zircons from basal quartzite units are 4350–3130 Ma (Wyche *et al.* 2004).

As with the terranes of the Eastern Goldfields Superterrane, the Southern Cross Domain displays a series of overlapping magmatic events:

(1) The first, at 2750–2700 Ma, is diffuse and forms two broad, spatially controlled groups. The Lake Johnston block displays a less reworked signature (*c.* εNd −2 to 0.8), while the Marda block consists mainly of crust with T_{DM}^2 ages of *c.* 3300 Ma (εNd *c.* −4.0).
(2) The second event at 2690–2680 Ma forms two groups clustered at T_{DM}^2 ages of *c.* 3050 and 3300 Ma (Fig. 8e). Magmatism in this event again appears to be spatially controlled, with each block reworking its respective pre-existing crust. This period correlates with the 2685–2680 Ma reworking period in the Kalgoorlie Terrane, suggesting some form of collisional event between the two blocks (Fig. 9f).
(3) The third event at *c.* 2665–2650 Ma dominantly displays reworking of the *c.* 3100 Ma source, suggesting that felsic magmatism at this time was mainly restricted to the Lake Johnston block. This event correlates with the juvenile pulse observed for the Kalgoorlie and Kurnalpi Terranes, suggesting a shared felsic magmatic event that tapped different source regions.
(4) The fourth magmatic event at *c.* 2640–2630 Ma forms an almost continuous array of Nd-isotope compositions from εNd *c.* −5.0 to −1.0 and T_{DM}^2 ages 3300–3100 Ma, indicating that crustal granites were tapping the source regions of both the Marda and Lake Johnston blocks (Fig. 9a–c), producing magmas with mixed isotopic compositions and suggesting that these blocks had amalgamated.

Youanmi Terrane: Murchison Domain. The Murchison Domain shows broadly similar crustal source

Fig. 13. (*Continued*) cross-section based on the Sm–Nd isotopic mapping and sections of Figure 12. This diagram demonstrates the changing lithospheric architecture between terranes of different isotopic composition and history. The thicker, older crust to the west is inferred to have focused the plume into the shallower area to the east as demonstrated here. This either created a set of rift-related terranes in the Kalgoorlie–Kurnalpi Terranes or reactivated a previous margin, which allowed high flux passage of hot, pre-existing komatiitic magmas to the surface. A similar process is inferred to have formed the *c.* 2.9 Ca komatiites and associated deposits in the Southern Cross Domain, but this cannot be proven using Sm–Nd isotopes as this map only covers the 2.8–2.6 Ga period. The approximate thickness of developed Archaean lithosphere (*c.* 250–150 km) was taken from Boyd *et al.* (1985) and Begg *et al.* (2009). The approximate scale of the plume head (*c.* 1600 km), tail (200–100 km) and thickness (150–100 km) were taken from Campbell *et al.* (1989) and Barnes *et al.* (2012). These values are proxies based on modern analogues and experiments.

characteristics to those of the Southern Cross Domain (Fig. 9g). However, the Murchison Domain appears to display a more well-defined temporal grouping, with four major felsic magmatic events:

(1) The oldest event occurs at *c.* 2950–2920 Ma and indicates that the crust of the Murchison Domain was already reworked, with a maximum T_{DM}^2 of 3700 Ma and εNd −5.9 at 2950 Ma. However, the occurrence of relatively juvenile material at *c.* 2920 Ma (T_{DM}^2 of *c.* 3000 Ma and εNd of *c.* 2.0) suggests juvenile input into older, heterogeneous crust. This interpretation is supported by the Lu–Hf data of Ivanic *et al.* (2012), which showed evidence for pre-existing 3800–3700 Ma crust and mantle input at *c.* 3040 Ma as well as mixing between a juvenile (mantle) source and a reworked, *c.* 3800–3700 Ma source at 2980 Ma. This juvenile input at *c.* 3000 Ma possibly represents the opening of the NE–SW 'rift' zone (see Figs 10 & 11) within pre-existing 3700–3300 Ma crust, and formation of the 2960–2930 Ma Golden Grove Group greenstone sequence (Wang *et al.* 1998, Spaggiari 2006; Van Kranendonk & Ivanic 2008). This juvenile zone possibly represents a 'failed continental rift' as postulated by Ivanic *et al.* (2010), and may have been reactivated during the emplacement of the *c.* 2810–2800 Ma mafic–ultramafic intrusions (Ivanic *et al.* 2010). This is supported by the moderately reworked nature of the coeval Norie Group mafic volcanics (εNd −0.5 to 0.9), suggesting contamination with older unradiogenic crustal material (Wyman & Kerrich 2012).

(2) The second felsic magmatic event at 2760–2740 Ma displays three groups documented in the Results section. The group with T_{DM}^2 values of *c.* 3000 Ma (εNd of *c.* 1.0) represents reworking of the juvenile crust created during the *c.* 3000 Ma crustal thinning event. The material with T_{DM}^2 ages of *c.* 3200 and 3300 Ma represents the marginal and distal flank regions of the rift, respectively (Fig. 10b). These areas represent original *c.* 3700–3300 Ma crust that experienced progressively less juvenile input away from the rift axis.

(3) The third felsic magmatic event occurs at 2700–2680 Ma. It reworked the previously established crustal sources resulting in a decrease in εNd for each T_{DM}^2 component.

(4) The final event at *c.* 2640–2620 Ma displays one main source with a T_{DM}^2 age of *c.* 3200 Ma (εNd *c.* −3.0). This suggests a significant change in source characteristics, whereby these younger granites were derived from more unradiogenic middle crust, as opposed to the more mafic lower crust inferred for older granites (Cassidy *et al.* 2002; Ivanic *et al.* 2012). Alternatively, felsic magmatism at this time was isolated in the older crust at the margins of the juvenile zone.

This interpretation of the Murchison Domain crustal history remains tentative owing to known geological events that are not represented in the compiled dataset. First, the formation of large layered intrusions/sills (e.g. Windimurra, Barambie) at *c.* 2810–2800 Ma and komatiitic basalts at *c.* 2735–2710 (Glen Group and Yalgowra suite; Ivanic *et al.* 2010; Wyman & Kerrich 2012) represents the input of a large amount of mafic, mantle-derived material into the crust (Ivanic *et al.* 2012), which is poorly represented in the Sm–Nd data. Second, the 2670–2650 Ma granite event, found throughout the Yilgarn Craton and clearly identified in the Lu–Hf work of Ivanic *et al.* (2012) from this domain, is not represented in the Sm–Nd dataset. If this group is added to the events identified above, the felsic magmatic episodes from the Southern Cross and Murchison Domains correlate well (Figs 6, 7, 9 & 11), with events in the Murchison occurring at *c.* 2760–2740, 2700–2680, 2670–2650 and 2640–2620 Ma, and at *c.* 2750–2700, 2690–2680, 2665–2650, 2640–2630 Ma in the Southern Cross Domain.

South West Terrane. In general, the South West Terrane shows the reworking of a heterogeneous *c.* 3400–3000 Ma crustal source (dominantly 3200 Ma), from *c.* 3000 to 2630 Ma (Fig. 9g). The only major magmatic event in the compiled dataset occurs at *c.* 2645–2630 Ma and represents reworking of this source. This dominant T_{DM}^2 age of *c.* 3200 Ma is likely to represent a mixing age owing to the heterogeneous nature of the crustal source for this terrane. The end members of this mixing trend, more representative of the added and pre-existing crust, occur at T_{DM}^2 ages *c.* 3000 and 3400 Ma, broadly correlating with events from the Youanmi Terrane.

Narryer Terrane. Nutman *et al.* (1993) summarized their Sm–Nd data from 3730–2620 Ma granites and granite–gneisses of the Narryer Terrane as demonstrating two broad crustal sources. The early Archaean (3700–3350 Ma) gneisses are typically tonalitic in composition and have T_{DM}^2 values of *c.* 3740–3500 Ma, with a number of samples intersecting the depleted mantle, suggesting crustal growth at this time. Younger 3350–3300 Ma gneisses appear to be the product of reworking of this source. The middle Archaean gneisses are granitic in composition, and appear to be the product

of variable reworking of a 3400–3200 Ma crustal reservoir, with the younger 2750–2620 Ma granites the result of further reworking of this source.

Data presented here are <3100 Ma and record a *c.* 3500–3200 Ma T_{DM}^2 age (Fig. 8h). This appears to be analogous to the 3400–3200 Ma source that produced the middle Archaean gneiss and late granites of Nutman *et al.* (1993). Consequently, the data presented here only capture the reworking history of a 3500–3200 Ma source, apart from a single 2648 Ma granite with T_{DM}^2 of *c.* 3700 Ma.

The change in source composition and age of crustal rocks of the Narryer Terrane at *c.* 3300–3000 Ma suggests that a juvenile event created new crust at this time (see Nutman *et al.* 1993), which underwent variable mixing with the older, 3700–3500 Ma early Archaean material. This led to a mixed 3400–3200 Ma source, demonstrated by the wide range of εNd (−3.7 to +3.2) for the middle Archaean granite–gneisses, which represent variable mixing between the new and old crust. Reworking of this mixed source at 2750–2620 Ma then formed the late Archaean granites. This conclusion is supported by the occurrence of *c.* 3700 Ma xenocrystic zircons in the younger granites of the Narryer Terrane (Nutman *et al.* 1993), as well as the 3700 Ma T_{DM}^2 age for a 2648 Ma granite (Fig. 8h).

Comparison of the West Yilgarn and Eastern Goldfields as crustal 'super-blocks'

The Sm–Nd analysis indicates that the West Yilgarn and Eastern Goldfields Superterrane have distinct crustal histories. In this section, these two regions are compared as 'super-blocks', that is, two crustal blocks, which consist of a number of amalgamated terranes with similar crustal histories.

It is likely that the majority of the crust of the Eastern Goldfields Superterrane was extracted from the mantle at *c.* 3100–3000 Ma (Wyche *et al.* 2012*b*). In addition, the presence of minor 3300–3200 Ma material as model ages and inherited zircons (Compston *et al.* 1986; Hill *et al.* 1989; Nelson 1997) suggests either the existence of precursor crust of this age or contamination of the *c.* 3100–3000 Ma source by older material of the adjacent Southern Cross Domain. Addition of juvenile material, possibly at *c.* 2800 Ma, led to bulk T_{DM}^2 values of 2900–2800 at *c.* 2700 Ma for this superterrane. The Kalgoorlie Terrane itself is 'zoned', with the older crustal component increasing to the west, suggesting that it is due to interaction with the older Southern Cross Domain, which consists of crust of the same age as the contaminating material (Fig. 9f). The occurrence of 3200–3100 Ma crust at the Burtville–Kurnalpi Terrane boundary indicates the presence of older material not associated with the West Yilgarn, possibly from the Burtville Terrane itself (Fig. 11a, b).

It has been suggested that the initial crust of the Burtville Terrane formed at the eastern edge of the Youanmi Terrane during a *c.* 3100–3000 Ma mantle extraction event (Wyche *et al.* 2012*b*; Pawley *et al.* 2012), also recorded in the older crust of the West Yilgarn. From *c.* 2960 to 2735 Ma, supracrustal sequences were emplaced throughout this 'proto-Yilgarn' (West Yilgarn 'subcraton' and adjacent Burtville Terrane), including a plume event which formed the *c.* 2810–2800 Ma mafic–ultramafic intrusions of the Murchison Domain (Ivanic *et al.* 2010) and *c.* 2805 Ma Duketon komatiites in the Burtville Terrane (Kositcin *et al.* 2008; Pawley *et al.* 2012) within plume-related rift-zones (Ivanic *et al.* 2010; Wyman & Kerrich 2012). This mantle input mixed with pre-existing *c.* 3100 Ma crust, resulting in a heterogenous isotopic signature (T_{DM}^2 3100–2850 Ma) for the Burtville Terrane (Fig. 8b). Extension and crustal thinning at *c.* 2720 Ma led to the separation of the Burtville and Youanmi Terranes and the formation of the Kalgoorlie and Kurnalpi Terranes (Pawley *et al.* 2012; Wyman & Kerrich 2012). This process added a significant amount of juvenile material to these regions (Fig. 8c, d), leading to mixed isotopic signatures ranging from *c.* 3200–3100 (older Burtville crust) to *c.* 2700 Ma (new juvenile crustal addition) with a net mixed T_{DM}^2 of *c.* 2900 Ma. The presence of >2720 Ma xenocrystic zircons and >3000 Ma Nd model ages in granites and mafic–ultramafic volcanics (Chauvel *et al.* 1985; Compston *et al.* 1986; Hill *et al.* 1989; Nelson 1997; Bateman *et al.* 2001; Cassidy *et al.* 2002; Barley *et al.* 2003; Champion & Cassidy 2007; Said & Kerrich 2009) suggests that older crust is present underneath the juvenile terranes, and that full continental rifting to produce oceanic crust did not occur.

In contrast to the Eastern Goldfields Superterrane, the West Yilgarn consists of three terranes with slightly different histories. The Narryer Terrane is the oldest, with T_{DM}^2 values as old as *c.* 3700 Ma, with most data suggesting a heterogeneous reworked source with T_{DM}^2 of *c.* 3400–3300 Ma (Nutman *et al.* 1993). The South West Terrane also appears to consist of heterogeneous source with T_{DM}^2 values dominantly at *c.* 3200 Ma (Fig. 8g). The Southern Cross and Murchison Domains of the Youanmi Terrane both demonstrate minor older crustal components with T_{DM}^2 ages of *c.* 3700–3500 Ma, indicative of the longevity of these domains. However, this precursor crust appears to have been extensively rejuvenated at some point, as *c.* 3300–3000 Ma crust dominates (Figs 8e–g & 9g). The occurrence of these sources appears to be spatially controlled as discussed in

the earlier sections. Interestingly, the Southern Cross Domain demonstrates a very minor juvenile component (Figs 8e & 11c), which correlates with the signature of the Eastern Goldfields Superterrane.

This information infers a minimum 1100 myr crustal history for the West Yilgarn (Fig. 7). Initially, pre-existing 3700–3500 Ma crust was rifted in the Cue area of the Murchison Domain at *c.* 3000 Ma, thinning the crust and extracting new material from the mantle. This event broadly correlates with the extraction of the Lake Johnston block and Burtville Terrane crust (Wyche *et al.* 2012*b*), potentially owing to the *c.* 3000 Ma plume event that produced the Southern Cross Domain komatiites (Perring *et al.* 1995; Wang *et al.* 1996; Perring *et al.* 1996). The Marda block, inferred to represent the core of the West Yilgarn, appears to represent older crust that had less juvenile input at this time. At *c.* 2810–2800 Ma, the Murchison rift was reactivated during emplacement of the mafic–ultramafic intrusions (Ivanic *et al.* 2010) and synchronous greenstone sequences (Norie Group; Van Kranendonk & Ivanic 2008). This event correlates with the *c.* 2805 Ma Duketon komatiites and the inferred juvenile input to the Burtville Terrane crust. Felsic magmatic activity from 2800 to 2600 Ma appears to have dominantly reworked the older, spatially segregated crustal sources. However, the occurrence of boninites in the Polelle Group suggests that subduction-derived magmas, probably related to the docking of the Narryer Terrane, were emplaced at *c.* 2800–2700 Ma (Wyman & Kerrich 2012; Occhipinti *et al.* 2001). This event is not clearly recorded in the Sm–Nd data (Fig. 8f).

The result of the comparison between the West Yilgarn and the Eastern Goldfields Superterrane indicates two major features:

(1) The Eastern Goldfields Superterrane is *c.* 400–600 myr younger than the West Yilgarn, and up to 800 myr if the oldest material of the Narryer Terrane is considered (Fig. 7).
(2) Both crustal blocks have been interacting (shared tectono-magmatic events and isotopic signatures) since *c.* 3100–3000 Ma, as suggested by contamination of basalts with older unradiogenic crust (Said *et al.* 2010; McCulloch & Compston 1981; Barley 1986), shared greenstone events (Burtville–Youanmi; Pawley *et al.* 2012; Van Kranendonk & Ivanic 2008) and plume magmatism (Ivanic *et al.* 2010; Kositcin *et al.* 2008), as well as the isotopic work of Wyche *et al.* (2012*b*), which demonstrated that after *c.* 2960 Ma the rocks of the Eastern Goldfields Superterrane and Youanmi Terrane were affected by contemporaneous magmatic events.

These significant differences in crustal evolution between the Eastern Goldfields Superterrane and the West Yilgarn suggest that the Ida Fault represents a long-lived lithospheric boundary between two cratonic blocks (Swager 1997; Drummond *et al.* 2000).

Influence of lithospheric architecture on komatiite-hosted nickel, orogenic gold and BIF-hosted iron mineral systems

Komatiite-hosted nickel

Spatial correlations with crustal architecture. When the spatial occurrences of the komatiites of the *c.* 2.9 Ga Southern Youanmi Terrane and *c.* 2.7 Ga Norseman–Wiluna belt are compared with the Sm–Nd isotope map (Fig. 13), there are some striking correlations. The 2.7 Ga komatiites of the Norseman–Wiluna belt (Kalgoorlie Terrane) occur on the juvenile side of a major isotopic boundary (structurally represented by the Ida Fault), and run adjacent to this boundary for *c.* 700 km (Fig. 13). This, together with the lack of synchronous komatiites in the Southern Cross Domain, suggests that the nature of the crust and associated margins provides a major first-order control on the emplacement of voluminous komatiite magmatism.

Figure 13 identifies a distinctive 'gap' in the komatiite belt around the central Kalgoorlie Terrane (Leonora district), possibly owing to a lack of greenstone material in this area (as shown in regional mapping and aeromagnetic datasets). However, this gap correlates with a well-defined, *c.* 200–150 km-long, eastward deviation in the Nd-isotope trend (Figure 10), from a generally linear, north–south path parallel to the Ida Fault (Figs 10–13). This potentially suggests that the high MgO komatiites may also be deflected to the east in this area (Fig. 13).

The 2.9 Ga komatiites technically fall outside of the temporal scope of the Nd map (Fig. 13), which was constructed using only 2.8–2.6 Ga crustal rocks. However, assuming that the Neoarchaean crustal architecture presented in Figure 10 is inherited from previous 'parent' architecture, it is possible to make some tentative correlations regarding large-scale controls.

The Southern Cross Domain hosts *c.* 2.9 Ga komatiites whose geochemistry, prospectivity and volcanology change markedly throughout the domain (Perring *et al.* 1995, 1996; Chen *et al.* 2003; Heggie *et al.* 2012*a*, *b*). The greenstone belts in the more reworked (T_{DM}^{2} *c.* 3300 Ma) Marda block are typically dominated by basalt (i.e. the lower sequence of the Marda greenstone belt; Chen *et al.* 2003), with komatiite occurring as rare, thin, low MgO, sheet flows. As a result, no

economic nickel sulphide mineralization is known to occur in komatiites of this belt (Barnes 2006*a*). In contrast, the less reworked (T_{DM}^2 *c.* 3100 Ma) Lake Johnston block, hosting the Southern Cross, Forrestania, Lake Johnston and Ravensthorpe greenstone belts (Cassidy *et al.* 2006), contains abundant komatiites, although only the latter three host nickel sulphide mineralization (Barnes 2006*a*). These mineralized belts contain thick, channelized, high MgO (MgO 20–40%) flows with abundant ortho-adcumulate bodies (Perring *et al.* 1995, 1996; Heggie *et al.* 2012*a*, *b*), which suggest high-flux eruption of komatiite magmas and high volume flow through of lava in large, submarine tubes (Hill *et al.* 1990, 1995; Arndt *et al.* 2008). As a result of these favourable features, numerous nickel sulphide deposits occur within these belts including Flying Fox, Spotted Quoll (Forrestania), Maggie Hays (Lake Johnston) and RAV-8 (Ravensthorpe).

Further to this, the highest concentration of high MgO komatiites, which occurs in the Forrestania greenstone belt, is found at the terrane margin between the Youanmi Terrane/Southern Cross Domain and the South West Terrane (Fig. 13). Lu–Hf isotope work by Mole *et al.* (2010) demonstrates that, at 3050–2820 Ma, the eastern South West Terrane is more reworked than the south Southern Cross Domain, which has positive εHf values. Subsequently, during the emplacement of the *c.* 2.9 Ga komatiites, the South West Terrane–Lake Johnston block boundary displayed a similar isotopic architecture to the Youanmi Terrane–Kalgoorlie Terrane boundary at 2.7 Ga.

Large-scale controls. The last few decades have seen a significant increase in our understanding of komatiites, particularly their generation, volcanology, geochemistry and associated Ni–Cu–PGE mineralization (Arndt *et al.* 1979; Gresham & Loftus-Hills 1981; Lesher *et al.* 1984; Huppert & Sparks 1985*b*; Arndt & Jenner 1986; Groves *et al.* 1986; Gole *et al.* 1987; Campbell *et al.* 1989; Herzberg 1992; Hill *et al.* 1995; Blichert-Toft & Arndt 1999; Barnes *et al.* 2004; Fiorentini *et al.* 2010, 2011; Barnes & Fiorentini 2012). However, most studies were focused at the deposit scale, whereas the understanding of the controls of komatiite emplacement at the terrane to craton scale has remained largely incomplete.

Building on previous work by Thompson & Gibson (1991) and Sleep (1997, 2005), Begg *et al.* (2010) used seismic tomography to demonstrate that the lithosphere can physically control the flow and lateral 'ponding' of plume material and subsequently the location of Ni–Cu–PGE deposits/camps. The Sm–Nd isotopic data can be used to infer an approximate three-dimensional intra-cratonic lithospheric architecture (Figs 11 & 13), where highly reworked crust, typically with $\varepsilon Nd < -3.0$, was assigned cratonic lithospheric thicknesses of 200–250 km (Boyd *et al.* 1985; Begg *et al.* 2009), while relatively juvenile crust, with εNd of 1.0–3.0, was assigned Phanerozoic lithospheric thicknesses of 80–60 km (Cawood *et al.* 2013). Crustal domains with εNd *c.* 0 were assigned intermediate crustal thicknesses. This proxy has been shown to work well in the Yellowstone area of the western USA (Ormerod *et al.* 1988; Nash *et al.* 2006; Manea *et al.* 2009; Pierce & Morgan 2009), and broadly agrees with recent geophysical studies from the Yilgarn Craton (Blewett *et al.* 2010*b*; Dentith *et al.* 2012, Fishwick & Rawlinson 2012). This three-dimensional crustal architecture, together with the 'plume-deflection' model of Begg *et al.* (2010), can be used to explain the localization of komatiite magmatism in the Yilgarn Craton.

At *c.* 2.7 Ga, a plume impinged on the thick, old lithosphere of the West Yilgarn (Barnes *et al.* 2012) and was focused eastward into the thinner, more juvenile Kalgoorlie Terrane (Fig. 13). Concurrently, attenuation caused by the rising plume re-activated a pre-existing lithospheric weakness along the isotopic boundary, leading to north–south orientated lithosphere-scale rifting. These trans-lithospheric faults or permeability zones were essential for the unrestricted rise of komatiite magma to the upper crust/surface. Owing to the high density of komatiitic magma relative to the continental crust (Herzberg *et al.* 1983; Huppert & Sparks 1985*a*), ultramafic melts can only ascend to the surface if they are able to form a continuous column of magma from the melting zone to the top of the crust (Naldrett 2010; Barnes & Fiorentini 2012). Rifting at the isotopic margin allows the formation of these pathways.

As a result of these features, komatiites emplaced at the isotopic margin are highly primitive and discharged at a high rate, resulting in channelization (Hill *et al.* 1995) and the formation of multiple, world-class nickel sulphide deposits (e.g. Mt Keith, Perseverance, Kambalda camp; Rosengren *et al.* 2005; Fiorentini *et al.* 2012). In contrast, the West Yilgarn consists of old, reworked and hence thicker crust, and as a result no komatiite magmatism of any form occurs here. The closest volcanic event is the eruption of the *c.* 2730 Ma andesites–rhyolites (Chen *et al.* 2003) of the Marda Complex within the Marda block. Their Nd isotopic signatures (εNd of *c.* −3; Table 2) suggest derivation from a crustal source, with geochemistry similar to a modern Andean-type margin (Chen *et al.* 2003), although evidence of other subduction-related features is lacking, that is, high-grade metamorphic rocks, tectonic mélanges, ophiolites, and so on (Bédard *et al.* 2012).

The lack of major, thick, high MgO, cumulate-rich komatiite sequences further to the east of the isotopic margin, in the Kurnalpi, Burtville and Yamarna Terranes (Fig. 13), suggests that the isotopic margin provides a fundamental physical control on komatiite localization (Figs 10–13). Komatiites are known to occur in these eastern terranes (Barnes & Fiorentini 2012), but they are neither as thick or hot, nor as extensive as those in the Kalgoorlie Terrane, suggesting a less focused melt source.

Within the Kalgoorlie Terrane itself, there are significant differences between the Agnew–Wiluna camp (felsic volcanic-hosted) and Kambalda camp (basalt-hosted) komatiites. The flows/sills of the northern camp typically demonstrate higher MgO values, more extensive cumulate (olivine adcumulate) zones and larger nickel deposits (Barnes 2006*a*; Barnes 2006*b*; Barnes & Fiorentini 2012). We suggest that this variation is controlled by the character of the crustal block and isotopic margin adjacent (west) of the related nickel camp. The crust to the west of the Kambalda camp (the Lake Johnston block) is slightly less reworked (thinner) than the block west of the Agnew–Wiluna belt (the Marda block; see Figs 10–13). This, together with the more pronounced isotopic boundary adjacent to the Agnew–Wiluna belt, suggests that plume magmas were focused to a greater extent at the northern margin.

The *c.* 2.9 Ga komatiites in the Southern Cross Domain also display a strong correlation between Nd isotopic architecture and komatiite location, character and nickel sulphide endowment. Rising plume magmas at this time would have been impeded by the presence of a thick overlying lithospheric 'lid' in the South West Terrane and Marda block. Consequently, magmatic fractionation, differentiation and crustal assimilation led to basalt-dominated greenstone sequences in the Marda block (Chen *et al.* 2003), and a complete lack of preserved volcanic rocks in the South West Terrane. In these environments, ore-forming processes that require turbulent emplacement of primitive magmas are not favoured (Lesher *et al.* 1981, 1984; Bekker *et al.* 2009).

In contrast, the Forrestania and Ravensthorpe belts are located along an inferred craton margin. This creates a lithospheric setting similar to that in the Eastern Goldfields at 2.7 Ga, where the South West Terrane forms the old, thick crustal block and the Lake Johnston block the thinner crust (see Fig. 13). As a result, similar plume-deflection processes (Begg *et al.* 2010) inferred for the 2.7 Ga komatiites led to the emplacement of komatiite magmas with the properties needed to form nickel sulphide deposits. In addition, the magnetotelluric work of Dentith *et al.* (2012) potentially shows the 'fossil' remnants of the lithospheric discontinuities that allowed komatiitic magmas to reach the surface unimpeded.

The Southern Cross komatiites appear to form a subgroup between the unprospective, low-MgO Marda flows and the prospective, high-MgO, Forrestania, Ravensthorpe and Lake Johnston magmas (Thébaud & Barnes 2012). These komatiites have high MgO contents, but appear to be unchannelized and have significantly less cumulate than the flows to the south. The transitional nature of these flows correlates with their location at the margin of the Marda and Lake Johnston blocks (Fig. 13).

In summary, the variable spatial location, character and nickel sulphide endowment of komatiites in two separate areas of the Yilgarn Craton, at two distinct times, appear to be governed by the same basic lithospheric architecture. The occurrence of a thin, young, juvenile crustal block adjacent to an older, thicker, more reworked block, together with the impingement of a mantle plume, appear to be vital to the formation of thick, channelized, high flux MgO-rich komatiite sequences and the onset of nickel sulphide ore-forming systems.

Orogenic gold

Spatial correlations with crustal architecture. While gold deposits can be found throughout the Yilgarn Craton (see Figs 3 & 12), they are particularly concentrated in the Kalgoorlie and Kurnalpi Terranes (e.g. Laverton belt) in the Eastern Goldfields Superterrane (Robert *et al.* 2005) and the central Murchison and Southern Cross Domains of the Youanmi Terrane.

In the Murchison Domain, gold deposits (e.g. Mt Magnet gold camp) are concentrated internal to, and on the margins of, the 'rift-like' juvenile architecture (Spaggiari 2006; McCuaig *et al.* 2010). The density of deposits appears to increase in the northern area of the 'rift' where large crustal structures appear to converge (Fig. 12).

In the Eastern Goldfields Superterrane, gold deposits are concentrated in the Kalgoorlie and Kurnalpi Terranes (Figs 3 & 12), with the Kalgoorlie–Norseman belt particularly prospective (Blewett *et al.* 2010*a*, *b*). Most deposits occur along major, terrane bounding structures or secondary structures (Groves *et al.* 1995; Witt & Vanderhor 1998; Robert *et al.* 2005). In general, the gold systems in the Kalgoorlie and Kurnalpi Terranes follow the isotopic boundary between the Eastern Goldfields Superterrane and West Yilgarn. Despite being the most juvenile crustal domain in the Yilgarn Craton (Fig. 10), the Kurnalpi Terrane does not appear to be more prospective than the Kalgoorlie Terrane. This suggests that, while juvenile crust is important for the formation of gold systems, large-scale structural networks may be more important

controls (Vearncombe 1998; Cox 1999; Blewett *et al.* 2010*b*).

This relationship is exemplified by the Southern Cross gold belt (e.g. Marvel Loch gold camp), which occurs along a major structure between the South West Terrane and Southern Cross Domain: two isotopically coherent regions which are both relatively reworked compared with the Murchison Domain and Kalgoorlie/Kurnalpi Terranes (Fig. 12). Although this margin is poorly defined in the Sm–Nd maps (Figs 10–12), time-resolved Lu–Hf mapping (Mole *et al.* 2010), together with granite age (U–Pb) mapping (Mole *et al.* 2012), show that this margin was much more pronounced at *c.* 2820–2720 Ma. As a result, the Southern Cross area demonstrates the significance of inherited, early architecture *c.* 200 myr older than the gold mineralizing event.

Large-scale controls. Gold deposits of the Yilgarn Craton generally formed in a craton-wide event at *c.* 2650–2630 Ma (Kent & McDougall 1995; Kent *et al.* 1996; Kent & Hagemann 1996), typically along lines of steep εNd gradient (Fig. 12) and in areas where multiple regional structures intersect and/or change direction (Cox 1999; Chen *et al.* 2001*b*; Blewett *et al.* 2010*a*, *b*). The large-scale hydrothermal systems that drove gold mineralization used lithospheric-crustal scale structures localized by the lithospheric architecture (Blewett *et al.* 2010*b*). This relationship is particularly clear in the gold-rich areas of the Murchison Domain, Southern Cross Domain and Kalgoorlie Terrane (Figs 3 & 12).

Gold mineralization in these areas is controlled by pre-existing lithospheric architecture, in tandem with major structures. This relationship is due to a number of factors:

(1) The addition of juvenile material into the crust before the initiation of a gold-forming event is critical to developing gold fertility (Cassidy *et al.* 2005; Bateman & Bierlein 2007, Hronsky *et al.* 2012). This can happen at anytime before gold mineralization, and suggests that the fertility of the Southern Cross and Murchison gold sources developed 350–150 myr before the gold mineralizing event at *c.* 2650–2630 Ma, as this is when juvenile material was added to the crust, creating a fertile source. However, the delay between juvenile input and gold mineralization in the Southern Cross district may explain the relatively small size of these deposits (McCuaig *et al.* 2010). In the Eastern Goldfields Superterrane, relatively juvenile crust (εNd > 0) dominated before and during gold mineralization. This suggests that the input of juvenile crust before and during gold mineralization created an especially gold-rich source, possibly explaining why deposits in this area are typically larger than those in the West Yilgarn.

(2) Deep-seated granite magmatism that drives large-scale hydrothermal systems is controlled by lithospheric architecture, that is, the geometry of the lithosphere controls where melts can rise and decompress. The late, 2650–2620 Ma Low-Ca granites, broadly synchronous with gold mineralization (Kent *et al.* 1996; Cassidy *et al.* 1998; Cassidy *et al.* 2002), are often localized at terrane boundaries and major structures where they can drive hydrothermal systems. These granites transferred large amounts of high heat-producing elements (U, Th, Rb) from the lower to upper crust (Champion & Sheraton 1997; Cassidy *et al.* 2002; Czarnota *et al.* 2007). This led to rapid cooling and cratonization of the lower crust, and also a significant increase in heat-flow in the upper crust, potentially responsible for the large hydrothermal systems involved in the craton-wide gold event.

(3) The 'Mafic' group of granites (sanukitoids; Cassidy *et al.* 2002) are associated with juvenile crust and appear to be an important factor in gold mineralization (Cassidy *et al.* 1998, 2002, 2005). These granites are relatively high in Ni, Cr and Mg# as well as large ion lithophile elements (Ba, Sr, light REE; Champion & Sheraton 1997) and such alkalic mafic magmas may have represented an important gold source (Wyman & Kerrich 1988; Müller 2002; Hronsky *et al.* 2012; Duuring *et al.* 2007). The Mafic granites utilized the same structures as gold and were emplaced at the start of the gold event at *c.* 2650 Ma (Cassidy *et al.* 2002). As a result, they are the preferred host for granite-hosted orogenic gold deposits (Cassidy *et al.* 1998; Duuring *et al.* 2007). These granites represent a link between the mantle, crust, gold source and deposition site and demonstrate the importance of juvenile crust to the gold fertility of a terrane.

(4) The location of major crustal structures (i.e. Ida, Hootanui, Ockerburry; Cassidy *et al.* 2006) typically occurs at or around the boundaries of crustal blocks. The correlation of gold deposits/camps with these structures (i.e. Laverton area and Celia crustal fault, Henson *et al.* 2010; Cue and Cunderloo shear zone, Mt Magnet and Mt Magnet fault, Spaggiari 2006) demonstrates their importance in the localization of hydrothermal systems and fluid flux (Groves 1993, Sibson 1994; Witt

& Vanderhor 1998; Vearncombe 1998; Cox 1999). These boundaries are also likely to be reactivated multiple times in their history, leading to increased permeability and the formation of the larger gold systems (Blewett *et al.* 2010*a*). In the Murchison Terrane, these structures appear to reach the mid-crust at *c.* 30–20 km, as shown by regional seismic data (Ivanic *et al.* 2013).

(5) Fluid flow – isotopic contrasts typically represent the boundary between rheologically and chemically different crustal blocks (Burov *et al.* 1998). These features, together with strain partitioning and inherited tectonic weakness, encourage the creation of large-scale, crustal and lithospheric faults together with complex subsidiary structural regimes (Henson *et al.* 2010; Blewett *et al.* 2010*a*, *b*). This complex and deep-tapping structural network allows the establishment of large hydrothermal cells (Groves *et al.* 1995; Vearncombe 1998; Cox 1999), possibly fuelled by deep-seated granites (Cassidy *et al.* 2002). The fluids would then have potentially fluxed through mafic alkaline igneous rocks, such as the Mafic granite suite (Cassidy *et al.* 2002; Duuring *et al.* 2007), picking up gold and depositing it further down the system in a trap or buffer (Groves *et al.* 1995, 1998; Hronsky & Groves 2008; McCuaig *et al.* 2010; Hronsky *et al.* 2012).

(6) Heat flow – the presence of younger, juvenile crust indicates that the lithosphere in that area may be thinner than in more reworked areas. This is because juvenile crust requires a variable amount of mantle input, whereas reworked signatures indicate crustal melting (Kemp *et al.* 2007). This is important as thinned crust allows more rapid and effective heat transfer to the upper crust, encouraging the generation of large hydrothermal cells and maintaining them over time (Champion & Sheraton 1997; Cassidy *et al.* 2002, 2005; Cassidy & Champion 2004; Champion & Cassidy 2007).

BIF-hosted iron

Spatial correlations with crustal architecture. Iron deposits of the Yilgarn Craton are spatially associated with older, more reworked crustal domains, with groups of deposits occurring internal to, and on the margins of, older crustal blocks of the West Yilgarn (Fig. 12). In contrast, BIF-hosted iron deposits appear rare to absent in the juvenile Eastern Goldfields Superterrane, where sulphidic black shales dominate sedimentary sequences and thick BIF units are lacking (Swager 1997; Barley *et al.* 2003; Bekker *et al.* 2009).

Within the West Yilgarn, three main iron camps occur in the Jack Hills, Murchison and central-north Southern Cross Domain areas (see Fig. 12). The Jack Hills camp (Crosslands, Mt Narryer, Taylor Range, Mt Hale) occurs within the Narryer Terrane (Occhipinti *et al.* 2001; Spaggiari *et al.* 2007), which is the oldest crustal terrane delineated by the Nd isotopes (see Figs 6g, h & 8h). BIF-hosted iron deposits in the Murchison Domain are mainly located on the margins of the NW–SE-trending juvenile crust (Figs 10 & 12). For example, the Weld Range deposits (e.g. Beebyn, Weld Range; Duuring *et al.* 2013) are situated along the northwestern margin, whereas the Yogi, Karara, Blue Hills and Mt Gibson deposits are located along the southern margin. The Koolanooka and Tallering Peak deposits are positioned off the isotopic margin, in old crust further to the SW. The reworked Marda block (Figs 11 & 12) also hosts numerous deposits (Windarling, Mt Jackson, Lake Giles; Angerer *et al.* 2012), while other deposits (Wiluna West, Central Mt Ida, Koolyanobbing; Angerer & Hagemann 2010) occur around the edge of this crustal block.

Large-scale controls. BIF-hosted iron deposits require the deposition of thick primary BIF sequences. These provide the iron source, which is later upgraded by silica-poor fluids localized by structures. This section demonstrates how lithospheric architecture potentially controls the location and extent of both processes.

The distinct absence of documented high-grade, BIF-hosted iron deposits in greenstone belts in the Eastern Goldfields Superterrane may be due to the rarity of laterally continuous, thick BIF in this region (Swager 1997; Gole 1981). Differences in ocean chemistry and crustal evolution during the Archaean may influence the primary abundance, distribution and composition of BIF (Gole 1981; Lascelles 2007; Bekker *et al.* 2010; Evans *et al.* 2012). Thus, the different crustal evolution of the West Yilgarn compared with the Eastern Goldfields Superterrane best explains the first-order differences in iron ore abundance between these areas.

In the West Yilgarn, the localization of iron deposits in the more reworked areas of the crust (Fig. 12) correlates with regional variations in the abundance of BIF (Gole 1981). This suggests that the older, more evolved and stable crustal regions were analogous to continental platform settings (Bekker *et al.* 2010). The edge of these crustal blocks could have represented passive margins, and this is supported by the presence of low-temperature hydrothermal VMS systems in the BIF and felsic volcanic footwall rocks of the Weld Range iron (Duuring & Hagemann 2013*a*, *b*). In these areas volcanism was episodic and of a relatively low-flux, resulting in a more stable

environment for the accumulation of thick BIF sequences (Bekker *et al.* 2010). In contrast, relatively juvenile regions represent more active, unstable environments where more continuous, rapid emplacement of komatiites and basalts, as well as associated hydrothermal systems, led to thinner BIF sequences (Lascelles 2007). This spatial variation can be observed in the different stratigraphy of the Marda (thick BIFs, basaltic volcanism) and Forrestania (thin BIFs and abundant komatiites) greenstone belts (Chen *et al.* 2003; Angerer & Hagemann 2010; Angerer *et al.* 2012*a*).

In general, there is an antithetic relationship between orogenic gold and BIF-hosted iron camps in the Yilgarn Craton (Fig. 12). This is because the fluids needed to form iron ore deposits must be silica-poor in order to remove chert from the BIF (Duuring & Hagemann 2013*b*). However, gold is invariably found associated with quartz, suggesting that a silica-rich fluid is involved (Phillips & Groves 1983). This is exemplified at the Mt Morgans gold camp in the Kurnalpi Terrane, where extensive hydrothermal alteration by the SiO_2–H_2O–S–CO_2-rich gold-bearing fluids resulted in the formation of quartz–carbonate–sulphide–gold veins, whereas addition of silica to the BIF resulted in the dilution of the iron content (Vielreicher *et al.* 1994). Consequently, as iron and gold show a preference for crustal domains with different histories, there is a correlation between fluid composition and crustal source, whereby older crust appears to favour silica-poor fluids, and juvenile crust silica-rich fluids. Further work is required to understand this relationship between fluid source and crustal evolution.

Large-scale structures, such as those described above for gold systems, are also fundamental in iron systems (Angerer & Hagemann 2010; Duuring *et al.* 2013). Iron camps (e.g. Weld Range, Windarling) form along major structures orientated parallel to isotopic margins (Angerer *et al.* 2012*a*; Duuring & Hagemann 2013*a*, *b*), suggesting an intimate regional relationship between major crustal boundaries and these localizing faults (Fig. 12).

Summary

The mineral systems approach to exploration targeting states that four primary features are required in the formation of any metallogenic camp/deposit: (1) a metal source; (2) an active pathway for fluid or magma; (3) a fluid throttle (physical); and (4) a deposition or trap site (Wyborn *et al.* 1994; Knox-Robinson & Wyborn 1997; Hronsky & Groves 2008; McCuaig *et al.* 2010). This study demonstrates that the large-scale crustal evolution of an Archaean craton and the subsequent lithospheric architecture exerts a significant control at each stage of camp formation in multiple metallogenic systems (Bierlein *et al.* 2006; Hronsky & Groves 2008; Begg *et al.* 2010; McCuaig *et al.* 2010). This work shows that each mineral system has specific correlations with the crustal architecture, suggesting ore-forming processes that require specific crustal settings. The findings of this study are summarized below:

- The Yilgarn Craton consists of two 'subcratons' with distinctly different crustal sources and histories: the Eastern Goldfields Superterrane and West Yilgarn.
- The Eastern Goldfields Superterrane is made up of four terranes with a similar bulk isotopic crustal source with a T_{DM}^2 of 2900–2800 Ma. This crust probably represents the mixing of juvenile addition (at *c.* 2800–2700 Ma) and pre-existing *c.* 3100 Ma crust. The addition of an older 3300–3200 Ma crustal component is spatially controlled, with the greatest amount occurring at the Kalgoorlie–Youanmi Terrane margin, and a lesser amount at the Kurnalpi–Burtville margin.
- The West Yilgarn 'super-block' is characterized by much older, and more reworked crust that typically shows $\varepsilon Nd < 0$. The Southern Cross Domain displays two, spatially controlled sources at *c.* 3300 and 3100 Ma. The Murchison Domain displays three broad crustal sources at *c.* 3000, 3200–3100 and 3300 Ma. These are inferred to reflect the relatively juvenile, NE–SW 'rift zone', the rift margins and the older crust outboard of the rift, respectively. The South West Terrane shows a *c.* 3200 Ma crustal source from 3000–2600 Ma with some minor scatter. Finally, the Narryer Terrane hints at a very old crustal source >3700 Ma.
- The felsic magmatic event that cratonized the terranes of the Yilgarn Craton occurred at 2650–2620 Ma. This episode was characterized by infra-crustal melting leading to reworking of established crustal sources and production of the Low-Ca granites.
- The broad cycling between reworking and juvenile input at 2720–2700 (J), 2700–2670 (RW), 2670–2650 (J) and 2650–2640 (RW) Ma, particularly evident in the Kalgoorlie Terrane, may suggest some form of tectonic cycling; either the opening and closing of rift basins, or possibly a change in melting depth.
- It is difficult to reconcile a subduction setting with the <2700 Ma granites of the Yilgarn Craton. Subduction is a linear process producing linear magmatic domains. The <2700 Ma granites occur craton-wide, suggesting that a large, non-linear tectonic process is required.

- Periods of reworking are inferred to represent compressive events, which led to orogenesis and the production of infra-crustal granites. Juvenile addition signifies crustal thinning, allowing magmatism to tap more mantle-derived, younger sources.
- Mantle input into the crust after *c.* 3000 Ma appears to be minor in the West Yilgarn. This may be due to thicker crust preventing mantle melts interacting with the mid-upper crust. Alternatively, owing to the older signature of the West Yilgarn crust, juvenile input does not necessarily result in >0 εNd values.
- Multiple periods of craton-wide granite magmatism, which tap a number of shared crustal sources at $<$2700 Ma, infer that the Yilgarn Craton was assembled by this time. Older shared features, such as greenstone ages and plume magmatism in the Burtville and Youanmi Terranes, suggest an even older relationship as far back as *c.* 3000 Ma.
- Crustal growth events, marked by the addition of mantle material, are inferred to have occurred at *c.* 3100–3000 Ma (formation of the Burtville Terrane, Murchison rift and Southern Cross komatiites), *c.* 2900 Ma (Yamarna Terrane formation?), *c.* 2800 Ma (Murchison mafic–ultramafic intrusions, Duketon komatiites, decrease in Eastern Goldfield Superterrane model ages) and *c.* 2720–2700 Ma (crustal stretching and thinning between Youanmi–Burtville and formation of Kalgoorlie and Kurnalpi Terranes, Norseman–Wiluna komatiites).
- BIF-hosted iron systems are concentrated in the older, more reworked crust of the West Yilgarn, internal to, and on the margins of, old crustal blocks.
- Orogenic gold systems typically occur internal to, and on the margins of, juvenile blocks. However, the occurrence of the Southern Cross gold belt in reworked crust demonstrates that the addition of juvenile material, which creates gold fertility in the crust, does not have to be synchronous with gold mineralization. The structural complexity common at the margins of crustal domains, together with juvenile crustal material where available, is a favourable location for gold mineralization.
- Gold mineralization throughout the craton appears to be coeval with cratonization and the last tectono-thermal event at *c.* 2640–2620 Ma.
- Komatiite-hosted nickel deposits are preferentially localized on the juvenile side of a margin with a more reworked crustal block. This architecture focused the plume source into the thinner juvenile crustal domain. Rifting occurred at or close to the isotopic margin, which represented a pre-existing crustal weakness. The formation of trans-lithospheric faults/pathways at this margin allowed komatiite magmas to be erupted unfractionated and with minimal crustal contamination.
- Lithospheric architecture is fundamental in localizing the source reservoir for a given commodity. In gold and nickel, the emplacement of juvenile magmas is governed by the age and configuration of crustal domains. In BIF-hosted iron systems, the development of thick BIF sequences that form the iron source is controlled by the age and stability of a crustal block.

Lithospheric architecture is a first-order control of mineral systems, and an important tool in assessing and understanding regional prospectivity. Our understanding of the effects of large-scale crustal architecture on camp/deposit localization is at an early stage, and further work needs to be done to understand how evolving lithospheric architecture controls the movement of prospective zones in space and time.

This project is funded by Australian Research Council (ARC) Linkage grants LP0776780 and LP100100647 with BHP Billiton Nickel West, Norilsk Nickel, St Barbara and the Geological Survey of Western Australia. Zircon U–Pb analyses were conducted using the SHRIMP ion microprobes at the John De Laeter Centre of Mass Spectrometry at Curtin University, Perth. A. Wilson and A. Clarke-Hale are thanked for assistance with logistics, support, and guidance in the field. T. Angerer is acknowledged for assistance and guidance with the BIF-hosted iron component of this paper. D. Champion is thanked for access to Geoscience Australia Sm–Nd data from the Yilgarn Craton. A. Naldrett and W. Maier are thanked for their reviews, which significantly improved the paper. The Geological Survey of Western Australia is acknowledged for field support, sample provision, and ongoing technical advice. C. L. Kirkland, S. S. Romano and M. P. Doublier publish with permission of the Executive Director of the Geological Survey of Western Australia. D. R. Mole acknowledges the receipt of a Scholarship for International Research Fees from the University of Western Australia. This is publication number **346** of the ARC Centre of Excellence Centre for Core to Crust Fluid Systems.

References

AHMAT, A. L. 1984. *Metamorphic patterns in the greenstone belts of the Southern Cross Province, Western Australia*. Geological Survey of Western Australia – Report 19, Professional Papers for 1984, 87.

ALLÈGRE, C. J., HART, S. R. & MINSTER, J. F. 1983. Chemical structure and evolution of the mantle and continents determined by inversion of Nd and Sr isotopic data, II. Numerical experiments and discussion. *Earth and Planetary Science Letters*, **66**, 191–213.

ALLIBONE, A. H., WINDH, J. *ET AL.* 1998. Timing relationships and structural controls on the location of Au–Cu

mineralization at the Boddington gold mine, Western Australia. *Economic Geology*, **93**, 245–270.

ANGERER, T. & HAGEMANN, S. G. 2010. The BIF-hosted high-grade iron ore deposits in the Archean Koolyanobbing Greenstone Belt, Western Australia: structural control on synorogenic- and weathering-related magnetite-, hematite-, and goethite-rich iron ore. *Economic Geology*, **105**, 917–945.

ANGERER, T., HAGEMANN, S. & DANYUSHEVSKY, L. 2012*a*. High-grade iron ore at Windarling, Yilgarn Craton: a product of syn-orogenic deformation, hypogene hydrothermal alteration and supergene modification in an Archean BIF-basalt lithostratigraphy. *Mineralium Deposita*, **48**, 1–32.

ANGERER, T., HAGEMANN, S. G. & DANYUSHEVSKY, L. V. 2012*b*. Geochemical evolution of the banded iron formation-hosted high-grade iron ore system in the Koolyanobbing Greenstone Belt, Western Australia. *Economic Geology*, **107**, 599–644.

ARNDT, N. T. & GOLDSTEIN, S. L. 1987. Use and abuse of crust-formation ages. *Geology*, **15**, 893–895.

ARNDT, N. T. & JENNER, G. A. 1986. Crustally contaminated komatiites and basalts from Kambalda, Western Australia. *Chemical Geology*, **56**, 229–255.

ARNDT, N. T., FRANCIS, D. & HYNES, A. J. 1979. The field characteristics and petrology of Archean–Proterozoic komatiites. *Canadian Mineralogist*, **17**, 147–163.

ARNDT, N. T., BARNES, S. J. & LESHER, C. M. 2008. *Komatiite*. Cambridge University Press, Cambridge.

ASHLEY, P. M., DUDLEY, R. J., LESH, R. H., MARR, J. M. & RYALL, A. W. 1988. The Scuddles Cu–Zn prospect, an Archean volcanogenic massive sulfide deposit, Golden Grove District, Western Australia. *Economic Geology*, **83**, 918–951.

BARLEY, M. E. 1986. Incompatible-element enrichment in Archean basalts: a consequence of contamination by older sialic crust rather than mantle heterogeneity. *Geology*, **14**, 947–950.

BARLEY, M. E., KRAPEZ, B., GROVES, D. I. & KERRICH, R. 1998. The Late Archaean bonanza: metallogenic and environmental consequences of the interaction between mantle plumes, lithospheric tectonics and global cyclicity. *Precambrian Research*, **91**, 65–90.

BARLEY, M. E., KERRICH, R., REUDAVY, I. & XIE, Q. 2000. Late Archaean Ti-rich, Al-depleted komatiites and komatiitic volcaniclastic rocks from the Murchison Terrane in Western Australia. *Australian Journal of Earth Sciences*, **47**, 873–883.

BARLEY, M. E., BROWN, S. J. A., CAS, R. A. F., CASSIDY, K. F., CHAMPION, D. C., GARDOLL, S. J. & KRAPEZ, B. 2003. *An integrated geological and metallogenic framework for the eastern Yilgarn Craton: developing geodynamic models of highly mineralised Archaean granite–greenstone terranes*. Amira International Limited, AMIRA Project P763.

BARLEY, M. E., BROWN, S. J. A., KRAPEZ, B. & KOSITCIN, N. 2008. Physical volcanology and geochemistry of a Late Archaean volcanic arc: Kurnalpi and Gindalbie Terranes, Eastern Goldfields Superterrane, Western Australia. *Precambrian Research*, **161**, 53–76.

BARNES, S. J. 2006*a*. *Komatiite-hosted Nickel Sulfide Deposits: geology, Geochemistry, and Genesis*. Society of Economic Geologists, Littleton, CO, Special Publications, **13**, 51–97.

BARNES, S. J. 2006*b*. *Komatiites: Petrology, Volcanology, Metamorphism and Geochemistry*. Society of Economic Geologists, Littleton, CO, Special Publications, **13**, 13–49.

BARNES, S. J. & FIORENTINI, M. L. 2012. Komatiite magmas and sulfide nickel deposits: a comparison of variably endowed Archean Terranes. *Economic Geology*, **107**, 755–780.

BARNES, S. J., HILL, R. E. T., PERRING, C. S. & DOWLING, S. E. 2004. Lithogeochemical exploration for komatiite-associated Ni-sulfide deposits: strategies and limitations. *Mineralogy and Petrology*, **82**, 259–293.

BARNES, S. J., VAN KRANENDONK, M. J. & SONNTAG, I. 2012. Geochemistry and tectonic setting of basalts from the Eastern Goldfields Superterrane. *Australian Journal of Earth Sciences*, **59**, 707–735.

BARRIE, C. T., LUDDEN, J. N. & GREEN, T. H. 1993. Geochemistry of volcanic rocks associated with Cu–Zn and Ni–Cu deposits in the Abitibi Subprovince. *Economic Geology*, **88**, 1341–1358.

BATEMAN, R. & BIERLEIN, F. P. 2007. On Kalgoorlie (Australia), Timmins–Porcupine (Canada), and factors in intense gold mineralisation. *Ore Geology Reviews*, **32**, 187–206.

BATEMAN, R., COSTA, S., SWE, T. & LAMBERT, D. 2001. Archaean mafic magmatism in the Kalgoorlie area of the Yilgarn Craton, Western Australia: a geochemical and Nd isotopic study of the petrogenetic and tectonic evolution of a greenstone belt. *Precambrian Research*, **108**, 75–112.

BATEMAN, R., AYER, J. A. & DUBÉ, B. 2008. The Timmins–Porcupine Gold Camp, Ontario: Anatomy of an Archean Greenstone Belt and Ontogeny of Gold Mineralization. *Economic Geology*, **103**, 1285–1308.

BÉDARD, J. H., HARRIS, L. B. & THURSTON, P. C. 2012. The hunting of the snArc. *Precambrian Research*, **229**, 20–48.

BEGG, G. C., GRIFFIN, W. L. *ET AL.* 2009. The lithospheric architecture of Africa: seismic tomography, mantle petrology, and tectonic evolution. *Geosphere*, **5**, 23–50.

BEGG, G. C., HRONSKY, J. A. M., ARNDT, N. T., GRIFFIN, W. L., O'REILLY, S. Y. & HAYWARD, N. 2010. Lithospheric, cratonic, and geodynamic setting of Ni–Cu–PGE sulfide deposits. *Economic Geology*, **105**, 1057–1070.

BEKKER, A., BARLEY, M. E., FIORENTINI, M. L., ROUXEL, O. J., RUMBLE, D. & BERESFORD, S. W. 2009. Atmospheric sulfur in Archean komatiite-hosted nickel deposits. *Science*, **326**, 1086–1089.

BEKKER, A., SLACK, J. F., PLANAVSKY, N., KRAPEZ, B., HOFMANN, A., KONHAUSER, K. O. & ROUXEL, O. J. 2010. Iron formation: the sedimentary product of a complex interplay among mantle, tectonic, oceanic, and biospheric processes. *Economic Geology*, **105**, 467–508.

BERESFORD, S., CAS, R., LAHAYE, Y. & JANE, M. 2002. Facies architecture of an Archean komatiite-hosted Ni-sulphide ore deposit, Victor, Kambalda, Western Australia: implications for komatiite lava emplacement. *Journal of Volcanology and Geothermal Research*, **118**, 57–75.

BIERLEIN, F., GROVES, D., GOLDFARB, R. & DUBÉ, B. 2006. Lithospheric controls on the formation of provinces hosting giant orogenic gold deposits. *Mineralium Deposita*, **40**, 874–886.

BIZZARRO, M., BAKER, J. A., HAACK, H., ULFBECK, D. & ROSING, M. 2003. Early history of Earth's crust–mantle system inferred from hafnium isotopes in chondrites. *Nature*, **421**, 931–933.

BLEWETT, R. S., CZARNOTA, K. & HENSON, P. A. 2010*a*. Structural-event framework for the eastern Yilgarn Craton, Western Australia, and its implications for orogenic gold. *Precambrian Research*, **183**, 203–229.

BLEWETT, R. S., HENSON, P. A., ROY, I. G., CHAMPION, D. C. & CASSIDY, K. F. 2010*b*. Scale-integrated architecture of a world-class gold mineral system: the Archaean eastern Yilgarn Craton, Western Australia. *Precambrian Research*, **183**, 230–250.

BLICHERT-TOFT, J. & ALBARÈDE, F. 1997. The Lu–Hf isotope geochemistry of chondrites and the evolution of the mantle–crust system. *Earth and Planetary Science Letters*, **148**, 243–258.

BLICHERT-TOFT, J. & ALBARÈDE, F. 2008. Hafnium isotopes in Jack Hills zircons and the formation of the Hadean crust. *Earth and Planetary Science Letters*, **265**, 686–702.

BLICHERT-TOFT, J. & ARNDT, N. T. 1999. Hf isotope compositions of komatiites. *Earth and Planetary Science Letters*, **171**, 439–451.

BOILY, M., LECLAIR, A., MAURICE, C., BÉDARD, J. H. & DAVID, J. 2009. Paleo- to Mesoarchean basement recycling and terrane definition in the northeastern Superior Province, Québec, Canada. *Precambrian Research*, **168**, 23–44.

BOYD, F. R., GURNEY, J. J. & RICHARDSON, S. H. 1985. Evidence for a 150–200-km thick Archaean lithosphere from diamond inclusion thermobarometry. *Nature*, **315**, 387–389.

BROWN, S. J. A., BARLEY, M. E., KRAPEZ, B., HAND, J. & CAS, R. A. F. 2001. The origin of TTD volcaniclastic rocks in the Kalgoorlie Terrane, Western Australia. *AGSO-Geoscience Australia Record 2001/37,* 131–133.

BUROV, E., JAUPART, C. & MARESCHAL, J. C. 1998. Large-scale crustal heterogeneities and lithospheric strength in cratons. *Earth and Planetary Science Letters*, **164**, 205–219.

CAMPBELL, I. H. & HILL, R. I. 1988. A two-stage model for the formation of the granite–greenstone terrains of the Kalgoorlie–Norseman area, Western Australia. *Earth and Planetary Science Letters*, **90**, 11–25.

CAMPBELL, I. H., GRIFFITHS, R. W. & HILL, R. I. 1989. Melting in an Archaean mantle plume: heads it's basalts, tails it's komatiites. *Nature*, **339**, 697–699.

CANTWELL, N., COOPER, M., MEYERS, J., MARTIN, N. & SAINTY, R. 2009. A review of the Jaguar Cu–Zn–Ag volcanogenic massive sulphide discovery and subsequent geophysical trials. *ASEG Extended Abstracts*, **2009**, 1–11.

CARLSON, R. L. & RASKIN, G. S. 1984. Density of the ocean crust. *Nature*, **311**, 555–558.

CASSIDY, K. F. & CHAMPION, D. C. 2004. Crustal evolution of the Yilgarn Craton from Nd isotopes and granite geochronology: implications for metallogeny. *In*: MUHLING, J. R. (ed.) *SEG 2004, Predictive Mineral Discovery Under Cover. Centre for Global Metallogeny*. University of Western Australia, Perth, 317–320.

CASSIDY, K. F., GROVES, D. I. & MCNAUGHTON, N. J. 1998. Late-Archean granitoid-hosted lode-gold deposits, Yilgarn Craton, Western Australia: deposit characteristics, crustal architecture and implications for ore genesis. *Ore Geology Reviews*, **13**, 65–102.

CASSIDY, K. F., BASTRAKOVA, I. V. *ET AL.* 2002. *Characterisation and metallogenic significance of Archaean granitoids of the Yilgarn Craton, Western Australia*. Australian Mineral Industries Research Association (AMIRA) Project P482, 222/P482.

CASSIDY, K. F., CHAMPION, D. C. & HUSTON, D. L. 2005. Crustal evolution constraints on the metallogeny of the Yilgarn Craton. *In*: MAO, J. & BIERLEIN, F. P. (eds) *Mineral Deposit Research: Meeting the Global Challenge: Proceedings of the Eight Biennia SGA Meeting*. Springer, Berlin, 901–904.

CASSIDY, K. F., CHAMPION, D. C. *ET AL.* 2006. *A revised geological framework for the Yilgarn Craton, Western Australia*. Geological Survey of Western Australia – Record 2006/8.

CAWOOD, P. A., HAWKESWORTH, C. J. & DHUIME, B. 2013. The continental record and the generation of continental crust. *Geological Society of America Bulletin*, **125**, 14–32.

CHAMPION, D. C. 2013. *Neodymium depleted mantle model age map of Australia: explanatory notes and user guide*. Geoscience Australia Record 2013/44.

CHAMPION, D. C. & CASSIDY, K. F. 2007. An overview of the Yilgarn Craton and its crustal evolution. *In*: BIERLEIN, F. P. & C. M. K.-R. (eds) *Proceedings of Geoconferences (WA) Inc. Kalgoorlie '07 Conference*. Kalgoorlie, Western Australia, Geoscience Australia Record 2007/14, 8–13.

CHAMPION, D. C. & SHERATON, J. W. 1997. Geochemistry and Nd isotope systematics of Archaean granites of the Eastern Goldfields, Yilgarn Craton, Australia: implications for crustal growth processes. *Precambrian Research*, **83**, 109–132.

CHAUVEL, C., DUPRÉ, B. & JENNER, G. A. 1985. The Sm–Nd age of Kambalda volcanics is 500 Ma too old!. *Earth and Planetary Science Letters*, **74**, 315–324.

CHEN, S. F., LIBBY, J. W., GREENFIELD, J. E., WYCHE, S. & RIGANTI, A. 2001*a*. Geometry and kinematics of large arcuate structures formed by impingement of rigid granitoids into greenstone belts during progressive shortening. *Geology*, **29**, 283–286.

CHEN, S. F., WITT, W. K. & LIU, S. 2001*b*. Transpression and restraining jogs in the northeastern Yilgarn craton, Western Australia. *Precambrian Research*, **106**, 309–328.

CHEN, S. F., RIGANTI, A., WYCHE, S., GREENFIELD, J. E. & NELSON, D. R. 2003. Lithostratigraphy and tectonic evolution of contrasting greenstone successions in the central Yilgarn Craton, Western Australia. *Precambrian Research*, **127**, 249–266.

CLAOUÉ-LONG, J. C., COMPSTON, W. & COWDEN, A. 1988. The age of the Kambalda greenstones resolved by ion-microprobe: implications for Archaean dating methods. *Earth and Planetary Science Letters*, **89**, 239–259.

CLOOS, M. 1993. Lithospheric buoyancy and collisional orogenesis: subduction of oceanic plateaus, continental

margins, island arcs, spreading ridges, and seamounts. *Geological Society of America Bulletin*, **105**, 715–737.

Compston, W., Williams, I. S., Campbell, I. H. & Gresham, J. J. 1986. Zircon xenocrysts from the Kambalda volcanics: age constraints and direct evidence for older continental crust below the Kambalda–Norseman greenstones. *Earth and Planetary Science Letters*, **76**, 299–311.

Cox, S. F. 1999. Deformational controls on the dynamics of fluid flow in mesothermal gold systems. *In*: McCaffrey, K., Lonergan, L. & Wilkinson, J. (eds) *Fractures, Fluid Flow and Mineralization*. Geological Society, London, Special Publications, **155**, 123–140.

Czarnota, K., Champion, D. C., Goscombe, B., Blewett, R. S., Henson, P. B., Cassidy, K. F. & Groenewald, B. 2007. *Geodynamics of the Eastern Goldfields Superterrane. Concepts to Targets: a scale-integrated mineral systems study of the Eastern Yilgarn Craton*. pmd*CRC Project Y4 Final Report.

Czarnota, K., Champion, D. C., Goscombe, B., Blewett, R. S., Cassidy, K. F., Henson, P. A. & Groenewald, P. B. 2010. Geodynamics of the eastern Yilgarn Craton. *Precambrian Research*, **183**, 175–202.

Dentith, M. C., Joly, A., Evans, S. & Thiel, S. 2012. Regional mineral exploration targeting based on crustal electrical conductivity variations from magnetotelluric data. *22nd International Geophysical Conference and Exhibition*, Brisbane, Australia.

DePaolo, D. J. 1981. Neodymium isotopes in the Colorado Front Range and crust–mantle evolution in the Proterozoic. *Nature*, **291**, 193–196.

DePaolo, D. J., Linn, A. M. & Schubert, G. 1991. The continental crustal age distribution: methods of determining mantle separation ages from Sm–Nd isotopic data and application to the southwestern United States. *Journal of Geophysical Research: Solid Earth*, **96**, 2071–2088.

Dhuime, B., Hawkesworth, C. J., Cawood, P. A. & Storey, C. D. 2012. A change in the geodynamics of continental growth 3 billion years ago. *Science*, **335**, 1334–1336.

Drummond, B. J., Goleby, B. R. & Swager, C. P. 2000. Crustal signature of Late Archaean tectonic episodes in the Yilgarn craton, Western Australia: evidence from deep seismic sounding. *Tectonophysics*, **329**, 193–221.

Duuring, P. & Hagemann, S. 2013*a*. Genesis of superimposed hypogene and supergene Fe orebodies in BIF at the Madoonga deposit, Yilgarn Craton, Western Australia. *Mineralium Deposita*, **48**, 371–395.

Duuring, P. & Hagemann, S. 2013*b*. Leaching of silica bands and concentration of magnetite in Archean BIF by hypogene fluids: Beebyn Fe ore deposit, Yilgarn Craton, Western Australia. *Mineralium Deposita*, **48**, 341–370.

Duuring, P., Cassidy, K. F. & Hagemann, S. G. 2007. Granitoid-associated orogenic, intrusion-related, and porphyry style metal deposits in the Archean Yilgarn Craton, Western Australia. *Ore Geology Reviews*, **32**, 157–186.

Duuring, P., Hagemann, S. G., Novikova, Y., Cudahy, T. & Laukamp, C. 2012. Targeting iron ore in banded iron formations using ASTER data: Weld Range Greenstone Belt, Yilgarn Craton, Western Australia. *Economic Geology*, **107**, 585–597.

Duuring, P., Angerer, T. & Hagemann, S. G. 2013. *Diversity in Iron Ore Deposits in Western Australia*. SGA, Uppsala.

Evans, K. A., McCuaig, T. C., Leach, D., Angerer, T. & Hagemann, S. G. 2012. Banded iron formation to iron ore: a record of the evolution of Earth environments? *Geology*, **41**, 99–102.

Fiorentini, M. L., Beresford, S. W., Rosengren, N., Barley, M. E. & McCuaig, T. C. 2010. Contrasting komatiite belts, associated Ni–Cu–(PGE) deposit styles and assimilation histories. *Australian Journal of Earth Sciences: An International Geoscience Journal of the Geological Society of Australia*, **57**, 543–566.

Fiorentini, M. L., Barnes, S. J., Maier, W. D., Burnham, O. M. & Heggie, G. 2011. Global variability in the platinum-group element contents of Komatiites. *Journal of Petrology*, **52**, 83–112.

Fiorentini, M., Beresford, S. *et al.* 2012. District to camp controls on the genesis of komatiitehosted nickel sulfide deposits, Agnew–Wiluna Greenstone Belt, Western Australia: insights from the multiple sulfur isotopes. *Economic Geology*, **107**, 781–796.

Fishwick, S. & Rawlinson, N. 2012. 3-D structure of the Australian lithosphere from evolving seismic datasets. *Australian Journal of Earth Sciences*, **59**, 809–826.

Fletcher, I. R. & Rosman, K. J. R. 1982. Precise determination of initial epsilon-Nd from Sm–Nd isochron data. *Geochimica et Cosmochimica Acta*, **46**, 1983–1987.

Fletcher, I. R., Rosman, K. J. R., Williams, I. R., Hickman, A. H. & Baxter, J. L. 1984. Sm–Nd geochronology of greenstone belts in the Yilgarn Block, Western Australia. *Precambrian Research*, **26**, 331–361.

Fletcher, I. R., Libby, J. W. & Rosman, K. J. R. 1994. *Sm–Nd model ages of granitoid rocks in the Yilgarn Craton. Western Australia Geological Survey Report*, **37**.

Goldstein, S. L., O'Nions, R. K. & Hamilton, P. J. 1984. A Sm–Nd isotopic study of atmospheric dusts and particulates from major river systems. *Earth and Planetary Science Letters*, **70**, 221–236.

Gole, M. J. 1981. Archean banded iron-formations, Yilgarn Block, Western Australia. *Economic Geology*, **76**, 1954–1974.

Gole, M. J., Barnes, S. J. & Hill, R. E. T. 1987. The role of fluids in the metamorphism of komatiites, Agnew nickel deposit, Western Australia. *Contributions to Mineralogy and Petrology*, **96**, 51–162.

Goleby, B. R., Blewett, R. S. *et al.* 2004. Deep seismic reflection profiling in the Archaean northeastern Yilgarn Craton, Western Australia: implications for crustal architecture and mineral potential. *Tectonophysics*, **388**, 119–133.

Goleby, B. R., Blewett, R. S. *et al.* 2006. An integrated multi-scale 3D seismic model of the Archaean Yilgarn Craton, Australia. *Tectonophysics*, **420**, 75–90.

Goscombe, B., Blewett, R. S., Czarnota, K., Groenewald, B. & Maas, R. 2009. *Metamorphic evolution and integrated terrane analysis of the eastern Yilgarn Craton: rationale, methods, outcomes and interpretation*. Geoscience Australia Record 2009/23.

GRESHAM, J. J. & LOFTUS-HILLS, G. D. 1981. The geology of the Kambalda nickel field, Western Australia. *Economic Geology*, **76**, 1373–1416.

GREY, K., HOCKING, R. M. *ET AL*. 2005. *Lithostratigraphic nomenclature of the Officer Basin and correlative parts of the Paterson Orogen, Western Australia*. Western Australia Geological Survey, Report 93.

GRIFFIN, W. L., BELOUSOVA, E. A., SHEE, S. R., PEARSON, N. J. & O'REILLY, S. Y. 2004. Archean crustal evolution in the northern Yilgarn Craton: U–Pb and Hf-isotope evidence from detrital zircons. *Precambrian Research*, **131**, 231–282.

GROVES, D. 1993. The crustal continuum model for late-Archaean lode-gold deposits of the Yilgarn Block, Western Australia. *Mineralium Deposita*, **28**, 366–374.

GROVES, D. I. & BATT, W. D. 1984. Spatial and temporal variations of Archaean metallogenic associations in terms of evolution of Granitoid–Greenstone Terrains with particular emphasis on the Western Australian Shield. *In*: KRÖNER, A., HANSON, G. N. & GOODWIN, A. M. (eds) *Archaean Geochemistry*. Springer, Berlin, 73–98.

GROVES, D. I., KORKIAKOSKI, E. A., MCNAUGHTON, N. J., LESHER, C. M. & COWDEN, A. 1986. Thermal erosion by komatiites at Kambalda, Western Australia and the genesis of nickel ores. *Nature*, **319**, 136–139.

GROVES, D. I., RIDLEY, J. R. *ET AL*. 1995. Lode-gold deposits of the Yilgarn block: products of Late Archaean crustal-scale overpressured hydrothermal systems. *In*: COWARD, M. E. & RIES, A. C. (eds) *Early Precambrian Processes*. Geological Society, London, Special Publications, **95**, 155–172.

GROVES, D. I., GOLDFARB, R. J., GEBRE-MARIAM, M., HAGEMANN, S. G. & ROBERT, F. 1998. Orogenic gold deposits: a proposed classification in the context of their crustal distribution and relationship to other gold deposit types. *Ore Geology Reviews*, **13**, 7–27.

HANNINGTON, M. D., BLEEKER, W. & KJARSGAARD, I. 1999*a*. Sulfide mineralogy, geochemistry, and ore genesis of Kidd Creek deposit: Part I. North, Central, and South orebodies. *In*: HANNINGTON, M. D. & BARRIE, C. T. (eds) *The Giant Kidd Creek Volcanogenic Massive Sulfide Deposit, Western Abitibi Subprovince, Canada*. Economic Geology Monograph, Society of Economic Geologists, Littleton, CO, 163–224.

HANNINGTON, M. D., BLEEKER, W. & KJARSGAARD, I. 1999*b*. Sulfide mineralogy, geochemistry, and ore genesis of Kidd Creek deposit: Part II. The bornite zone. *In*: HANNINGTON, M. D. & BARRIE, C. T. (eds) *The Giant Kidd Creek Volcanogenic Massive Sulfide Deposit, Western Abitibi Subprovince, Canada*. Economic Geology Monograph, Society of Economic Geologists, Littleton, CO, 225–266.

HARRISON, T. M., BLICHERT-TOFT, J., MÜLLER, W., ALBAREDE, F., HOLDEN, P. & MOJZSIS, S. J. 2005. Heterogeneous Hadean Hafnium: evidence of Continental Crust at 4.4 to 4.5 Ga. *Science*, **310**, 1947–1950.

HAWKESWORTH, C. J. & KEMP, A. I. S. 2006. Evolution of the continental crust. *Nature*, **443**, 811–817.

HAWKESWORTH, C., CAWOOD, P., KEMP, T., STOREY, C. & DHUIME, B. 2009. A matter of preservation. *Science*, **323**, 49–50.

HAWKESWORTH, C. J., DHUIME, B., PIETRANIK, A. B., CAWOOD, P. A., KEMP, A. I. S. & STOREY, C. D. 2010. The generation and evolution of the continental crust. *Journal of the Geological Society*, **167**, 229–248.

HEGGIE, G. J., FIORENTINI, M. L., BARNES, S. J. & BARLEY, M. E. 2012*a*. Maggie Hays Ni deposit: Part 1. Stratigraphic controls on the style of komatiite emplacement in the 2.9 Ga Lake Johnston Greenstone Belt, Yilgarn Craton, Western Australia. *Economic Geology*, **107**, 797–816.

HEGGIE, G. J., FIORENTINI, M. L., BARNES, S. J. & BARLEY, M. E. 2012*b*. Maggie Hays Ni deposit: Part 2. Nickel mineralization and the spatial distribution of PGE ore-forming signatures in the Maggie Hays Ni System, Lake Johnston Greenstone Belt, Western Australia. *Economic Geology*, **107**, 817–833.

HENSON, P. A., BLEWETT, R. S., ROY, I. G., MILLER, J. M. & CZARNOTA, K. 2010. 4D architecture and tectonic evolution of the Laverton region, eastern Yilgarn Craton, Western Australia. *Precambrian Research*, **183**, 338–355.

HERZBERG, C. 1992. Depth and degree of melting of komatiites. *Journal of Geophysical Research*, **97**, 4521–4540.

HERZBERG, C., FYFE, W. & CARR, M. 1983. Density constraints on the formation of the continental Moho and crust. *Contributions to Mineralogy and Petrology*, **84**, 1–5.

HERZBERG, C., ASIMOW, P. D. *ET AL*. 2007. Temperatures in ambient mantle and plumes: donstraints from basalts, picrites, and komatiites. *Geochemistry Geophysics Geosystems*, **8**, http://dx.doi.org/10.1029/2006GC001390

HILL, R. E. T. 2001. Komatiite volcanology, volcanological setting and primary geochemical properties of komatiite-associated nickel deposits. *Geochemistry Exploration, Environment, Analysis*, **1**, 365–381.

HILL, R. I.,, CAMPBELL, I. H. & COMPSTON, W. 1989. Age and origin of granitic rocks in the Kalgoorlie–Norseman region of Western Australia: implications for the origin of archaean crust. *Geochimica et Cosmochimica Acta*, **53**, 1259–1275.

HILL, R. E. T., BARNES, S. J., GOLE, M. J. & DOWLING, S. E. 1990. *The physical volcanology of komatiites in the Norseman–Wiluna Belt, Western Australia*. Geological Society of Australia, Excursion Guidebook **1**.

HILL, R. E. T., BARNES, S. J., GOLE, M. J. & DOWLING, S. E. 1995. The volcanology of komatiites as deduced from field relationships in the Norseman–Wiluna greenstone belt, Western Australia. *Lithos*, **34**, 159–188.

HOATSON, D. M., JAIRETH, S. & JAQUES, A. L. 2006. Nickel sulfide deposits in Australia: characteristics, resources, and potential. *Ore Geology Reviews*, **29**, 177–241.

HOULÉ, M. G., GIBSON, H. L., LESHER, C. M., DAVIS, P. C., CAS, R. A. F., BERESFORD, S. W. & ARNDT, N. T. 2008. Komatiitic sills and multigenerational Peperite at Dundonald Beach, Abitibi Greenstone Belt, Ontario: volcanic architecture and nickel sulfide distribution. *Economic Geology*, **103**, 1269–1284.

HOULÉ, M., LESHER, C. M. & DAVIS, P. 2012. Thermomechanical erosion at the Alexo Mine, Abitibi greenstone belt, Ontario: implications for the genesis of komatiite-associated Ni–Cu–(PGE) mineralization. *Mineralium Deposita*, **47**, 105–128.

Hronsky, J. M. A. & Groves, D. I. 2008. Science of targeting: definition, strategies, targeting and performance measurement. *Australian Journal of Earth Sciences*, **55**, 3–12.

Hronsky, J. A., Groves, D., Loucks, R. & Begg, G. 2012. A unified model for gold mineralisation in accretionary orogens and implications for regional-scale exploration targeting methods. *Mineralium Deposita*, **47**, 339–358.

Huppert, H. E. & Sparks, R. S. J. 1985*a*. Cooling and contamination of mafic and ultramafic magmas during ascent through continental crust. *Earth and Planetary Science Letters*, **74**, 371–386.

Huppert, H. E. & Sparks, R. S. J. 1985*b*. Komatiites I: eruption and flow. *Journal of Petrology*, **26**, 694–725.

Ispolatov, V., Lafrance, B., Dubé, B., Creaser, R. & Hamilton, M. 2008. Geologic and structural setting of gold mineralization in the Kirkland Lake–Larder Lake Gold Belt, Ontario. *Economic Geology*, **103**, 1309–1340.

Ivanic, T. J., Wingate, M. T. D., Kirkland, C. L., Van Kranendonk, M. J. & Wyche, S. 2010. Age and significance of voluminous mafic–ultramafic magmatic events in the Murchison Domain, Yilgarn Craton. *Australian Journal of Earth Sciences*, **57**, 597–614.

Ivanic, T. J., Van Kranendonk, M. J., Kirkland, C. L., Wyche, S., Wingate, M. T. D. & Belousova, E. A. 2012. Zircon Lu–Hf isotopes and granite geochemistry of the Murchison Domain of the Yilgarn Craton: evidence for reworking of Eoarchean crust during Meso-Neoarchean plume-driven magmatism. *Lithos*, **148**, 112–127.

Ivanic, T. J., Korsch, R. J. *et al.* (eds) 2013. *Preliminary Interpretation of the 2010 Youanmi Deep Seismic Reflection Lines and Magnetotelluric Data for the Windimurra Igneous Complex*. Youanmi and Southern Carnarvon seismic and magnetotelluric (MT) workshop 2013: extended abstracts volume. Geological Survey of Western Australia, Record 2013/6. Geological Survey of Western Australia, Perth.

Jacobsen, S. B. & Wasserburg, G. J. 1979. Mean age of mantle and crustal reservoirs. *Journal of Geophysical Research*, **84**, 7411–7428.

Kemp, A. I. S., Hawkesworth, C. J. *et al.* 2007. Magmatic and crustal differentiation history of Granitic Rocks from Hf–O Isotopes in Zircon. *Science*, **315**, 980–983.

Kent, A. J. R. & Hagemann, S. G. 1996. Constraints on the timing of lode-gold mineralisation in the Wiluna greenstone belt, Yilgarn Craton, Western Australia. *Australian Journal of Earth Sciences*, **43**, 573–588.

Kent, A. J. R. & McDougall, I. 1995. ^{40}Ar–^{39}Ar and U–Pb age constraints on the timing of gold mineralization in the Kalgoorlie gold field, Western Australia. *Economic Geology*, **90**, 845–859.

Kent, A. J. R., Cassidy, K. F. & Mark Fanning, C. 1996. Archean gold mineralization synchronous with the final stages of cratonization, Yilgarn Craton, Western Australia. *Geology*, **24**, 879–882.

Ketchum, J. W. F., Ayer, J. A., van Breemen, O., Pearson, N. J. & Becker, J. K. 2008. Pericontinental crustal growth of the southwestern Abitibi Subprovince, Canada–U–Pb, Hf, and Nd Isotope Evidence. *Economic Geology*, **103**, 1151–1184.

Khan, R. M. K. & Naqvi, S. M. 1996. Geology, geochemistry and genesis of BIF of Kushtagi schist belt, Archaean Dharwar Craton, India. *Mineralium Deposita*, **31**, 123–133.

Kinny, P. D., Williams, I. S., Froude, D. O., Ireland, T. R. & Compston, W. 1988. Early archaean zircon ages from orthogneisses and anorthosites at Mount Narryer, Western Australia. *Precambrian Research*, **38**, 325–341.

Kirkland, C. L., Spaggiari, C. V., Wingate, M. T. D., Smithies, R. H., Belousova, E. A., Murphy, R. & Pawley, M. J. 2011. *Inferences on crust–mantle interaction from Lu–Hf isotopes: a case study from the Albany–Fraser Orogen*. Geological Survey of Western Australia, Record 2011/12.

Knox-Robinson, C. M. & Wyborn, L. A. I. 1997. Towards a holistic exploration strategy: using Geographic Information Systems as a tool to enhance exploration. *Australian Journal of Earth Sciences*, **44**, 453–463.

Kositcin, N., Brown, S. J. A., Barley, M. E., Krapez, B., Cassidy, K. F. & Champion, D. C. 2008. SHRIMP U–Pb zircon age constraints on the Late Archaean tectonostratigraphic architecture of the Eastern Goldfields Superterrane, Yilgarn Craton, Western Australia. *Precambrian Research*, **161**, 5–33.

Krapez, B. & Hand, J. L. 2008. Late Archaean deep-marine volcaniclastic sedimentation in an arc-related basin: The Kalgoorlie Sequence of the Eastern Goldfields Superterrane, Yilgarn Craton, Western Australia. *Precambrian Research*, **161**, 89–113.

Krapez, B., Brown, S. J. A., Hand, J., Barley, M. E. & Cas, R. A. F. 2000. Age constraints on recycled crustal and supracrustal sources of Archaean metasedimentary sequences, Eastern Goldfields Province, Western Australia: evidence from SHRIMP zircon dating. *Tectonophysics*, **322**, 89–133.

Kumagai, I., Davaille, A. & Kurita, K. 2007. On the fate of thermally buoyant mantle plumes at density interfaces. *Earth and Planetary Science Letters*, **254**, 180–193.

Kumagai, I., Davaille, A., Kurita, K. & Stutzmann, E. 2008. Mantle plumes: thin, fat, successful, or failing? Constraints to explain hot spot volcanism through time and space. *Geophysical Research Letters*, **35**, L16301.

Lascelles, D. F. 2007. Black smokers and density currents: a uniformitarian model for the genesis of banded iron-formations. *Ore Geology Reviews*, **32**, 381–411.

Lesher, C. M., Lee, R. F., Groves, D. I., Bickle, M. J. & Donaldson, M. J. 1981. Geochemistry of komatiites at Kambalda: chalcophile element depletion – a consequence of sulfide liquid separation from komatiitic magmas. *Economic Geology*, **76**, 1714–1728.

Liew, T. C. & Hofmann, A. W. 1988. Precambrian crustal components, plutonic associations, plate environment of the Hercynian Fold Belt of central Europe: indications from a Nd and Sr isotopic study. *Contributions to Mineralogy and Petrology*, **98**, 129–138.

Maas, R., Kamenetsky, M. B., Sobolev, A. V., Kamenetsky, V. S. & Sobolev, N. V. 2005. Sr, Nd, and Pb isotope evidence for a mantle origin of alkali chlorides and carbonates in the Udachnaya kimberlite, Siberia. *Geology*, **33**, 549–552.

MAIER, W. D. 2005. Platinum-group element (PGE) deposits and occurrences: mineralization styles, genetic concepts, and exploration criteria. *Journal of African Earth Sciences*, **41**, 165–191.

MAMUSE, A., PORWAL, A., KREUZER, O. & BERESFORD, S. W. 2010. Spatial statistical analysis of the distribution of komatiite-hosted nickel sulfide deposits in the Kalgoorlie Terrane, Western Australia: clustered or not? *Economic Geology*, **105**, 229–242.

MANEA, V. C., MANEA, M., LEEMAN, W. P. & SCHUTT, D. L. 2009. The influence of plume head-lithosphere interaction on magmatism associated with the Yellowstone hotspot track. *Journal of Volcanology and Geothermal Research*, **188**, 68–85.

MCCUAIG, T. C., BEHN, M. *ET AL.* 2001. *The Boddington gold mine: a new style of Archaean Au–Cu deposit*. AGSO-Geoscience Australia. Record 2001/*37*, 453–455.

MCCUAIG, T. C., BERESFORD, S. & HRONSKY, J. 2010. Translating the mineral systems approach into an effective exploration targeting system. *Ore Geology Reviews*, **38**, 128–138.

MCCULLOCH, M. T. 1987. Sm–Nd isotopic constraints on the evolution of Precambrian crust in the Australian continent. *In*: KRONER, A. (ed.) *Proterozoic Lithospheric Evolution*. AGU, Washington, DC, 115–130.

MCCULLOCH, M. T. & COMPSTON, W. 1981. Sm–Nd age of Kambalda and Kanowna greenstones and heterogeneity in the Archaean mantle. *Nature*, **294**, 322–327.

MCCULLOCH, M. T., COMPSTON, W. & FROUDE, D. 1983. Sm–Nd and Rb–Sr dating of Archaean gneisses, eastern Yilgarn Block, Western Australia. *Journal of the Geological Society of Australia*, **30**, 149–153.

MOLE, D. R. 2012. *Evaluating the Lithospheric Architecture of the Yilgarn Craton in Space and Time: Implications for Komatiite Volcanism and Earth Evolution*. University of Western Australia, Perth.

MOLE, D. R., FIORENTINI, M. *ET AL.* 2010. Lithospheric controls on the localization of komatiite-hosted nickel-sulfide deposits. *In*: TYLER, I. M. & KNOX-ROBINSON, C. M. (eds) *5th International Archean Symposium*, Perth, Western Australia. Geological Survey of Western Australia Record 2010/18, 101–103.

MOLE, D. R., FIORENTINI, M. *ET AL.* 2012. Spatio-temporal constraints on lithospheric development in the southwest-central Yilgarn Craton, Western Australia. *Australian Journal of Earth Sciences*, **59**, 625–656.

MÜLLER, D. 2002. Gold-copper mineralization in alkaline rocks. *Mineralium Deposita*, **37**, 1–3.

MYERS, J. S. 1995. The generation and assembly of an Archaean supercontinent: evidence from the Yilgarn Craton, Western Australia. *In*: COWARD, M. P. & RIES, A. C. (eds) *Early Precambrian Processes*. Geological Society, London, Special Publications, **95**, 143–154.

MYERS, J. S. 1997. Preface: Archaean geology of the Eastern Goldfields of Western Australia: A regional overview. *Precambrian Research*, **83**, 1–10.

MYERS, J. S. & WILLIAMS, I. R. 1985. Early Precambrian crustal evolution at Mount Narryer, Western Australia. *Precambrian Research*, **27**, 153–163.

NAERAA, T., SCHERSTEN, A., ROSING, M. T., KEMP, A. I. S., HOFFMANN, J. E., KOKFELT, T. F. & WHITEHOUSE, M. J. 2012. Hafnium isotope evidence for a transition in the dynamics of continental growth 3.2 Gyr ago. *Nature*, **485**, 627–630.

NALDRETT, A. J. 2010. Secular variation of magmatic sulfide deposits and their source magmas. *Economic Geology*, **105**, 669–688.

NASH, B. P., PERKINS, M. E., CHRISTENSEN, J. N., LEE, D.-C. & HALLIDAY, A. N. 2006. The Yellowstone hotspot in space and time: Nd and Hf isotopes in silicic magmas. *Earth and Planetary Science Letters*, **247**, 143–156.

NELSON, D. R. 1995. *Compilation of SHRIMP U–Pb zircon geochronology data, 1994–2001*. Geological Survey of Western Australia Record 2003/2.

NELSON, D. R. 1997. Evolution of the Archaean granite–greenstone terranes of the Eastern Goldfields, Western Australia: SHRIMP U–Pb zircon constraints. *Precambrian Research*, **83**, 57–81.

NEMCHIN, A. A., PIDGEON, R. T. & WILDE, S. A. 1994. Timing of Late Archaean granulite facies metamorphism in the southwestern Yilgarn Craton of Western Australia: evidence from U–Pb ages of zircons fro mafic granulites. *Precambrian Research*, **68**, 307–321.

NISBET, E. G., CHEADLE, M. J., ARNDT, N. T. & BICKLE, M. J. 1993. Constraining the potential temperature of the Archaean mantle: a review of the evidence from komatiites. *Lithos*, **30**, 291–307.

NUTMAN, A. P., KINNY, P. D., COMPSTON, W. & WILLIAMS, I. S. 1991. SHRIMP U–Pb zircon geochronology of the Narryer Gneiss Complex, Western Australia. *Precambrian Research*, **52**, 275–300.

NUTMAN, A. P., BENNETT, V. C., KINNY, P. D. & PRICE, R. 1993. Large-scale crustal structure of the northwestern Yilgarn Craton, western Australia: evidence from Nd isotopic data and zircon geochronology. *Tectonics*, **12**, 971–981.

OCCHIPINTI, S. A., SHEPPARD, S., MYERS, J. S., TYLER, I. M. & NELSON, D. R. 2001. *Archean and Paleoproterozoic geology of the Narryer Terrane (Yilgarn Craton) and the Southern Gascoyne Complex (Capricorn Orogen), Westen Australia – a field guide*. Western Australia Geological Survey Record 2001/8.

O'NIONS, R. K., EVENSEN, N. M., HAMILTON, P. J., SMITH, J. V. & BAILEY, D. K. 1980. Differentiation and evolution of the mantle. [And Discussion.] *Philosophical Transactions of the Royal Society of London. Series A, Mathematical and Physical Sciences*, **297**, 479–493.

ORMEROD, D. S., HAWKESWORTH, C. J., ROGERS, N. W., LEEMAN, W. P. & MENZIES, M. A. 1988. Tectonic and magmatic transitions in the Western Great Basin, USA. *Nature*, **333**, 349–353.

PAWLEY, M. J., WINGATE, M. T. D., KIRKLAND, C. L., WYCHE, S., HALL, C. E., ROMANO, S. S. & DOUBLIER, M. P. 2012. Adding pieces to the puzzle: episodic crustal growth and a new terrane in the northeast Yilgarn Craton, Western Australia. *Australian Journal of Earth Sciences*, **59**, 603–623.

PERRING, C. S., BARNES, S. J. & HILL, R. E. T. 1995. The physical volcanology of Archaean komatiite sequences from Forrestania, Southern Cross Province, Western Australia. *Lithos*, **34**, 189–207.

PERRING, C. S., BARNES, S. J. & HILL, R. E. T. 1996. Geochemistry of komatiites from Forrestania, Southern

Cross Province, Western Australia: evidence for crustal contamination. *Lithos*, **37**, 181–197.

PHILLIPS, G. N. & GROVES, D. I. 1983. The nature of Archaean gold-bearing fluids as deduced from gold deposits of Western Australia. *Journal of the Geological Society of Australia*, **30**, 25–39.

PIDGEON, R. T. & HALLBERG, J. A. 2000. Age relationships in supracrustal sequences of the northern part of the Murchison Terrane, Archaean Yilgarn Craton, Western Australia: a combined field and zircon U–Pb study. *Australian Journal of Earth Sciences*, **47**, 153–165.

PIDGEON, R. T. & WILDE, S. A. 1990. The distribution of 3.0 Ga and 2.7 Ga volcanic episodes in the Yilgarn Craton of Western Australia. *Precambrian Research*, **48**, 309–325.

PIDGEON, R. T., WILDE, S. A., COMPSTON, W. & SHIELD, M. W. 1990. Archaean evolution of the Wongan Hills Greenstone Belt, Yilgarn Craton, Western Australia. *Australian Journal of Earth Sciences*, **37**, 279–292.

PIERCE, K. L. & MORGAN, L. A. 2009. Is the track of the Yellowstone hotspot driven by a deep mantle plume? Review of volcanism, faulting, and uplift in light of new data. *Journal of Volcanology and Geothermal Research*, **188**, 1–25.

QIU, Y. M. 1997. *Long-lived Granitoid Magmatism in the Southern Cross Province, Yilgarn Craton, Western Australia, and its Relationship with Archean Gold Mineralization*. School of Earth and Environment, University of Western Australia, Perth.

RACZEK, I., JOCHUM, K. P. & HOFMANN, A. W. 2003. Neodymium and strontium isotope data for USGS reference materials BCR-1, BCR-2, BHVO-1, BHVO-2, AGV-1, AGV-2, GSP-1, GSP-2 and eight MPI-DING reference glasses. *Geostandards Newsletter*, **27**, 173–179.

ROBERT, F., POULSEN, K. H., CASSIDY, K. F. & HODGSON, C. J. 2005. Gold Metallogeny of the Superior and Yilgarn Cratons. *In*: HEDENQUIST, J. W., THOMPSON, J. F. H., GOLDFARB, R. J. & RICHARDS, J. P. (eds) *Economic Geology One Hundredth Anniversary Volume (1905–2005)*, Littleton, CO, Society of Economic Geologists.

ROSENGREN, N. M., BERESFORD, S. W., GRGURIC, B. A. & CAS, R. A. F. 2005. An intrusive origin for the komatiitic dunite-hosted Mount Keith disseminated nickel sulfide deposit, Western Australia. *Economic Geology*, **100**, 149–156.

RUDNICK, R. L. 1995. Making continental crust. *Nature*, **378**, 571–578.

SAID, N. & KERRICH, R. 2009. Geochemistry of coexisting depleted and enriched Paringa Basalts, in the 2.7 Ga Kalgoorlie Terrane, Yilgarn Craton, Western Australia: evidence for a heterogeneous mantle plume event. *Precambrian Research*, **174**, 287–309.

SAID, N., KERRICH, R. & GROVES, D. 2010. Geochemical systematics of basalts of the Lower Basalt Unit, 2.7 Ga Kambalda Sequence, Yilgarn Craton, Australia: plume impingement at a rifted craton margin. *Lithos*, **115**, 82–100.

SCHIOTTE, L. & CAMPBELL, I. H. 1996. Chronology of the Mount Magnet granite–greenstone terrain, Yilgarn Craton, Western Australia: implications for field based predictions of the relative timing of granitoid emplacement. *Precambrian Research*, **78**, 237–260.

SHIREY, S. B. & RICHARDSON, S. H. 2011. Start of the Wilson cycle at 3 Ga shown by diamonds from subcontinental mantle. *Science*, **333**, 434–436.

SIBSON, R. H. 1994. Crustal stress, faulting and fluid flow. *In*: PARNELL, J. (ed.) *Geofluids: Origin, Migration and Evolution of Fluids in Sedimentary Basins*, Geological Society, London, Special Publications, **78**, 69–84.

SIRCOMBE, K. N., CASSIDY, K. F., CHAMPION, D. C. & TRIPP, G. 2007. *Compilation of SHRIMP U–Pb geochronological data, Yilgarn Craton, Western Australia, 2004–2006*. Geoscience Australia Record, 2007/01.

SLEEP, N. H. 1997. Lateral flow and ponding of starting plume material. *Journal of Geophysical Research*, **102**, 10001–10012.

SLEEP, N. H. 2005. Evolution of the continental lithosphere. *Annual Review of Earth and Planetary Sciences*, **33**, 369–393.

SMITHIES, R. H., CHAMPION, D. C. & CASSIDY, K. F. 2003. Formation of Earth's early Archaean continental crust. *Precambrian Research*, **127**, 89–101.

SPAGGIARI, C. V. 2006. *Interpreted bedrock geology of the northern Murchison Domain, Youanmi Terrane, Yilgarn Craton*. Western Australia Geological Survey, Record 2006/10.

SPAGGIARI, C. V., PIDGEON, R. T. & WILDE, S. A. 2007. The Jack Hills greenstone belt, Western Australia: Part 2: lithological relationships and implications for the deposition of ≥4.0 Ga detrital zircons. *Precambrian Research*, **155**, 261–286.

STEIN, H. J., MARKEY, R. J., MORGAN, J. W., SELBY, D., CREASER, R. A., MCCUAIG, T. C. & BEHN, M. 2001. Re–Os Dating of Boddington Molybdenite, SW Yilgarn: two Au Mineralization Events. *In*: CASSIDY, K. F., CASSIDY, J. M. & VAN KRANENDONK, M. J. (eds) *4th International Archean Symposium, Perth Western Australia*. AGSO-Geoscience Australia. Record 2001/37, 453–455.

SWAGER, C. P. 1997. Tectono-stratigraphy of late Archaean greenstone terranes in the southerrn Eastern Goldfields, Western Australia. *Precambrian Research*, **83**, 11–42.

TAYLOR, S. R. & MCLENNAN, S. M. 1985. *The Continental Crust: its Composition and Evolution*. Blackwell Scientific, Oxford.

TAYLOR, S. R. & MCLENNAN, S. M. 1995. The Geochemical Evolution of the Continental Crust. *Reviews of Geophysics*, **33**, 241–265.

THÉBAUD, N. & BARNES, S. J. 2012. Geochemistry of komatiites in the Southern Cross Belt, Youanmi Terrane, Western Australia. *Australian Journal of Earth Sciences*, **59**, 234–246.

THÈBAUD, N. & MILLER, J. M. 2009. U–Pb age constraints on the siliciclastic sediments from the upper supracrustal cover in the Southern Cross greenstone belt, Youanmi Terrane, Western Australia, *In: Abstract Volume, Tenth Biennial SGA meeting, Townsville*.

THÉBAUD, N., BARNES, S. & FIORENTINI, M. 2012. Komatiites of the Wildara–Leonora Belt, Yilgarn Craton, WA: the missing link in the Kalgoorlie Terrane? *Precambrian Research*, **196–197**, 234–246.

THOMPSON, R. N. & GIBSON, S. A. 1991. Subcontinental mantle plumes, hotspots and pre-existing thinspots. *Journal of the Geological Society*, London, **148**, 973–977.

VANCE, D. & THIRLWALL, M. 2002. An assessment of mass discrimination in MC-ICPMS using Nd isotopes. *Chemical Geology*, **185**, 227–240.

VAN KRANENDONK, M. J. & IVANIC, T. J. 2008. A new lithostratigraphic scheme for the northeastern Murchison Domain, Yilgarn Craton. *Geological Survey of Western Australia Annual Review*, **2007–2008**, 34–53.

VEARNCOMBE, J. R. 1998. Shear zones, fault networks, and Archean gold. *Geology*, **26**, 855–858.

VIELREICHER, R. M., GROVES, D. I., RIDLEY, J. R. & MCNAUGHTON, N. J. 1994. A replacement origin for the BIF-hosted gold deposit at Mt. Morgans, Yilgarn Block, W.A. *Ore Geology Reviews*, **9**, 325–347.

WANG, Q., SCHIOTTE, L. & CAMPBELL, I. H. 1996. Geochronological constraints on the age of komatiites and nickel mineralisation in the Lake Johnston greenstone belt, Yilgarn Craton, Western Australia. *Australian Journal of Earth Sciences*, **43**, 381–385.

WANG, Q., SCHIOTTE, L. & CAMPBELL, I. H. 1998. Geochronology of the supracrustal rocks from the Golden Grove area, Murchison Province, Yilgarn block, Western Australia. *Australian Journal of Earth Sciences*, **45**, 571–577.

WATKINS, K. P., FLETCHER, I. R. & DE LAETER, J. R. 1991. Crustal evolution of Archaean granitoids in the Murchison Province, Western Australia. *Precambrian Research*, **50**, 311–336.

WILDE, S. A. & PIDGEON, R. T. 1986. Geology and geochronology of the Saddleback Greenstone Belt in the Archaean Yilgarn Block, southwestern Australia. *Australian Journal of Earth Sciences*, **33**, 491–501.

WILDE, S. A., MIDDLETON, M. F. & EVANS, B. J. 1996. Terrane accretion in the southwestern Yilgarn Craton: evidence from a deep seismic crustal profile. *Precambrian Research*, **78**, 179–196.

WILDE, S. A., VALLEY, J. W., PECK, W. H. & GRAHAM, C. M. 2001. Evidence from detrital zircons for the existence of continental crust and oceans on the Earth 4.4 Gyr ago. *Nature*, **409**, 175–178.

WITT, W. K. 1999. The Archaean Ravensthorpe Terrane, Western Australia: synvolcanic Cu–Au mineralization in a deformed island arc complex. *Precambrian Research*, **96**, 143–181.

WITT, W. K. & VANDERHOR, F. 1998. Diversity within a unified model for Archaean gold mineralization in the Yilgarn Craton of Western Australia: an overview of the late-orogenic, structurally-controlled gold deposits. *Ore Geology Reviews*, **13**, 29–64.

WITT, W. K., STEIN, H. J., CASSIDY, K. F., BLACK, L., CHAMPION, D. C. & FLETCHER, I. R. 2001. A >2.75 Ga basement enclave at Leonora: a domain of uplift and 2.75 Ga gold within the 2.71–2.66 Ga Eastern Goldfields Province. *AGU Chapman Conference*, Perth, Western Australia, 176–177.

WYBORN, L. A. I., PAGE, R. W. & MCCULLOCH, M. T. 1988. Petrology, geochronology and isotope geochemistry of the post-1820 Ma granites of the Mount Isa Inlier: mechanisms for the generation of Proterozoic anorogenic granites. *Precambrian Research*, **40–41**, 509–541.

WYBORN, L. A. L., HEINRICH, C. A. & JAQUES, A. L. 1994. Australian Proterozoic mineral systems: essential ingredients and mappable criteria. *Australian Institute of Mining and Metallurgy Annual Conference Proceedings*, Melbourne, 109–115.

WYCHE, S., NELSON, D. R. & RIGANTI, A. 2004. 4350–3130 Ma detrital zircons in the Southern Cross Granite–greenstone terrane, Western Australia: implications for the early evolution of the Yilgarn Craton. *Australian Journal of Earth Sciences*, **51**, 31–45.

WYCHE, S., FIORENTINI, M. L., MILLER, J. L. & MCCUAIG, T. C. 2012*a*. Geology and controls on mineralisation in the Eastern Goldfields region, Yilgarn Craton, Western Australia. *Episodes*, **35**, 273–282.

WYCHE, S., KIRKLAND, C. L., RIGANTI, A., PAWLEY, M. J., BELOUSOVA, E. & WINGATE, M. T. D. 2012*b*. Isotopic constraints on stratigraphy in the central and eastern Yilgarn Craton, Western Australia. *Australian Journal of Earth Sciences*, **59**, 657–670.

WYMAN, D. & KERRICH, R. 1988. Alkaline magmatism, major structures, and gold deposits; implications for greenstone belt gold metallogeny. *Economic Geology*, **83**, 454–461.

WYMAN, D. A. & KERRICH, R. 2012. Geochemical and isotopic characteristics of Youanmi Terrane volcanism: the role of mantle plumes and subduction tectonics in the western Yilgarn Craton. *Australian Journal of Earth Sciences*, **59**, 1–24.

YEATS, C. J., MCNAUGHTON, N. J. & GROVES, D. I. 1996. SHRIMP U–Pb geochronological constraints on Archean volcanic-hosted massive sulfide and lode gold mineralization at Mount Gibson, Yilgarn Craton, Western Australia. *Economic Geology*, **91**, 1354–1371.

ZIENTEK, M. L., COOPER, R. W., CORSON, S. R. & GERAGHTY, E. P. 2002. Platinum-group element mineralization in the Stillwater Complex, Montana. *In*: CABRI, L. J. (ed.) *The Geology, Geochemistry, Mineralogy and Mineral Beneficiation of Platinum-group Elements*. Canadian Institute of Mining, Metallurgy and Petroleum Special Volumes, **54**, 459–481.